Titre: Title:	Évolution thermodynamique d'une cible de silicium soumise à de brèves impulsions laser
Auteur: Author:	Patrick Lorazo
Date:	2006
Type:	Mémoire ou thèse / Dissertation or Thesis
Référence: Citation:	Lorazo, P. (2006). Évolution thermodynamique d'une cible de silicium soumise à de brèves impulsions laser [Thèse de doctorat, École Polytechnique de Montréal]. PolyPublie. https://publications.polymtl.ca/7565/

UNIVERSITÉ DE MONTRÉAL

ÉVOLUTION THERMODYNAMIQUE D'UNE CIBLE DE SILICIUM SOUMISE À DE BRÈVES IMPULSIONS LASER

PATRICK LORAZO
DÉPARTEMENT DE GÉNIE PHYSIQUE
ÉCOLE POLYTECHNIQUE DE MONTRÉAL

THÈSE PRÉSENTÉE EN VUE DE L'OBTENTION
DU DIPLÔME DE PHILOSOPHIÆ DOCTOR
(GÉNIE PHYSIQUE)
FÉVRIER 2006

Your file Votre référence
ISBN: 978-0-494-17007-6
Our file Notre référence
ISBN: 978-0-494-17007-6

UNIVERSITÉ DE MONTRÉAL

ÉCOLE POLYTECHNIQUE DE MONTRÉAL

Cette thèse intitulée:

ÉVOLUTION THERMODYNAMIQUE D'UNE CIBLE DE SILICIUM SOUMISE À DE BRÈVES IMPULSIONS LASER

présentée par: LORAZO Patrick

en vue de l'obtention du diplôme de: Philosophiæ Doctor

a été dûment acceptée par le jury d'examen constitué de:

M. FRANCOEUR Sébastien, Ph.D., président

M. MEUNIER Michel, Ph.D., membre et directeur de recherche

M. LEWIS Laurent J., Ph.D., membre et codirecteur de recherche

M. ROORDA Sjoerd, Ph.D., membre

M. SOKOLOWSKI-TINTEN Klaus, Ph.D., membre

À ma charmante femme, Agnieszka, qui a fait de moi une meilleure personne...

À mes enfants aussi, Philippe et Dominika, qui égaient ma vie de leurs rires et de leurs pleurs...

REMERCIEMENTS

L'aboutissement de ce travail n'eût été possible sans l'indéfectible soutien et la sollicitude que m'ont témoignés de nombreuses personnes au cours des dernières années.

À cet égard, je tiens tout d'abord à exprimer ma très profonde gratitude à mes directeurs de recherche, les professeurs Laurent J. Lewis (département de physique de l'Université de Montréal) et Michel Meunier (département de génie physique de l'École Polytechnique de Montréal): tous deux, par leur rigueur, leur exceptionnelle patience et leur attention dévouée, ont su me mener à bon port malgré les affres et les écueils qui ont ponctué ce long parcours.

Je souhaite aussi adresser de très chaleureux remerciements à mon sagace collègue et ami Danny Perez pour les nombreuses et éclairantes discussions que nous avons eues et sans le génie duquel je n'eusse pu espérer un jour compléter cette thèse.

Je ne saurais également oublier ma femme, Agnieszka, pour qui — et à juste titre — ces derniers mois ont été éprouvants et qui, malgré tout, n'a cessé de m'offrir son soutien.

À vous aussi, Dominika et, surtout, Philippe, qui lirez peut-être ces lignes un jour et qui, je l'espère, aurez pardonné à votre père ses nombreuses sautes d'humeur.

À ma belle-mère Anna pour toutes ces heures à garder mes enfants et à me préparer de succulents *pierogi*, de même qu'à mon beau-frère Adam pour ces agréables moments — et amères défaites — vécus aux commandes de sa console de jeux *PlayStation*.

À ma mère, mon éternelle petite soeur Julie et, surtout, mon père qui n'ont cessé de m'encourager tout au long de mes études.

Je souhaite aussi remercier les diverses personnes à la DGTIC de l'Université de Montréal — notamment Bernard Lorazo, Richard Lefebvre et Patrick McNeil — pour leur précieuse et indispensable collaboration.

Je tiens également à exprimer ma reconnaissance à tous les membres du jury — et tout particulièrement les professeurs Sébastien Francoeur, Sjoerd Roorda et Klaus Sokolowski-Tinten — d'avoir accepté de participer au processus de soutenance de cette thèse de doctorat.

Enfin, à vous tous, Alexis, Anna, Cristiano, et Ralf, auprès de qui j'ai passé d'agréables années.

RÉSUMÉ

En dépit de son omniprésence dans de nombreux secteurs technologiques, les mécanismes à l'origine des modifications structurales — fusion, ablation et solidification — induites dans la matière par le rayonnement laser sont encore mal compris. Un modèle unique combinant les techniques Monte Carlo et de dynamique moléculaire est proposé afin de simuler l'irradiation laser d'une cible de silicium avec des impulsions dont la durée varie de 500 fs à 100 ps; à l'aide d'un calcul simultané des densité, température et pression associées à diverses sections de la cible, l'évolution thermodynamique du système sur une échelle de temps de l'ordre de la nanoseconde est obtenue.

Les simulations mettent en exergue des modifications structurales *thermiques* qui, de manière générale, impliquent des états métastables ou instables résultant d'un rapide chauffage ou refroidissement du matériau irradié.

À cet effet, les résultats font état de deux contributions importantes: (i) en régime femtoseconde au voisinage du seuil d'ablation, le système, initialement à hautes température et pression suivant la fusion du cristal covalent *instable* et le chauffage isochore du liquide métallique qui en découle, est refroidi suite à une rapide expansion adiabatique vers la région de coexistence liquide-vapeur où la germination homogène de bulles de gaz qui s'ensuit n'est *pas* le résultat de fluctuations thermiques dans le liquide surchauffé mais, plutôt, la conséquence d'une conversion directe de l'énergie de translation en énergie de surface; autrement dit, l'*explosion de phase* du liquide métastable est un phénomène dont la nature est, en partie, *mécanique.* (ii) En régime picoseconde, le liquide en expansion *sous-critique* et relativement lente est refroidi le long de la binodale par diffusion de la chaleur: le système n'a *pas* accès à la région de coexistence liquide-vapeur et *aucune explosion de phase n'est observée.* Ceci implique un temps — plus court — d'équilibration du liquide métallique avec sa vapeur $\tau_{\mathrm{LV}} \sim 10^{-11} - 10^{-10}$ s et un processus d'explosion

de phase qui est donc propre aux impulsions *femtoseconde* — et *non* aux impulsions nanoseconde.

Dans ce contexte, l'ablation en régime picoseconde (ainsi que sous irradiation femtoseconde relativement loin du seuil) implique la *fragmentation* d'un fluide homogène en expansion *supercritique*.

Finalement, les simulations confirment la possibilité d'une germination *homogène* de liquide dans le cristal surchauffé à l'échelle de la picoseconde. La solidification du liquide non ablaté et *surfondu* vers un cristal ou un verre est, quant à elle, observée en un temps de l'ordre de 10^{-9} s, et ce, indépendamment de la durée de l'impulsion.

ABSTRACT

In spite of its ubiquitous nature in many areas of technology, the mechanisms by which structural modifications — melting, ablation, and solidification — are induced in a solid by laser radiation have yet to be understood.

A unique model combining the Monte Carlo and molecular-dynamics techniques is proposed to simulate the irradiation of a silicon target by 500 fs to 100 ps laser pulses; by simultaneously tracking the density, temperature and pressure of various sections of the target, the complete thermodynamic evolution of the irradiated material is obtained on a nanosecond time scale.

Simulations reveal *thermal* structural modifications driven by metastable or unstable states of rapidly heated or promptly cooled matter.

In particular, the results reveal two important findings: (i) Under femtosecond laser irradiation near the ablation threshold, the system, initially at high temperature and pressure following melting of the *unstable* covalent crystal and subsequent isochoric heating of the resulting metallic liquid, is adiabatically cooled to the liquid-vapor regime where homogeneous nucleation of gas bubbles in the superheated liquid is *not* the result of large, local, thermal fluctuations but, rather, follows from a direct conversion of translational energy into surface energy; in other words, the *phase explosion* of the metastable liquid is, to a significant extent, *mechanical* in nature. (ii) Under picosecond laser irradiation, the liquid under *subcritical* and relatively slow expansion is efficiently cooled along the binodal by thermal conduction: the system does *not* access the liquid-vapor regime and *phase explosion is not observed.* This points to a — shorter — liquid-vapor equilibration time $\tau_{LV} \sim 10^{-11} - 10^{-10}$ s and, consequently, a phase-explosion process that is typical of femtosecond — *not* nanosecond — irradiation.

In this context, ablation under picosecond pulses (as well as under far-from-threshold femtosecond laser irradiation) is driven by the *fragmentation* of an initially homo-

geneous fluid under *supercritical* expansion.

Finally, simulations confirm the possibility of a melting process occurring on a picosecond time scale by *homogeneous* nucleation of liquid inclusions in a superheated solid. Solidification of the nonablated, *supercooled* liquid to a crystal or a glass is observed in a time on the order of a nanosecond, irrespective of the pulse duration.

TABLE DES MATIÈRES

LISTE DES FIGURES

LISTE DES NOTATIONS ET DES SYMBOLES

CCD :	Charge-Coupled Device
CO_2 :	Carbon dioxide
IR :	Infrarouge
LASER :	Light Amplification by Stimulated Emission of Radiation
MET :	Microscopie Électronique en Transmission
Nd:YAG :	Neodymium-doped Yttrium Aluminium Garnet
PAM :	Plasma Annealing Model
SSRW :	Self-Similar Rarefaction Wave
SW :	Stillinger-Weber
TAM :	Thermal Annealing Model
UV :	Ultraviolet

LISTE DES TABLEAUX

INTRODUCTION

Depuis son invention il y a près de 50 ans, le laser occupe une place importante dans de nombreux secteurs technologiques où il est couramment employé pour effectuer des tâches aussi diverses que micro-usiner (Borowiec *et al.*, 2003) et nettoyer (Zapka *et al.*, 1991) des surfaces, faire croître des couches minces de compositions complexes (Chrisey and Hubler, 1994) ou, plus récemment, produire des nanoparticules de divers matériaux dans le vide (Amoruso *et al.*, 2004) et en milieu liquide (Sylvestre *et al.*, 2004); plus près de nous, il est, par exemple, à la base des lecteurs optiques que nous côtoyons au quotidien.

À un niveau plus fondamental, l'interaction du rayonnement laser avec la matière donne habituellement lieu à une complexe succession de phénomènes à de multiples échelles de temps (femtoseconde à microseconde) et d'espace (électronique à macroscopique). À cet égard, la figure 1 illustre un montage expérimental type dédié à l'étude des phénomènes engendrés par l'absorption d'une impulsion laser dans un matériau. Une impulsion excitatrice est d'abord focalisée à la surface d'une cible à l'aide d'une lentille sur une largeur de quelques micromètres. Afin de sonder l'évolution de l'échantillon irradié, une seconde impulsion, de beaucoup plus faible intensité et retardée par rapport à la première, est quant à elle focalisée en surface par l'intermédiaire d'un microscope dont elle remplace la source de lumière. La partie du faisceau sonde qui est réfléchie (ou transmise) par l'échantillon est ensuite redirigée vers une caméra CCD, ce qui permet d'obtenir une "image" de la cible à tout instant suivant son excitation. Cette technique de microscopie résolue en temps (*time-resolved microscopy*), introduite par Downer *et al.* (1985) il y a vingt ans, offre une résolution temporelle et une résolution spatiale déterminées, respectivement, par la durée de l'impulsion sonde et le microscope; tel que décrit au chapitre 2, elle permet, entre autres choses, de déduire les échelles de temps as-

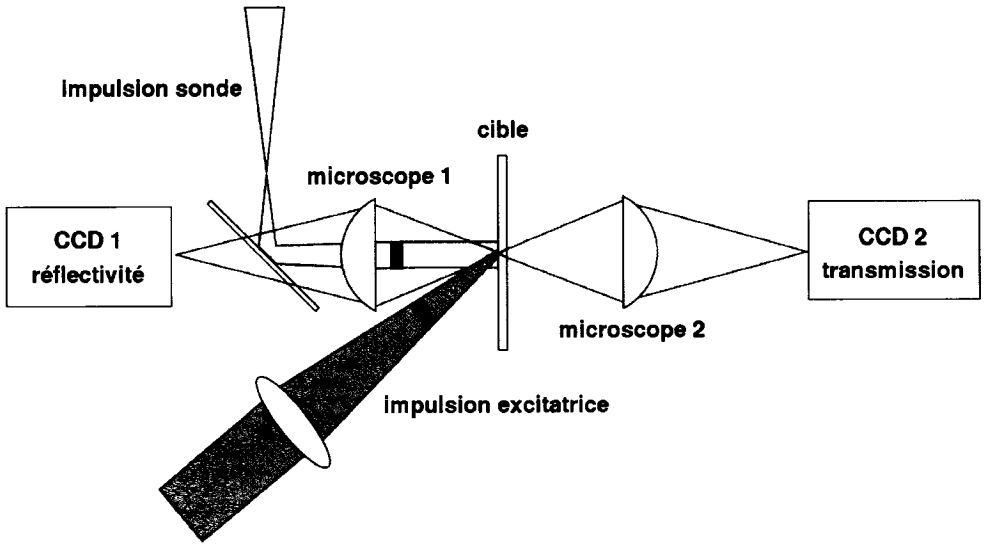

Figure 1 Schéma d'un montage expérimental employant la technique de microscopie résolue en temps. [Adapté de Sokolowski-Tinten *et al.* (1998a)]

sociées aux diverses modifications structurales induites dans un matériau par une brève impulsion laser.

La nature exacte de ces modifications est fonction de nombreux paramètres parmi lesquels la durée (typiquement de quelques femtosecondes à quelques nanosecondes), la longueur d'onde [généralement entre 193 nm (UV) et 1064 nm (IR)] et l'énergie par unité de surface (fluence) de l'impulsion, de même que la nature du matériau irradié qui, dans le contexte qui nous occupe, peut être un solide absorbant (métal ou semi-conducteur) ou un isolant (diélectrique). Cela suggère un large éventail de phénomènes qui, malgré l'apparente complexité du problème, peuvent être classés en deux groupes selon que ces phénomènes sont *thermiques ou non*: si les premiers sont observés dans les solides absorbants, les seconds, bien que pouvant survenir dans les semi-conducteurs à des irradiances (énergie par unité de surface et de temps) élevées, sont habituellement propres aux diélectriques carac-

térisés par une large bande interdite et, conséquemment, des processus d'absorption de l'énergie lumineuse qui sont non linéaires.

Afin de mieux saisir l'origine et l'importance de cette distinction, il convient de présenter un bref rappel historique des événements et observations qui ont conduit certains à s'interroger sur les processus et phénomènes qui découlent de l'interaction de brèves impulsions laser avec la matière.

0.1 Un peu d'histoire...

C'est en 1960 que Theodore Maiman parvient à concrétiser d'importants travaux théoriques aux fondements édifiés 40 ans plus tôt par Albert Einstein: produire un faisceau de lumière monochromatique et cohérent par l'émission stimulée de photons (Maiman, 1960). Cette nouvelle forme de radiation, baptisée LASER (*Light Amplification by Stimulated Emission of Radiation*) par le physicien américain Gordon Gould en 1959, permet de concentrer d'importantes quantités d'énergie au point de focalisation et est, de ce fait, rapidement mise à profit pour façonner la matière. Ainsi, dès 1963, des lasers CO_2, ruby, et Nd:YAG de relativement faible puissance sont utilisés pour fondre, vaporiser et faire "exploser" des échantillons de divers matériaux, principalement des métaux (Wood *et al.*, 1984).

Il faut cependant attendre les années 1974-1976, et la découverte par des chercheurs soviétiques que de brèves impulsions laser permettent d'annihiler les défauts produits par l'implantation de dopants dans les semi-conducteurs (Shtyrkov *et al.*, 1976; Khaibullin *et al.*, 1977), afin qu'un intérêt marqué pour les procédés laser et, de façon plus générale pour l'interaction du rayonnement laser avec la matière, se manifeste.

À cette époque, l'activation électrique des dopants, de même que l'annihilation

des défauts résultant de leur implantation dans un matériau semi-conducteur, sont habituellement réalisées en plaçant l'échantillon dopé dans un four à haute température (environ 1000°C). Cependant, cette technique a pour principal désavantage de chauffer l'ensemble de l'échantillon et, par conséquent, d'endommager les régions situées au-delà de la zone d'implantation (Wood *et al.*, 1984).

Il est observé que ces effets indésirables peuvent être éludés en chauffant l'échantillon avec une impulsion laser dont la durée, la longueur d'onde et la fluence ont été, au préalable, soigneusement choisies: l'absorption de l'énergie lumineuse se faisant, pour l'essentiel, sur une profondeur variant typiquement de quelques centaines à quelques milliers d'angströms, il devient ainsi possible de cibler avec précision la zone d'implantation. Cette technique de recuit par laser, aujourd'hui connue sous le nom de *laser annealing*, offre deux autres avantages.

À cet effet, la figure 2 illustre la structure de divers échantillons de silicium dopés par implantation ionique et ayant subi, selon le cas, un recuit thermique (c'est-à-dire au four) ou laser: si les images obtenues par microscopie électronique en transmission (MET) indiquent, dans le premier cas, la présence de boucles de dislocation, elles démontrent en revanche que, dans le second cas, aucun défaut (à une échelle de l'ordre de 10 Å) n'est présent dans le matériau traité au laser.

Les propriétés électriques résultant d'un recuit laser sont également plus avantageuses. Ainsi qu'en témoigne la figure 3 pour du silicium dopé au bore, la concentration électronique par carré (*sheet carrier concentration*) suivant un recuit thermique plafonne au-delà d'une dose d'implantation d'environ 1.5×10^{16} cm^{-2}; la concentration de dopants correspondante est de 6×10^{20} cm^{-3}, soit la limite de solubilité du bore dans le silicium. En revanche, cela n'est pas observé avec un recuit laser au cours duquel les dopants sont incorporés (de façon substitutionnelle) dans le silicium à des concentrations bien au-delà de la limite de solubilité, sug-

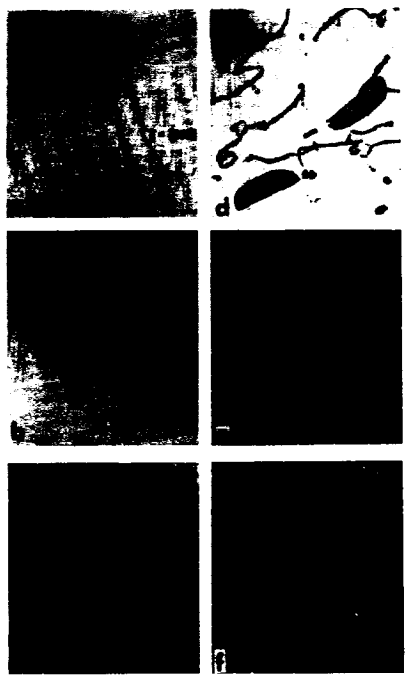

Figure 2 Images obtenues par MET de divers échantillons de silicium [orientés (001)] d'abord dopés par implantation ionique, puis soumis à un recuit laser [(a) à (c)] ou thermique [(d) à (f)]. La nature et l'énergie des ions implantés, de même que les doses utilisées, sont: (a) et (d) ^{11}B, 35 keV et 3×10^{15} cm^{-2}; (b) et (e) ^{31}P, 80 keV et 1×10^{15} cm^{-2}; (c) et (f) ^{75}As, 100 keV et 1×10^{16} cm^{-2}. Les échantillons dopés au bore et au phosphore [(d) et (e)] ont été chauffés au four pendant 30 minutes à 1100°C; l'échantillon dopé à l'arsenic (f) a, quant à lui, subi un recuit thermique à 900°C pendant 30 minutes. [Source: Wood (1984)]

gérant par le fait même un processus se produisant relativement loin de l'équilibre thermodynamique (Khaibullin *et al.*, 1978).

Si ces découvertes suscitent un engouement nouveau pour les procédés laser, elles éveillent aussi un vif intérêt et soulèvent de nombreuses questions en rapport avec l'interaction de brèves impulsions laser avec la matière. Ainsi, très tôt, plusieurs travaux mettent en évidence l'apparition d'une phase caractérisée par une grande réflectivité à la surface de matériaux semi-conducteurs irradiés par une impulsion

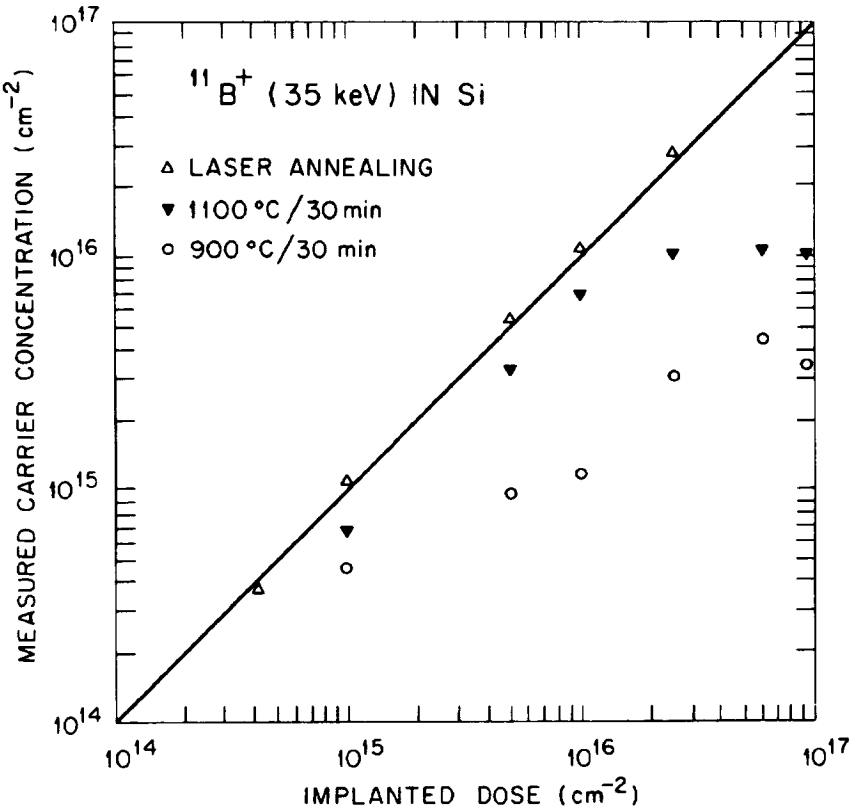

Figure 3 Concentration électronique par carré en fonction de la dose d'implantation dans des échantillons de silicium d'abord dopés au bore, puis soumis à un recuit thermique ou laser. [Source: Wood (1984)]

de fluence suffisamment élevée (Sooy *et al.*, 1964; Blinov *et al.*, 1967; Auston *et al.*, 1978; Lowndes and Wood, 1981). À peu près à la même époque, et tel que l'illustre la figure 4, des mesures par spectrométrie de rétrodiffusion Rutherford mettent aussi en lumière un élargissement important de la distribution des dopants après irradiation avec un faisceau laser (Kachurin *et al.*, 1976; Young *et al.*, 1978; Celler *et al.*, 1978; White *et al.*, 1978).

Pour les uns (Young *et al.*, 1978; Auston *et al.*, 1978; White *et al.*, 1978; Liu and Wang, 1979a), plus nombreux, ces observations peuvent être expliquées par

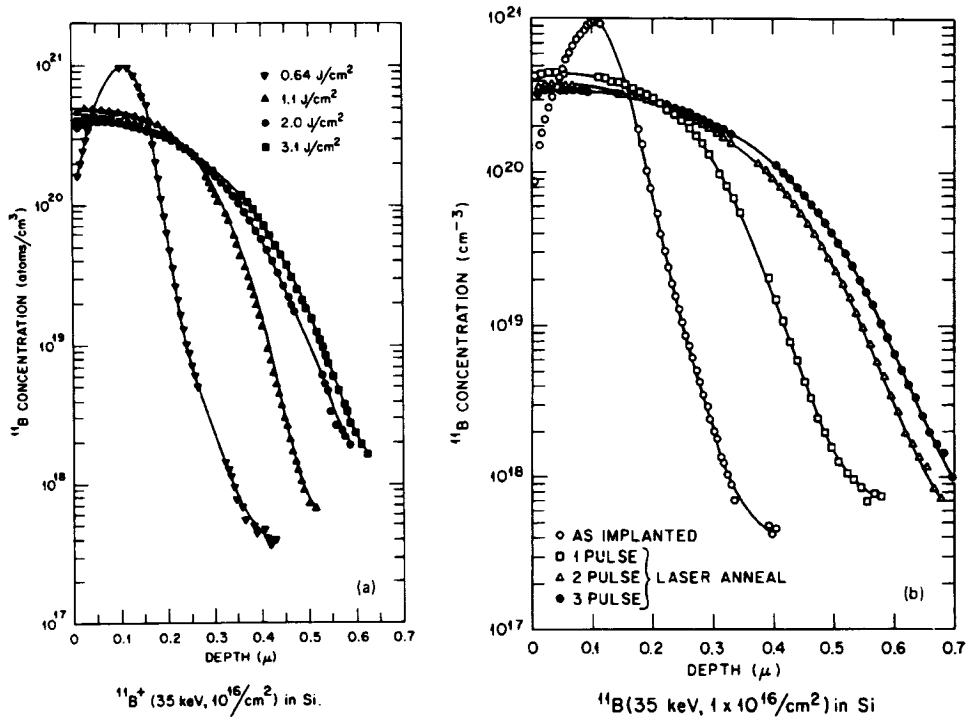

Figure 4 Distribution des dopants (bore) dans un échantillon de silicium avant et après recuit laser: (a) élargissement de la distribution en fonction de la fluence; (b) effet du nombre d'impulsions sur la distribution pour une fluence de 1.1 J cm^{-2}. [Source: Wood (1984)]

le modèle *thermique* ou TAM (*Thermal Annealing Model*): l'énergie fournie par l'impulsion laser (d'une durée de l'ordre de la nanoseconde) est d'abord absorbée par l'intermédiaire d'excitations électroniques, puis rapidement transférée au réseau atomique. Il s'ensuit la fusion du cristal semi-conducteur et l'apparition d'une couche liquide *métallique* dont la réflectivité est plus élevée et qui s'étend au-delà de la zone d'implantation. Au cours de la cristallisation qui suit par la solidification épitaxiale du liquide en contact avec le substrat parfaitement cristallin, les divers défauts sont éliminés et les dopants incorporés de façon substitutionnelle dans le matériau nouvellement solidifié; dans ce contexte, l'élargissement de la distribution

des dopants résulte de leur rapide diffusion en phase *liquide.*

Pour les autres (Van Vechten *et al.*, 1979; Lo and Compaan, 1980), tenants du modèle *non thermique* ou PAM (*Plasma Annealing Model*), le laser crée de nombreuses paires électron-trou (dont la concentration est de l'ordre de 10^{21} à 10^{22} cm^{-3}) qui n'interagissent que peu ou pas avec les modes de vibration atomiques sur une échelle de temps d'environ 10^{-8} à 10^{-7} s. Il en résulte un réseau cristallin relativement "froid" et plus "souple" (suite à la rupture de liens covalents par l'excitation d'électrons à la bande de conduction) qui favorise l'annihilation des défauts et une diffusion plus efficace des dopants; de plus, la forte hausse de la réflectivité est attribuable non pas à la formation d'une couche liquide mais, plutôt, à la présence du gaz électronique en surface.

Dans ce contexte, deux échelles de temps sont importantes: (i) le temps caractéristique, τ_E, pour que les électrons et trous, par l'émission de phonons, parviennent à l'équilibre avec les ions. À cet égard, un phénomène (tel que la fusion) est dit *thermique* s'il se produit alors qu'il y a (à tout le moins localement) équilibre électron-ion; en revanche, il est dit *non thermique* s'il est observé avant qu'un transfert substantiel d'énergie du gaz d'électrons vers le gaz de phonons ait eu lieu (et donc avant qu'un chauffage significatif du matériau se soit produit). (ii) La durée de vie des porteurs: si la hausse de réflectivité est due à la présence de paires électron-trou, celles-ci doivent pouvoir survivre à tout processus de recombinaison sur une échelle de temps supérieure à la durée de l'impulsion.

En une période marquée par beaucoup de fébrilité et une certaine confusion, divers travaux viennent apporter un éclairage déterminant au débat: ainsi, des mesures par diffusion Raman (von der Linde and Wartmann, 1982), spectrométrie de masse à de temps de vol (Stritzker *et al.*, 1981), diffraction de rayons X (Larson *et al.*, 1982) et réflectivité (Lompré *et al.*, 1983) démontrent que le matériau irradié

peut être chauffé à des températures avoisinant ou dépassant le point de fusion; l'observation d'une émission d'ions suivant l'absorption d'une impulsion picoseconde vient également étayer l'idée d'une fonte du matériau près de la surface (Liu *et al.*, 1981). De plus, les travaux de Svantesson *et al.* (1971) réalisés quelques années plus tôt suggèrent fortement que la recombinaison de paires électron-trou dans le silicium est médiée par un processus non radiatif sur une échelle de temps nettement inférieure à la nanoseconde.

Enfin, plusieurs travaux reposant sur une résolution numérique de l'équation de diffusion de la chaleur [et qui tiennent compte des possibles transitions de phase (fusion et évaporation) ainsi que de la dépendance en température des propriétés thermiques et optiques du matériau irradié] confirment la nature *thermique* des transformations induites dans un semi-conducteur ou un métal par une impulsion picoseconde ou nanoseconde (Wang *et al.*, 1978; Baeri *et al.*, 1979; Surko *et al.*, 1979; Wood and Giles, 1981); entre autres choses, ces études prédisent des distributions de dopants suivant un recuit laser qui sont en très bon accord avec les observations expérimentales.

0.2 Et aujourd'hui?

Il est désormais généralement admis qu'un équilibre électron-trou est atteint en un temps $\tau_E \sim 10^{-12} - 10^{-11}$ s (Liu *et al.*, 1981; Liu *et al.*, 1982; Bloembergen, 1985); de même, la recombinaison de paires électron-trou est un phénomène se produisant habituellement sur une échelle de temps de l'ordre de la picoseconde (Yoffa, 1980). À cet égard, une impulsion de durée τ_L supérieure à τ_E agit comme une source très rapide de *chaleur* donnant lieu à des transformations purement *thermiques* dans le matériau irradié.

Cependant, diverses recherches menées au cours des années 1980 et 1990 démontrent que des transitions *non* thermiques sont également possibles si $\tau_L < \tau_E$: comme l'avait imaginé Van Vechten (1979) — à tort — pour une impulsion nanoseconde, l'irradiation de la surface d'un semi-conducteur (tel que le silicium) par une impulsion *femtoseconde* permet, au-delà d'une fluence seuil, de rompre un nombre suffisant de liens covalents pour provoquer un affaiblissement et, éventuellement, un effondrement du réseau cristallin vers une structure désordonnée et métallique (Shank *et al.*, 1983a; Sokolowski-Tinten *et al.*, 1995); autrement dit, il y a fusion très rapide ($\lesssim 1$ ps) du cristal avant qu'un transfert substantiel d'énergie du gaz électronique vers le réseau atomique ait eu lieu.

Si, de manière générale, il existe aujourd'hui un consensus au sujet de la nature des processus *électroniques* (et échelles de temps associées) qui résultent de l'irradiation de matériaux par une brève impulsion laser, il en va autrement des phénomènes qui ont subséquemment cours aux échelles atomique, mésoscopique et macroscopique.

En effet, l'interaction d'un rayonnement laser avec la matière donne lieu à diverses transformations structurales qu'il convient de séparer en deux groupes (Sokolowski-Tinten *et al.*, 1998b; von der Linde and Sokolowski-Tinten, 2000): le premier, qui concerne une modification de l'*ordre à longue portée*, regroupe les mécanismes de fusion et de solidification; le second, qui a trait à une modification de l'*état d'aggrégation* du matériau, implique l'ablation (c'est-à-dire l'éjection) d'importantes quantités de matière de la surface sous la forme, selon le cas, d'atomes isolés, d'agrégats et/ou de gouttelettes au-delà d'une fluence seuil bien définie.

De tous les possibles phénomènes, l'ablation est certainement celui dont les mécanismes et les origines ont suscité le plus de débats au cours des dernières années. Dans les diélectriques, où l'excitation d'électrons de valence à la bande de conduction (par l'absorption simultanée de plusieurs photons) requiert une irradiance élevée et, con-

séquemment, des impulsions *femtoseconde*, l'éjection de matière est, pour certains, le résultat d'un claquage optique et d'une ionisation complète du matériau qui subit une transition directe d'un solide vers un plasma (von der Linde and Schüler, 1996; Sokolowski-Tinten *et al.*, 1998a); pour d'autres, l'émission d'électrons par effet photoélectrique conduit à une rupture de la neutralité en surface et, éventuellement, à une forte répulsion électrostatique entre les ions positifs qui sont subséquemment éjectés par un processus dit d'explosion de Coulomb (Stoian *et al.*, 2002).

Dans les métaux, de même que dans les semi-conducteurs à des irradiances inférieures au seuil de formation de plasma, l'absorption de l'énergie laser se produit par l'intermédiaire de transitions optiques linéaires et les modifications structurales qui s'ensuivent sont essentiellement thermiques (Sokolowski-Tinten *et al.*, 1998a). Dans un tel contexte, il est proposé dès les années 1970 que l'éjection de matière suivant une irradiation par une impulsion de très longue durée ($\sim 10^{-7} - 10^{-5}$ s) est le résultat d'une germination *homogène* de bulles de gaz dans un liquide métastable (et surchauffé) *alors que celui-ci est rapidement chauffé* (Martynyuk, 1976): ce scénario baptisé "explosion de phase" (ou *phase explosion*) est, bien que jamais démontré à ce jour, fréquemment invoqué afin de décrire l'ablation de solides absorbants par des impulsions femtoseconde (Cheng and Xu, 2005), picoseconde (Zhigilei and Garrison, 2000; Willis and Xu, 2002a) et nanoseconde (Miotello and Kelly, 1995; Song and Xu, 1998; Yoo *et al.*, 2000; Bulgakova and Bulgakov, 2001).

Cependant, cette interprétation n'est pas valable en régime femtoseconde où le matériau, qui est chauffé à volume constant, est converti en un liquide surchauffé au cours du *refroidissement* qui suit par expansion adiabatique dans le vide (Sokolowski-Tinten *et al.*, 1998b; Lorazo *et al.*, 2003).

Les mécanismes par lesquels le solide irradié fond sont également le sujet de nombreuses hypothèses: si les premières études ont suggéré une fusion *hétérogène* du

cristal métastable par la propagation (de la surface vers le volume) d'une interface solide-liquide dont la vitesse est fonction du degré de surchauffe (Bucksbaum and Bokor, 1984; Fabricius *et al.*, 1986), de récents travaux théoriques évoquent aussi la possibilité d'une fusion par germination *homogène* d'embryons liquides dans une matrice solide (Rethfeld *et al.*, 2002). De même, la solidification peut être décrite par des processus de cristallisation hétérogène et/ou homogène dans un liquide surfondu (Stiffler *et al.*, 1988); l'obtention d'une structure *amorphe* est aussi parfois évoquée (Thompson *et al.*, 1983).

De manière générale, les travaux effectués à ce jour pour des solides absorbants mettent en exergue des modifications thermiques impliquant des états métastables (surchauffés ou surfondus) dans la matière soumise à de brèves impulsions laser.

Cette thèse est consacrée à l'étude des mécanismes *thermiques* menant à la fusion, l'ablation et la solidification dans les semi-conducteurs et métaux irradiés par des impulsions femtoseconde, picoseconde et nanoseconde. À cet effet, une approche numérique unique associant la méthode Monte Carlo à celle de la dynamique moléculaire est employée afin de décrire, respectivement, les dynamiques électronique et atomique découlant de l'irradiation d'une cible de silicium par une impulsion laser femtoseconde ou picoseconde. En suivant simultanément l'évolution du matériau irradié dans l'espace thermodynamique constitué de la densité, de la température et de la pression (ρ-T-P), il est démontré que les états métastables engendrés par l'absorption de l'impulsion laser peuvent être mis en évidence et les mécanismes à l'origine des diverses modifications structurales identifiés; tel que détaillé aux chapitres 4 à 6, il en résulte une vision nouvelle et unifiée des possibles trajectoires thermodynamiques suivies dans les solides absorbants soumis à un rayonnement laser.

Ce travail est présenté comme suit: les notions théoriques nécessaires à la com-

préhension de l'interaction laser-matière sont tout d'abord résumées au chapitre suivant. Le chapitre 2 présente ensuite une *brève* revue de la littérature afin d'illustrer les principaux enjeux et questions liés à l'absorption d'impulsions laser dans les semi-conducteurs et métaux. Les objectifs visés par cette étude sont subséquemment énoncés au chapitre 3. Les chapitres 4 et 5 (qui ont fait l'objet de publications dans des périodiques scientifiques) constituent le coeur même de ce travail: alors que le premier est exclusivement consacré à une comparaison des mécanismes d'ablation sous irradiation femtoseconde et picoseconde, le second offre une synthèse détaillée des modifications structurales se produisant dans les solides absorbants irradiés par des impulsions dont la durée varie de la femtoseconde à la nanoseconde. Ceci est suivi d'une brève discussion générale ainsi que d'une conclusion mettant en exergue les principaux apports de ce travail à la compréhension du problème.[1]

[1]Une justification du choix de la valeur de certains paramètres composant le modèle décrit aux chapitres 4 et 5 est également fournie en annexe.

CHAPITRE 1

THÉORIE

Ce premier chapitre a pour objectif de fournir les connaissances nécessaires à la compréhension de la physique de l'interaction de brèves impulsions laser avec les matériaux, plus particulièrement avec les semi-conducteurs et les métaux.

Une description des processus d'excitation et de relaxation électroniques dans les solides soumis à un rayonnement laser est tout d'abord présentée. Les diverses modifications structurales (thermiques ou non) qui s'ensuivent aux échelles atomique, mésoscopique et macroscopique sont ensuite discutées.

Le présent travail portant sur une étude des transformations *thermiques* reposant, pour l'essentiel, sur une analyse des propriétés thermodynamiques du matériau irradié (cf. chapitres 4 et 5), un énoncé des principales caractéristiques des diagrammes des phases des semi-conducteurs et métaux est également donné. Une présentation du modèle SSRW, qui illustre l'évolution *thermique* de ces derniers lorsque chauffés par une impulsion femtoseconde, clôt ce chapitre.

1.1 L'interaction laser-matière

L'absorption d'une impulsion laser d'irradiance suffisamment élevée donne lieu, dans le matériau irradié, à une complexe succession de phénomènes à de nombreuses échelles de temps et d'espace.

Ceci est illustré à la figure 1.1 pour un semi-conducteur à bande interdite directe

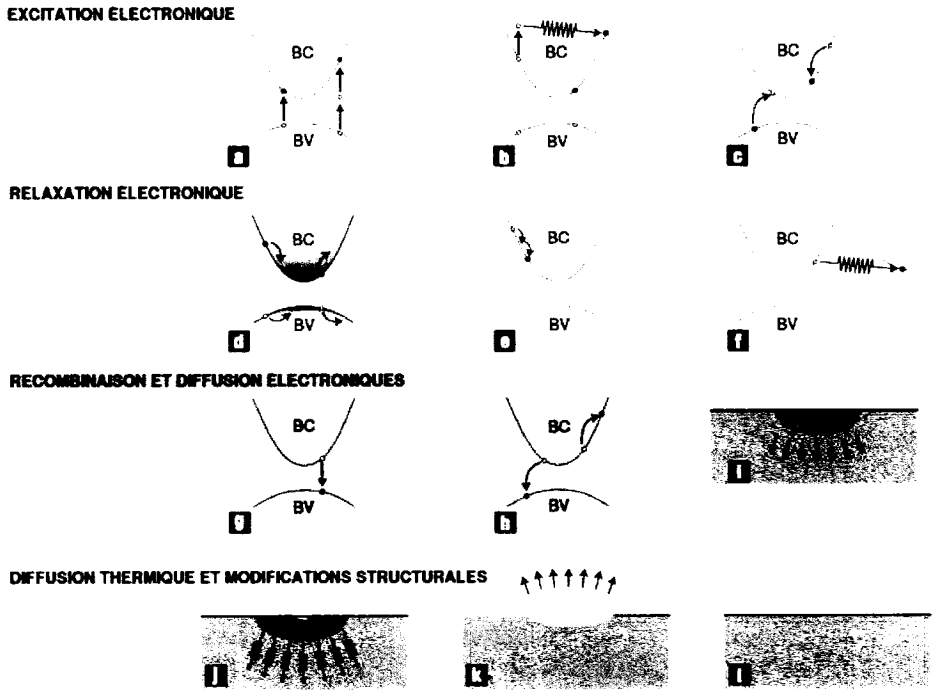

Figure 1.1 Illustration schématique des divers processus d'excitation et de relaxation électroniques, ainsi que des possibles modifications structurales, dans un semiconducteur dont la largeur de la bande interdite (directe dans ce cas) est inférieure à l'énergie des photons incidents: (a) absorption interbande à un ou deux photons; (b) absorption intrabande par un électron dans la bande de conduction; (c) création d'une paire électron-trou suite à une ionisation par impact; (d) collisions électron-électron, trou-trou et électron-trou; collisions électron-phonon (e) "intravallée" et (f) "intervallée"; (g) recombinaison radiative; (h) recombinaison Auger; (i) diffusion électronique; (j) diffusion thermique et fusion; (k) ablation; (l) solidification. BC et BV identifient respectivement les bandes de conduction et de valence. [Adapté de Sundaram et Mazur (2002)]

tel que le GaAs. Il est à noter que la description phénoménologique qui suit est, en régime *thermique*, essentiellement indépendante de la durée de l'impulsion; cependant, les échelles de temps associées aux divers processus (et tout particulièrement les modifications structurales) peuvent varier.

1.1.1 Absorption du laser et dynamique à l'échelle électronique

L'absorption de photons d'énergie supérieure à la largeur de la bande interdite donne d'abord lieu à des transitions *interbandes*, et donc à la création de paires électron-trou, dans le matériau cristallin initialement non excité et non dopé [à gauche sur la figure 1.1(a)]; de telles transitions sont également possibles dans les semi-conducteurs à bande interdite indirecte tel que le silicium, mais requièrent l'absorption ou l'émission d'un phonon afin d'assurer la conservation de la quantité de mouvement. À des irradiances élevées, une transition interbande peut aussi se produire par l'absorption simultanée — et donc non linéaire — de plusieurs photons [à droite sur la figure 1.1(a)]; dans les diélectriques, ce processus constitue d'ailleurs le principal mécanisme par lequel l'énergie lumineuse associée à une impulsion femtoseconde est absorbée dans le matériau caractérisé par une large bande interdite.

Lorsque la concentration d'électrons promus à la bande de conduction N atteint et éventuellement dépasse la valeur critique (Sokolowski-Tinten *et al.*, 1998c)

$$N_{\mathrm{cr}} = m^*_{\mathrm{opt}} \epsilon_0 \epsilon \left(\frac{2\pi c}{e\lambda_L} \right)^2 , \tag{1.1}$$

où m^*_{opt} est la masse effective optique, ϵ la permittivité diélectrique, c la vitesse de la lumière, e la charge électronique et λ_L la longueur d'onde de l'impulsion laser, le gaz électronique devient hautement réfléchissant et absorbant; dans un tel contexte,

des transitions *intrabandes*, par lesquelles toute l'énergie du photon est transmise à l'électron de conduction, se produisent dans une proportion qui est fonction de N [figure 1.1(b)]. Ce processus, que l'on nomme également *bremsstrahlung inverse*, constitue le principal mécanisme d'absorption dans les métaux de même que dans la phase *liquide métallique* des semi-conducteurs covalents appartenant aux groupes IV et III-V (Godlevsky *et al.*, 1998).

Une transition intrabande produit un porteur très énergétique qui, s'il n'est pas extrait de la surface par effet photoélectrique ou thermoélectronique, peut aussi créer une nouvelle paire électron-trou suite à une ionisation par impact avec un électron de valence [figure 1.1(c)].

L'absorption des quanta de lumière devant respecter certains principes de conservation, l'excitation d'un semi-conducteur par une impulsion laser donne initialement lieu à des populations hors équilibre d'électrons et de trous dont les distributions en fonction de l'énergie et de la quantité de mouvement reflètent les transitions optiques permises. Ceux-ci parviennent ensuite à un équilibre mutuel, d'une part, et avec les ions, d'autre part, par l'intermédiaire de collisions de diverses natures et décrites ci-après.

Le gaz d'électrons et de trous atteint tout d'abord un équilibre *interne* [représenté par une distribution de Fermi-Dirac à une température électronique T_e supérieure à celle du réseau d'ions T ($T_e \gg T$)] à la suite de collisions répétées entre ses particules constituantes [figure 1.1(d)]; à des concentrations électroniques au-delà d'environ 10^{18} cm^{-3}, le temps caractéristique séparant deux collisions est de l'ordre de 10 fs (Wood *et al.*, 1984; Siegal *et al.*, 1995) et un équilibre est ainsi atteint après quelques dizaines à quelques centaines de femtosecondes.

Les porteurs tentent simultanément d'atteindre un équilibre avec les ions par l'émission

de phonons longitudinaux optiques (Siegal *et al.*, 1995): ceux-ci ne transportant que relativement peu d'énergie (typiquement une dizaine de meV), le processus de relaxation implique de nombreuses collisions [figures 1.1(e) et 1.1(f)]. À titre d'exemple, une centaine de collisions seront nécessaires pour qu'un électron possédant une énergie de 1 eV regagne le minimum de la bande de conduction; en supposant un temps caractéristique de collision électron-phonon d'environ 10 fs (Eesley, 1986; Fischetti and Laux, 1988), il en résulte qu'un équilibre électron-phonon est atteint après quelques picosecondes. L'énergie thermique est ensuite éventuellement partagée entre tous les modes de vibration (notamment acoustiques) selon une distribution de Bose-Einstein à une température $T \approx T_e$ (von der Linde *et al.*, 1997).

Une fois les électrons et ions parvenus à un équilibre, une température peut être (à tout le moins localement) définie. Cependant, la concentration électronique est, à ce stade, encore supérieure à la valeur strictement associée à la température locale. Dans ce contexte, le retour vers l'équilibre est assuré par les processus de recombinaison radiatif et Auger: dans le premier cas [figure 1.1(g)], l'énergie issue de la recombinaison d'un électron et d'un trou est convertie sous la forme de lumière (photon); dans le second cas [figure 1.1(h)], l'énergie excédentaire est remise à un électron de conduction avoisinant et la température électronique se retrouve, de ce fait, momentanément majorée. Il est à noter que le processus Auger (dont le temps caractéristique peut avoisiner la picoseconde) constitue généralement le mécanisme de recombinaison dominant, la recombinaison radiative étant habituellement observée sur une échelle de temps supérieure à la nanoseconde (Landsberg, 1991).

La diffusion de porteurs en volume contribue également à réduire la concentration électronique dans la région irradiée [figure 1.1(i)]; cependant, et contrairement aux processus de recombinaison, le nombre total de porteurs est cette fois conservé. Notons que la diffusion peut être accélérée par l'accroissement de la pression de Fermi du gaz d'électrons dont la concentration augmente (Young and van Driel,

1982) ou, au contraire, ralentie suite à des effets de confinement électronique liés à la variation de la largeur de la bande interdite avec la température (Siegal *et al.*, 1995).

1.1.2 La dynamique aux échelles atomique, mésoscopique et macroscopique

Tel que discuté précédemment, les électrons parviennent à un équilibre avec les ions en un temps $\tau_E \sim 10^{-12} - 10^{-11}$ s. Celui-ci est d'importance capitale puisqu'il permet de différencier les impulsions "longues" (picoseconde et nanoseconde) des impulsions "brèves" (femtoseconde): en effet, si $\tau_L \gg \tau_E$, un équilibre électron-ion est atteint très tôt durant l'irradiation du solide semi-conducteur ou métallique et les modifications structurales qui s'ensuivent sont purement thermiques; en revanche, si $\tau_L < \tau_E$, le matériau est fortement excité avant qu'un équilibre thermique ait pu s'établir, ouvrant de ce fait la voie à de *possibles* phénomènes non thermiques dans les semi-conducteurs et diélectriques.

1.1.2.1 Le régime thermique

Si le semi-conducteur n'est pas irradié par une impulsion dont l'irradiance est suffisamment élevée pour engendrer des modifications non thermiques telles que, par exemple, la fusion ultrarapide du cristal covalent (voir plus bas), la diffusion de chaleur de la surface encore solide vers les zones plus froides en volume se produit sur une échelle de temps qui peut être aussi brève que $\sim 10^{-11}$ s [figure 1.1(j)]; le détail est fonction du gradient de température au voisinage de la surface, et donc des propriétés optiques et thermiques du matériau soumis à l'impulsion laser (von der Linde *et al.*, 1997).

Au-delà d'une fluence seuil, l'irradiation laser provoque la *fonte* du matériau [figure 1.1(j)]. Avec une impulsion nanoseconde, la transition de phase se produit près de la température de fusion à l'équilibre suite à la germination *hétérogène* de liquide en surface et la propagation ultérieure d'une interface solide-liquide en un temps de l'ordre de 10^{-9} à 10^{-7} s (Wood *et al.*, 1984). En revanche, diverses études expérimentales avec des impulsions picoseconde indiquent que le *solide cristallin* peut être chauffé quelques centaines de degrés au-dessus de la température de fusion (Bucksbaum and Bokor, 1984; Fabricius *et al.*, 1986); la vitesse de l'interface solide-liquide — qui peut atteindre plusieurs centaines de mètres par seconde (sans toutefois dépasser la vitesse du son) — est alors fonction du degré de surchauffe du cristal *métastable.*

La fusion par germination *homogène* (c'est-à-dire en l'absence de surfaces ou de défauts) d'embryons liquides dans un solide métastable est également possible avec des impulsions femtoseconde (Rethfeld *et al.*, 2002; Ashitkov *et al.*, 2002); le cristal surchauffé fond alors sur une échelle de temps de l'ordre du temps d'équilibration électron-ion, constituant de ce fait un processus plus rapide que la germination hétérogène mais néanmoins plus lent que la possible fusion non thermique dans les semi-conducteurs covalents (voir plus bas).

L'ablation du matériau irradié se traduit par l'éjection de matière solide ou liquide au-delà d'une fluence qui est également bien définie [figure 1.1(k)]: dans le premier cas, la rupture par *spallation* résulte du passage d'une onde de pression tensile dans le solide (Zhigilei and Garrison, 2000; Perez and Lewis, 2003); dans le second cas, l'*explosion de phase* par germination homogène de bulles de gaz dans un liquide métastable et surchauffé (Miotello and Kelly, 1995; Sokolowski-Tinten *et al.*, 1998b; Zhigilei and Garrison, 2000; Bulgakova and Bulgakov, 2001; Perez and Lewis, 2003), la *décomposition spinodale* d'un liquide mécaniquement instable (Vidal *et al.*, 2001), la *fragmentation* d'un fluide supercritique en expansion (Perez and Lewis,

2002; Perez and Lewis, 2003) et la simple vaporisation du matériau peuvent donner lieu à l'éjection d'atomes isolés, d'agrégats et/ou de gouttelettes dont la taille peut atteindre le micromètre (Chrisey and Hubler, 1994).

Enfin, l'excitation du solide par une impulsion laser implique à terme (s'il y a préalablement eu fusion du matériau) une solidification par germination *hétérogène* ou *homogène* d'une phase cristalline dans le liquide non ablaté et surfondu [figure 1.1(l)]; l'obtention d'une phase *amorphe* est également possible si la vitesse du front de solidification est suffisamment élevée (Thompson *et al.*, 1983; Bucksbaum and Bokor, 1984).

1.1.2.2 Le régime non thermique

Bien qu'ils ne soient pas au coeur de la présente étude, il convient de rappeler que de multiples phénomènes *non thermiques* peuvent aussi entraîner des transformations de nature structurale dans un solide irradié par une impulsion femtoseconde.

Ainsi, dans les semi-conducteurs covalents tels que le Ge (Siders *et al.*, 1999), le GaAs (Saeta *et al.*, 1991) et le Si (Sokolowski-Tinten and von der Linde, 2000), la génération d'un gaz électronique dont la concentration dépasse la valeur critique $N_c \approx 10^{22}$ cm^{-3} entraîne l'effondrement du réseau cristallin et la formation d'un liquide métallique en un temps de l'ordre de quelques centaines de femtosecondes.

Au-delà d'une irradiance $I_{\text{break}} \sim 10^{13}$ W cm^{-2} (von der Linde and Schüler, 1996; Sokolowski-Tinten *et al.*, 1998a), une transition directe d'un solide vers un plasma par claquage optique (*optical breakdown*) est observée dans les semi-conducteurs et isolants soumis à une irradiation femtoseconde très intense. L'ablation par répulsion électrostatique en surface (explosion de Coulomb) est également possible dans les diélectriques irradiés par des impulsions ultrabrèves (Stoian *et al.*, 2002).

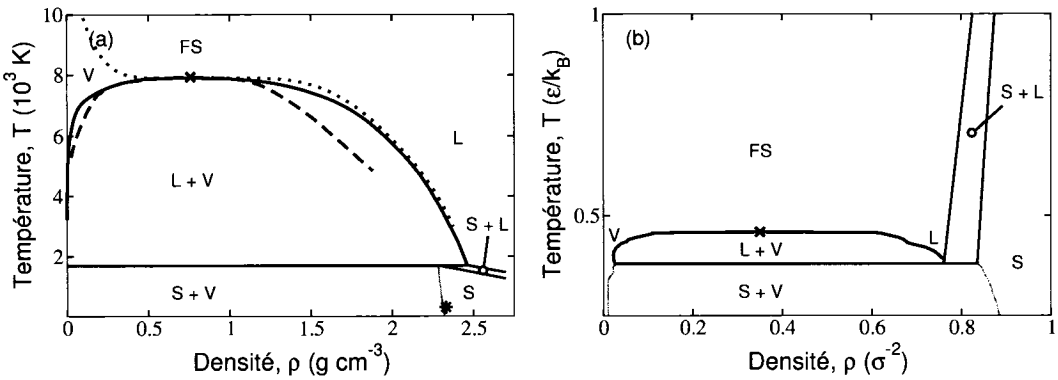

Figure 1.2 Diagramme des phases (projection ρ-T) du (a) silicium (tel qu'obtenu à partir du potentiel de SW) et (b) d'un système de Lennard-Jones bidimensionnel pour lequel la densité et la température sont exprimées en unités réduites [σ et ϵ représentent, respectivement, les échelles de longueur et d'énergie]. Trait continu noir: binodale (coexistence liquide-vapeur); trait bleu: ligne triple (coexistence solide-liquide-vapeur); trait vert: coexistence solide-vapeur; traits rouges: coexistence solide-liquide; trait discontinu: spinodale; pointillé: isobare critique; croix: point critique ($\rho_c = 0.76$ g cm^{-3}, $T_c = 7925$ K et $P_c = 185$ MPa pour le Si). S: solide; L: liquide; V: vapeur; FS: fluide supercritique (pour $T > T_c$ et $P > P_c$).

1.2 Thermodynamique de l'interaction laser-matière

1.2.1 Le diagramme des phases

Tel que mentionné plus tôt et détaillé aux chapitres 4 et 5, l'identification des mécanismes à l'origine des modifications thermiques repose sur une analyse thermodynamique dans le diagramme des phases du matériau irradié.

1.2.1.1 Les semi-conducteurs

À cet effet, la figure 1.2(a) illustre le diagramme des phases du potentiel de Stillinger-Weber (SW) (Stillinger and Weber, 1985) qui décrit l'interaction entre les divers

atomes composant la cible de silicium modélisée dans cette étude.

Les régions d'intérêt sont: (i) la zone *métastable* à droite du point critique — située entre la binodale (le long de laquelle le liquide coexiste à l'équilibre avec sa vapeur saturée) et la spinodale [qui correspond à la limite de stabilité mécanique $(\partial P/\partial \rho)_T = 0$] — où un liquide homogène est dit surchauffé; dans cette région, une énergie libre de la phase gazeuse inférieure à celle du liquide favorise (par l'intermédiaire, en principe, de fluctuations thermiques locales) la germination homogène de bulles de gaz à un taux qui dépend fortement du degré de surchauffe (Sokolowski-Tinten *et al.*, 1998b). (ii) La zone *instable* [identifiée par l'inégalité $(\partial P/\partial \rho)_T > 0$] située sous la spinodale et à l'intérieur de laquelle tout liquide homogène se dissocie presque instantanément en un mélange liquide-gaz par un processus de décomposition spinodale (Koch *et al.*, 1983). (iii) La région supercritique où le système (qui n'est pas nécessairement homogène) n'est ni un liquide ni un gaz, mais un fluide.

Le diagramme des phases du potentiel de SW est représentatif des semi-conducteurs covalents appartenant aux groupes IV et III-V (Moran and Shapiro, 2000); en particulier, il reproduit adéquatement l'existence d'une phase liquide dont la densité est *supérieure* à celle de la phase solide.

1.2.1.2 Les métaux

Le diagramme des phases (pour un système de Lennard-Jones bidimensionnel) représenté à la figure 1.2(b) donne une illustration *qualitative* des propriétés thermodynamiques des métaux (Perez and Lewis, 2003; Lorazo *et al.*, 2004).

En raison d'une phase liquide dont la densité est, cette fois, *inférieure* à celle du solide, l'état initial du système (c'est-à-dire avant toute irradiation laser) ne se situe

pas sous la ligne triple [contrairement à l'état initial du silicium identifié par un astérisque à la figure 1.2(a)]; comme en font foi les résultats présentés au chapitre 5, cela a d'importantes conséquences sur les trajets thermodynamiques menant à la fusion en régime femtoseconde.

Cependant, en raison de diagrammes des phases aux caractéristiques de coexistence liquide-vapeur et supercritiques communes, les semi-conducteurs et métaux partagent des trajets thermodynamiques menant à l'ablation qui, à l'exception de la spallation, sont très semblables (cf. chapitre 5).

1.2.2 Le modèle SSRW

Bien que, en principe, il ne soit valable que pour un solide de densité uniforme ρ_i instantanément et uniformément chauffé, le modèle SSRW (*Self-Similar Rarefaction Wave*) permet néanmoins de décrire (à tout le moins qualitativement) la propagation en volume de l'onde de raréfaction (associée à la baisse de densité) accompagnant l'expansion *adiabatique*, par exemple, d'une couche liquide formée suite au chauffage *isochore* d'un semi-conducteur par une impulsion femtoseconde (Sokolowski-Tinten *et al.*, 1998a).

Selon ce modèle, l'accroissement de la vitesse de translation (ou d'écoulement) $\mathrm{d}u$ pour une augmentation infinitésimale de la densité $\mathrm{d}\rho$ est proportionnelle à la vitesse du son $\mathrm{c}(\rho)$; la vitesse de translation à une densité ρ_f s'écrit alors

$$u_f(\rho_f, S) = -\int_{\rho_i}^{\rho_f} \left(\frac{c(\rho)}{\rho}\right)_S d\rho, \tag{1.2}$$

où S représente l'entropie.

Comme nous le verrons au chapitre 5, la valeur de $\mathrm{c}(\rho)$ est, dans le présent contexte,

d'importance capitale. En effet, la région liquide-vapeur est caractérisée par une vitesse du son très faible (de l'ordre de quelques mètres par seconde) qui se traduit par un système en zone métastable dont la vitesse de translation est essentiellement indépendante de ρ_f et de S (Perez and Lewis, 2003). En régime femtoseconde au voisinage du seuil d'ablation, le refroidissement du matériau par expansion adiabatique vers la région de coexistence liquide-vapeur donne lieu à une germination homogène de bulles de gaz dans un liquide surchauffé caractérisé par une *interface nette* le séparant du vide et dont l'existence est révélée par l'apparition d'anneaux d'interférence lors de mesures par microscopie résolue en temps (cf. chapitre 2).

CHAPITRE 2

REVUE DE LA LITTÉRATURE

Ce chapitre se veut un bref survol de la littérature dont un compte rendu exhaustif est présenté au chapitre 5. Ainsi, seuls les travaux essentiels à la compréhension des principaux enjeux de cette étude — essentiellement liés aux mécanismes d'ablation *thermiques* dans les semi-conducteurs et métaux — sont discutés ci-après.

2.1 Irradiation par des impulsions nanoseconde

Les premiers fondements d'une théorie visant à expliquer l'importante quantité de matière éjectée sous la forme de gouttelettes de grande taille ($\sim 10^{-6}$ m) — et non d'atomes isolés tel qu'on s'y attendrait pour une simple évaporation — suite à l'irradiation laser d'un métal ont été édifiés par Martynyuk (1976).

Le scénario, d'abord proposé pour de relativement longues ($\sim 10^{-7} - 10^{-5}$ s) impulsions, repris il y a une dizaine d'années par Miotello et Kelly (1995) pour des impulsions nanoseconde et par la suite maintes fois invoqué pour des impulsions femtoseconde (Cheng and Xu, 2005), picoseconde (Zhigilei and Garrison, 2000; Willis and Xu, 2002a) et nanoseconde (Miotello and Kelly, 1995; Song and Xu, 1998; Yoo *et al.*, 2000; Bulgakova and Bulgakov, 2001), repose sur des principes illustrés à la figure 2.1 et s'énonçant comme suit pour une impulsion de durée τ_L: (i) si $\tau_L \gg \tau_{\mathrm{LV}}$, où $\tau_{\mathrm{LV}} \sim 10^{-9}-10^{-8}$ s est le temps requis pour qu'un liquide métallique parvienne à l'équilibre avec sa vapeur saturée (Bulgakova and Bulgakov, 2001), le liquide en expansion est stable et sa trajectoire suit la binodale (indiquée par *equi-*

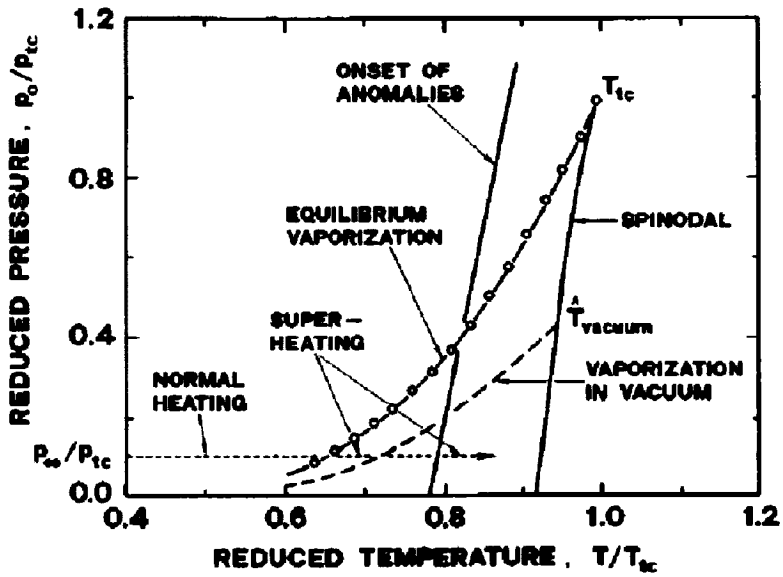

Figure 2.1 Évolution thermodynamique (dans la projection T-P du diagramme des phases) d'un métal irradié par une impulsion nanoseconde selon Miotello et Kelly (1995); $T_{\rm tc}$ et $P_{\rm tc}$ représentent, respectivement, les température et pression critiques.

librium vaporization). En revanche, si $\tau_L \lesssim \tau_{\rm LV}$, une partie de l'énergie du laser est emmagasinée dans le liquide avant d'être consommée sous la forme de chaleur latente de vaporisation. Dans ce contexte, ce dernier tente de s'équilibrer avec sa vapeur sous-saturée (la pression de saturation est celle donnée par la binodale) et, conséquemment, est poussé en zone métastable *alors qu'il est rapidement chauffé* (indiqué par *vaporization in vacuum*). (ii) Si la fluence est suffisamment élevée, le métal liquide près de la spinodale est surchauffé à une température $\approx 0.9T_c$ à l'approche de laquelle se manifestent d'importantes fluctuations thermiques et de densité (indiqué par *onset of anomalies*). (iii) Il en résulte une explosion de phase du liquide métastable par germination homogène de bulles de gaz en un temps caractéristique $\tau_{\rm NUC} \sim 10^{-9} - 10^{-7}$ s. À cet effet, l'existence d'une fluence seuil, au-delà de laquelle il y a éjection (iv) d'importantes quantités de matière sous la

forme (v) de gouttelettes liquides, est expliquée par la rapide hausse du taux de germination à l'approche de la spinodale (Bulgakova and Bulgakov, 2001; Song and Xu, 1998; Miotello and Kelly, 1995; Zhigilei and Garrison, 2000; Kelly and Miotello, 1999; Lu *et al.*, 2002; Garrison, 2003).

2.2 Irradiation par des impulsions femtoseconde

Cependant, l'interprétation de Miotello et Kelly n'est, de toute évidence, pas valide sous irradiation femtoseconde où, d'une part, les très hautes pressions associées au chauffage isochore entraînent initialement l'*éloignement* du système de la région métastable et où, d'autre part, cette dernière est plutôt atteinte lors du *refroidissement* qui suit par expansion adiabatique du matériau dans le vide (Sokolowski-Tinten *et al.*, 1998b; Perez and Lewis, 2003; Lorazo *et al.*, 2003).

2.2.1 Études expérimentales

À cet égard, une étude expérimentale des mécanismes d'ablation par irradiation laser femtoseconde dans les semi-conducteurs et métaux réalisée par Sokolowski-Tinten *et al.* (1998a, 1998b) a apporté un éclairage nouveau à la compréhension des phénomènes en jeu.

Ceci est mis en évidence à la figure 2.2 par une série d'images obtenues par microscopie résolue en temps (cf. figure 1) et illustrant l'évolution d'une surface de silicium suite à son excitation par une impulsion ultrabrève *au voisinage du seuil d'ablation.* L'absorption de l'énergie provenant du laser crée tout d'abord un dense gaz électronique à l'origine de la hausse initiale de la réflectivité en surface (0.1 ps). L'augmentation plus marquée de la réflectivité au cours des quelques centaines de

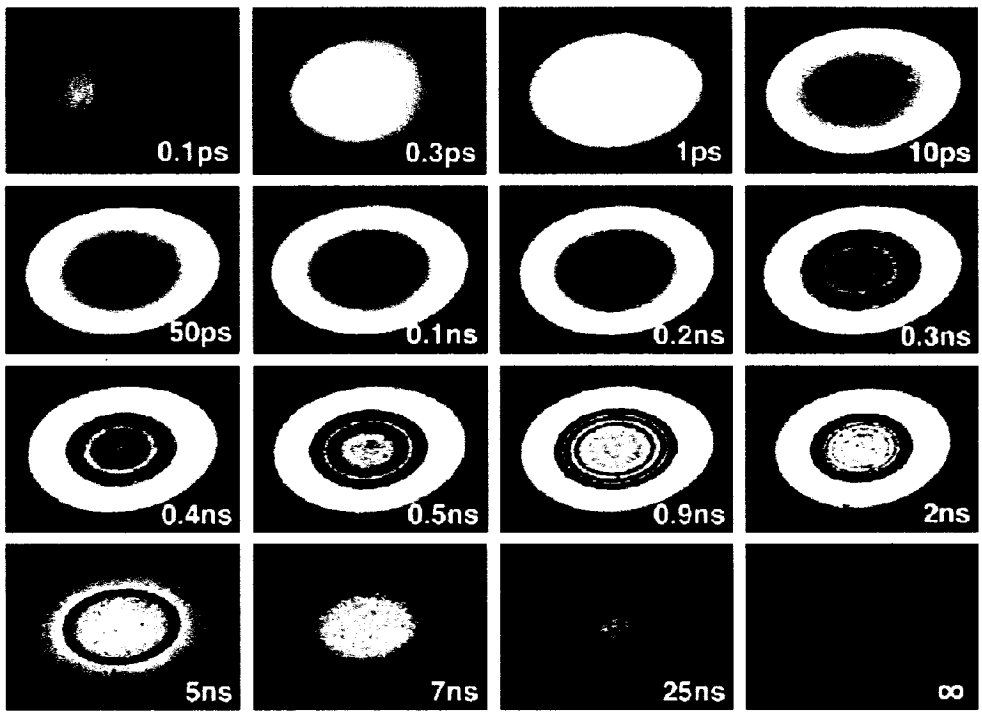

Figure 2.2 Images obtenues par microscopie résolue en temps et illustrant l'évolution d'une surface de silicium suite à son excitation par une impulsion de 100 fs à une fluence de 0.47 J cm^{-2}. Taille réelle des images: 300 μm$\times$200 μm. [Source: Sokolowski-Tinten *et al.* (1998a)]

femtosecondes suivantes indique la subséquente fusion ultrarapide et *non thermique* du cristal covalent (cf. chapitre 1). Au terme des quelques picosecondes qui suivent, une *tache sombre* associée à la rapide expansion et dilution du liquide métallique (et l'amorce du processus d'ablation) apparaît au centre de la zone irradiée (10 ps). Cette tache sombre fait ensuite place à un ensemble d'*anneaux concentriques* dont la séparation diminue (le nombre d'anneaux croît) sur une période de temps s'étalant sur plusieurs centaines de picosecondes. Après quelques nanosecondes, ces derniers disparaissent et la réflectivité retrouve éventuellement sa valeur originelle alors que le liquide demeuré en surface (c'est-à-dire qui n'a pas été éjecté) se solid-

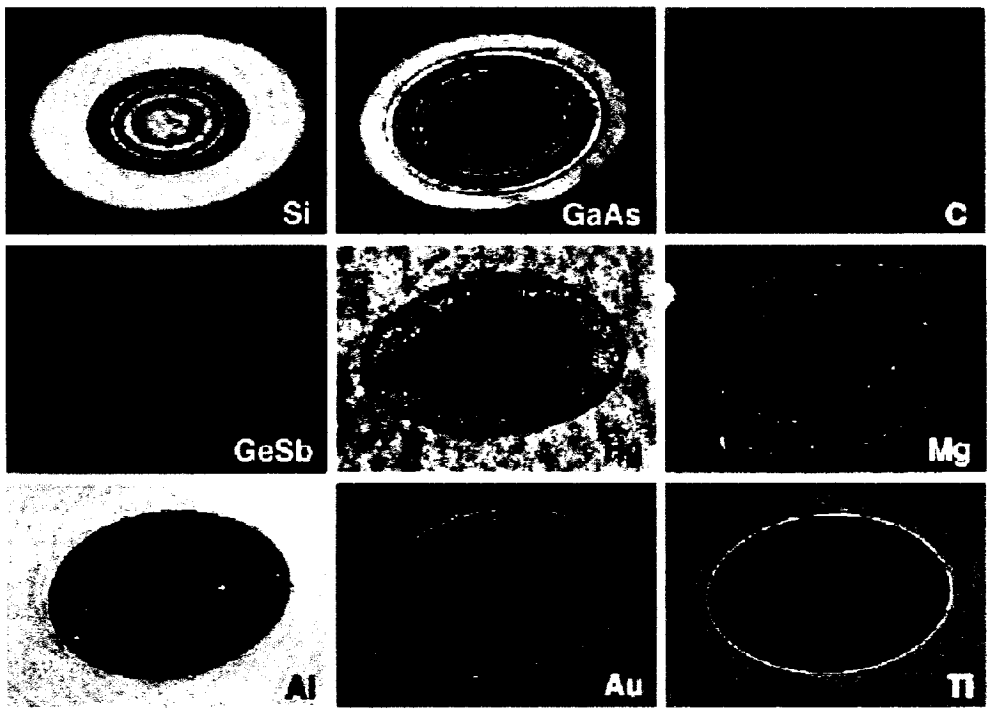

Figure 2.3 Images obtenues par microscopie résolue en temps et illustrant la nature *universelle* de la structure annulaire. [Source: Sokolowski-Tinten *et al.* (1998a)]

ifie; l'anneau visible en périphérie de la zone irradiée sur l'image finale (identifiée par le symbole ∞) est attribuable à la formation d'une phase *amorphe.*

La structure annulaire, dont l'étendue coïncide parfaitement avec la région ablatée, est intimement liée au phénomène d'ablation; observée, ainsi qu'en témoigne la figure 2.3, pour de nombreux autres métaux et semi-conducteurs, elle suggère des mécanismes d'éjection de matière *universels* dans les solides absorbants irradiés par des impulsions laser ultrabrèves.

Sokolowski-Tinten *et al.* ont démontré que la structure annulaire observée au voisinage du seuil d'ablation n'est pas associée à la morphologie de la surface mais, plutôt, à une figure d'interférence (anneaux de Newton) qui révèle l'expansion

(avec une vitesse d'écoulement de quelques centaines de mètres par seconde) d'un matériau non homogène et relativement transparent *entre deux interfaces nettes.*

Afin d'expliquer ces observations, Sokolowski-Tinten *et al.* ont proposé un scénario reposant sur le modèle SSRW (cf. chapitre 1): le solide est d'abord chauffé à volume constant, produisant de ce fait un matériau à très hautes température et pression. Ce dernier entreprend ensuite une expansion adiabatique dans le vide jusqu'à la région de coexistence liquide-vapeur où la forte chute de la vitesse du son, d'une part, et la germination homogène de bulles de gaz dans le liquide métastable et surchauffé, d'autre part, donnent lieu à une structure bulleuse comprise entre deux interfaces nettes (le front d'ablation et l'interface séparant la région ablatée de la région non ablatée).

À des fluences plus élevées (mais néanmoins inférieures au seuil de formation de plasma dans les semi-conducteurs), les anneaux d'interférence ne sont plus observés [cf. figure 2.3 au centre de l'échantillon de GaAs où la fluence (localement) du faisceau gaussien est plus élevée], suggérant de ce fait une expansion supercritique (c'est-à-dire au-dessus de la région liquide-vapeur) du matériau irradié au cours de laquelle aucune chute abrupte de la vitesse du son n'entraîne la formation d'un front d'ablation bien défini.

2.2.2 Études numériques

Aussi utiles soient elles, les mesures par microscopie résolue en temps ne permettent pas de directement sonder l'évolution des propriétés thermodynamiques du solide irradié. En revanche, cela est possible avec des approches numériques employant, par exemple, la dynamique moléculaire (Allen and Tildesley, 1987).

À cet égard, Perez et Lewis (2002, 2003) ont été les premiers à calculer explicite-

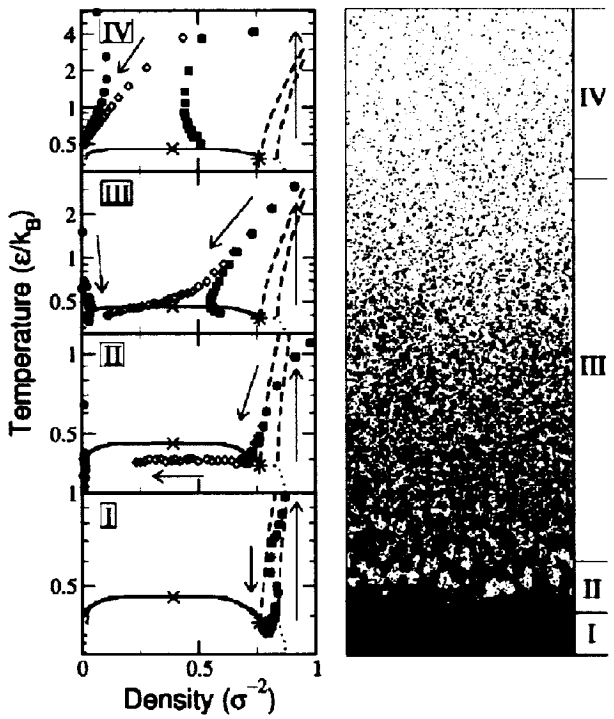

Figure 2.4 Évolutions thermodynamique (à gauche) et morphologique (à droite) d'un système de Lennard-Jones bidimensionnel irradié par une impulsion laser femtoseconde. Carrés noirs: branche dense; cercles noirs: branche gazeuse; losanges blancs: branche moyenne. Les flèches indiquent l'écoulement du temps. Le diagramme des phases détaillé est illustré à la figure 1.2(b). [Source: Perez et Lewis (2002)]

ment l'évolution thermodynamique d'un matériau soumis à une impulsion laser ultrabrève à partir de simulations reposant sur la dynamique moléculaire.

Les résultats de leurs calculs pour un système de Lennard-Jones bidimensionnel sont illustrés à la figure 2.4. L'originalité de la démarche réside dans le suivi de l'évolution des principales variables thermodynamiques (densité, température et pression) de petites sections (tranches) de la cible selon une technique décrite au chapitre 5. Ainsi, trois trajectoires, ou "branches", sont associées à chacune des

sections de l'échantillon: dense (pour les phases solide et/ou liquide), gazeuse et macroscopique (ou moyenne); en déterminant où, dans le diagramme des phases, les branches dense et moyenne se séparent, le mécanisme d'ablation responsable (localement) de la rupture du matériau peut être identifié.

L'étude réalisée par Perez et Lewis confirme les conclusions des travaux de Sokolowski-Tinten *et al.*: à des énergies près du seuil d'ablation, le matériau, suite à un chauffage isochore, entreprend une expansion adiabatique qui le mène à la région liquide-vapeur où une explosion de phase par germination homogène de bulles de gaz dans un liquide surchauffé s'ensuit (région II sur la figure 2.4).

Les simulations mettent aussi en exergue un nouveau mécanisme d'éjection: plus près de la surface où l'énergie déposée est plus importante, la rapide expansion supercritique du matériau entraîne (localement) sa dissociation en un ensemble d'agrégats (dont la taille moyenne dépend du *gradient* de vitesse local) par un processus de *fragmentation* "non trivial" (région III); il est à noter que, à l'opposé, un processus de fragmentation est dit "trivial" si la décomposition du fluide se produit au voisinage de l'équilibre thermodynamique (comme nous le verrons pour des impulsions picoseconde aux chapitres 4 et 5).

Enfin, encore plus près de la surface, la très grande quantité d'énergie absorbée entraîne la vaporisation pure et simple de la cible (région IV).[1]

Ainsi, les travaux de Sokolowski-Tinten *et al.*, de même que ceux de Perez et Lewis, ont contribué de façon remarquable à une meilleure compréhension des mécanismes thermiques responsables de l'éjection de matière dans les solides irradiés par des impulsions femtoseconde.

En revanche, ces études ne nous renseignent pas sur la nature de l'ablation occa-

[1] Aucune ablation ne se produit dans la région I.

sionnée par des impulsions de plus longue durée (picoseconde et nanoseconde) pour lesquelles la validité du modèle de Miotello et Kelly reste à être démontrée.

CHAPITRE 3

OBJECTIFS ET MÉTHODOLOGIE

L'objectif premier de cette étude consiste à mettre en exergue les mécanismes qui gouvernent les possibles modifications structurales *thermiques* dans les semiconducteurs et métaux irradiés par des impulsions femtoseconde, picoseconde et nanoseconde.

À cet effet, la première étape (et non la moindre!) implique la conception d'un modèle qui puisse *simultanément* rendre compte des transitions optiques ainsi que de la complexe dynamique aux échelles électronique et atomique, et ce, sur une échelle de temps allant de la femtoseconde à la nanoseconde.

Ce modèle unique, résumé au chapitre 4 et discuté dans le moindre détail au chapitre 5, combine une approche novatrice pour la description de l'interaction du laser avec la cible à une méthode jumelant les techniques Monte Carlo et de dynamique moléculaire décrivant, respectivement, les dégrés de liberté électroniques et atomiques.

En complémentant le modèle par un suivi simultané de l'évolution thermodynamique de la cible selon une procédure décrite au chapitre 5, les états métastables et instables induits dans le matériau par le laser peuvent être observés et les mécanismes à l'origine de la fusion, de l'ablation et de la solidification identifiés.

En raison de l'importance technologique que revêt ce matériau, la présente analyse est appliquée au cas d'une cible de silicium. Cependant, comme nous le verrons aux chapitres suivants, les conclusions de cette étude sont également valables pour

les autres semi-conducteurs appartenant aux groupes IV et III-V ainsi que, dans une certaine mesure, aux métaux.

Les principales questions auxquelles nous nous proposons de répondre concernent, en ordre d'importance, les mécanismes d'ablation, de fusion et de solidification.

Ainsi, nous cherchons tout d'abord à savoir si le modèle de Miotello et Kelly (1995), bien que ne pouvant de toute évidence s'appliquer à une irradiation par une impulsion femtoseconde, est valable en régimes picoseconde et nanoseconde. En particulier,

(i) Existe-t-il des conditions permettant à un liquide d'accéder à la région métastable alors que celui-ci est *rapidement chauffé par une impulsion laser*? Autrement dit, quel est le temps d'équilibration du liquide métallique avec sa vapeur τ_{LV}?

(ii) Lors d'une explosion de phase, l'ablation se produit-elle forcément à une température $\approx 0.9T_c$?

(iii) Quel est le temps caractéristique de germination d'une bulle (critique) de gaz dans un liquide surchauffé, τ_{NUC}? Si l'explosion de phase est possible suivant une irradiation laser femtoseconde, la valeur de τ_{NUC} doit, dans ce cas, être nettement inférieure à celle avancée par Martynyuk (cf. chapitre 2).

(iv) Des mécanismes autres que l'explosion de phase peuvent-ils expliquer l'existence d'un seuil d'ablation bien défini?

(v) Enfin, quelle est la *nature* de ce seuil dans les semi-conducteurs irradiés par des impulsions ultrabrèves? Ainsi, la germination de bulles de gaz est-elle le seul résultat de fluctuations thermiques dans le liquide surchauffé ou est-il possible que l'importante énergie de translation caractérisant le système à son entrée en zone métastable puisse également y jouer un rôle?

Dans un second temps, nous nous attardons aux mécanismes par lesquels il y a fusion sous l'action d'un rayonnement laser. Ainsi, cette fusion est-elle toujours la conséquence d'un processus de germination hétérogène ou si, tel que proposé par Rethfeld *et al.* (2002), une germination homogène, voire une instabilité mécanique dans le cristal fortement surchauffé, est également possible?

Enfin, nous cherchons à mieux comprendre la dynamique hors équilibre régissant la solidification (et la possible amorphisation) du liquide non ablaté et surfondu. :

CHAPITRE 4

SHORT-PULSE LASER ABLATION OF SOLIDS: FROM PHASE EXPLOSION TO FRAGMENTATION

Ce chapitre est exclusivement consacré aux mécanismes d'*ablation* prévalant dans les semi-conducteurs et métaux irradiés par des impulsions femtoseconde et picoseconde. Ainsi, par le biais de simulations reposant, d'une part, sur un modèle unique décrivant la dynamique aux échelles électronique et atomique dans une cible de silicium soumise à un rayonnement laser et, d'autre part, sur un suivi de l'évolution thermodynamique du matériau irradié, il est démontré que l'explosion de phase est un phénomène propre aux impulsions ultrabrèves — et non au régime nanoseconde tel que l'affirment Miotello et Kelly (1995). À ce titre, ce qui suit constitue une introduction à l'étude, plus générale, de l'ensemble des modifications structurales (fusion, ablation et solidification) pouvant être induites dans les solides absorbants par une irradiation laser et détaillées au chapitre 5. Ce chapitre a fait l'objet d'une publication en 2003 dans la revue *Physical Review Letters*.[1]

Short-Pulse Laser Ablation of Solids: From Phase Explosion to Fragmentation

Patrick Lorazo,[1,2,*] Laurent J. Lewis,[2] and Michel Meunier[1]

[1] Département de Génie Physique et Groupe de Recherche en Physique et Technologie des Couches Minces (GCM), École Polytechnique de Montréal, C.P.

[1]LORAZO, P., LEWIS, L. J., MEUNIER, M. «Short-Pulse Laser Ablation of Solids: From Phase Explosion to Fragmentation». *Physical Review Letters*. 91:22 (2003). 225502.

*Electronic address: lorazop@MAGELLAN.UMontreal.CA

6079, Succursale Centre-Ville, Montréal, Québec, Canada, H3C 3A7

[2] Département de Physique et Groupe de Recherche en Physique et Technologie des Couches Minces (GCM), Université de Montréal, C.P. 6128, Succursale Centre-Ville, Montréal, Québec, Canada H3C 3J7

The mechanisms of laser ablation in silicon are investigated close to the threshold energy for pulse durations of 500 fs and 50 ps. This is achieved using a unique model coupling carrier and atom dynamics within a unified Monte Carlo and molecular-dynamics scheme. Under femtosecond laser irradiation, isochoric heating and rapid adiabatic expansion of the material provide a natural pathway to phase explosion. This is not observed under slower, nonadiabatic cooling with picosecond pulses where fragmentation of the hot metallic fluid is the only relevant ablation mechanism.

PACS numbers: 61.80.Az, 79.20.Ds, 79.20.Ap

Laser ablation is the process by which macroscopic amounts of material are ejected from the surface of a solid irradiated by a short, intense, laser pulse. In spite of its ubiquitous nature in many areas of technology (von Allmen and Blatter, 1995), a satisfactory understanding of the fundamentals of laser ablation has been hampered by a complex phenomenology involving multiple length and time scales (Sokolowski-Tinten *et al.*, 1998b).

In metals and semiconductors, below the threshold energy for dielectric breakdown and plasma formation ($I_p \sim 10^{13}$ W cm^{-2}) (Sokolowski-Tinten *et al.*, 1998b; von der Linde and Schüler, 1996), it is often argued that a system is pushed into the metastable region as a result of *rapid heating* (Miotello and Kelly, 1995; Yoo *et al.*, 2000; Zhigilei *et al.*, 2003a; Vidal *et al.*, 2001); phase separation follows from large, local, density fluctuations, i.e., homogeneous bubble nucleation in the metastable

(superheated) liquid. This process, known as phase explosion or explosive boiling, has often been suggested based on the observation of liquid droplets in the plume for typical pulse durations of $\sim$ 10 ns (Kelly and Miotello, 1999). However, the above interpretation fails for ultrashort ($\lesssim$ 1 ps) pulses where heating is isochoric and explosive boiling takes place, instead, as the system adiabatically *cools* into the metastable region (Sokolowski-Tinten *et al.*, 1998b; Perez and Lewis, 2002). Moreover, using molecular dynamics (MD) and a simple Lennard-Jones model, Perez and Lewis have established the occurrence of fragmentation in the fs regime, thereby revealing a new path for the ejection of liquid droplets (Perez and Lewis, 2002; Perez and Lewis, 2003). Thus, if a clear picture of ultrashort-pulse laser ablation is beginning to emerge, a definite assessment for longer (ps to ns) pulses has yet to come.

In this Letter, we report on the fundamental mechanisms of matter removal during short-pulse laser irradiation of Si for energies close to the ablation threshold but below that for plasma formation. Using a combined MD and Monte Carlo (MC) approach capable of capturing both microscopic and mesoscopic-scale dynamics, we follow the thermodynamic trajectory of the system in the temperature-density (ρ-T) plane during heating, expansion, and cooling for pulse durations of 500 fs and 50 ps. We show that, in spite of similarities between the expanding plumes (see figure 4.1), the mechanisms of matter removal are fundamentally different. In brief, rapid heating is observed to pull the system *away* from the metastable region, in contrast to the scenario reported by, e.g., Miotello and Kelly (1995). The extent to which thermal diffusion takes place as the system subsequently cools towards the liquid-gas regime is found to be determinant for the ablation process. As shown below, this suggests a pulse duration upper limit for phase explosion of $\sim 10^{-11}$ s.

A complete description of our model will be given elsewhere. In short, classical MD is used to follow the motion of atoms which interact via the Stillinger-Weber

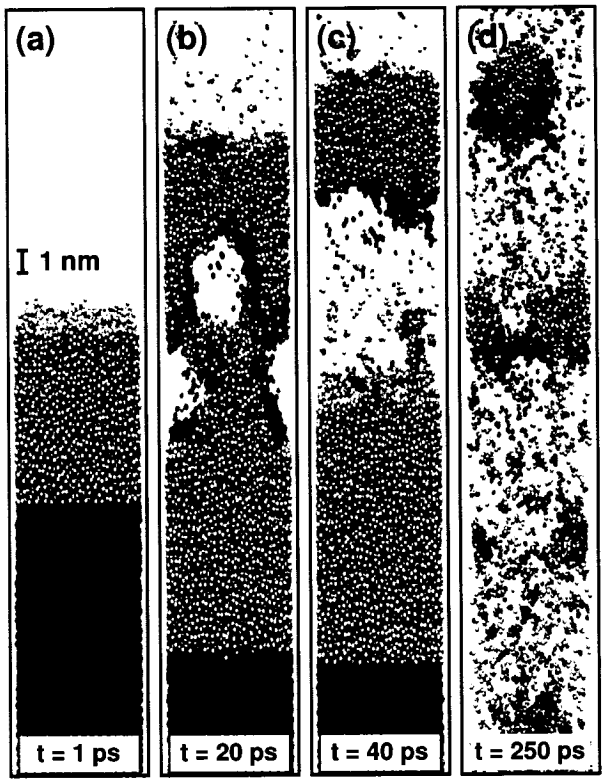

Figure 4.1 Snapshots showing the ejection of molten material for two pulse durations at 266 nm: (a)-(c) 500 fs at a fluence of 0.375 J cm^{-2}; (d) 50 ps at a fluence of 0.55 J cm^{-2}; each pulse begins at $t = 0$. Dark gray: crystalline silicon; light gray: (metallic) liquid silicon.

(SW) potential (Stillinger and Weber, 1985). Two systems, consisting of 99000 ($8 \times 8 \times 30$ nm^3) and 165600 ($8 \times 8 \times 50$ nm^3) atoms embedded into a $8 \times 8 \times 500$ nm^3 supercell, are used for pulse durations of 500 fs and 50 ps, respectively. Periodic boundary conditions are applied in the x and y directions. In the z direction, normal to the surface, we proceed as follows: (i) to simulate heat diffusion into an infinite bulk, the crystal is terminated by a Langevin heat bath (Allen and Tildesley, 1987); (ii) to mimic the propagation of pressure waves beyond the bottom of the supercell, a single atomic layer, to which an appropriate set of forces are applied, is added (Zhigilei *et al.*, 2003a).

The laser pulse of duration τ_L (FWHM) has $\lambda_L = 266$ nm ($h\nu = 4.66$ eV) and is Gaussian in time but spatially constant; it is simulated by the successive arrival of photons which couple to "carriers". Here, a carrier is a particle (electron or hole) which follows Drude dynamics while undergoing various scattering events, each with its own characteristic collision time τ. The position at which a photon is absorbed along the z axis is determined from Beer's law, i.e., it has a probability $1-\exp(-\alpha l_c)$ of being absorbed within each of the cells of side $l_c \sim 5$ Å dividing the supercell; α is the local absorption coefficient with contributions from interband and intraband transitions [$\sim (5\text{ nm})^{-1}$ for c-Si and l-Si]. In an interband event, an electron-hole pair is created with total kinetic energy $h\nu - E_G$, where E_G is the band gap energy: each carrier is given velocity $\mathbf{v}$ and kinetic energy $m^* v^2/2$, where the effective mass m^* (the only free parameter in the model) is chosen such as to reproduce the experimental melting threshold fluence at λ_L and $\tau_L = 15$ ps (Malvezzi *et al.*, 1984). In an intraband transition, which is the only absorption process in the metallic molten material (see below), the carrier energy is increased by $h\nu$.

As mentioned above, the hot electrons and holes relax through a cascade of scattering events (von Allmen and Blatter, 1995). This is taken into account using a standard MC approach (Lundstrom, 1990). In the present model, carrier-carrier scattering allows carriers to exchange energy [$\tau_{\text{c-c}} \sim 10$ fs (von Allmen and Blatter, 1995)]. Heating, and eventually equilibrium at a common lattice (T) and electronic (T_e) temperature, is achieved through carrier-phonon scattering whereby a quantum of energy of 62.6 meV [c-Si (Lundstrom, 1990)] or 50 meV (l-Si) is given to nearby atoms if $T_e > T$ [$\tau_{\text{c-ph}} \sim 10$ fs (Eesley, 1986)]. In the crystal, additional scattering processes include Auger recombination and impact ionization (van Driel, 1987). As a final point, Si, like other group IV and III-V semiconductors, is metallic in the liquid state (Godlevsky *et al.*, 1998): coordination increases from 4 to 6 and the electron density jumps to $\sim 10^{23}$ cm^{-3}. In our model, the semiconductor-

to-metal transition is simulated by generating electrons (up to four per atom) at the rate at which the local coordination increases.

All simulations started from a Si(100) substrate at 300 K. Figures 4.1(a)-4.1(c) display the early stages of matter removal for a 500 fs pulse slightly above the threshold fluence for ablation, $F_{\rm th}^{\rm a} = 0.35$ J cm^{-2}; the corresponding irradiance is 7×10^{11} W cm^{-2}, well below I_p. About 1 ps after the beginning of the pulse, a hot ($\sim$ 8000 K) and highly pressurized ($\sim$ 10 GPa) liquid layer has formed at the surface [figure 4.1(a)]. The subsequent scenario is as follows: (i) more solid material is transformed into a liquid metal as the melt front propagates further into the bulk; (ii) closer to the surface, the relaxation of the pressure buildup within the liquid layer causes the latter to rapidly expand into vacuum, eventually leading to void nucleation [figure 4.1(b)] and to the ejection of a large piece of material with a velocity $\approx$ 200 m s^{-1} [figure 4.1(c)], i.e., ablation occurs. Note that the strongly excited Si crystal may, under fs laser irradiation, undergo an ultrafast, nonthermal melting transition which cannot be accounted for by empirical potentials such as SW (Sokolowski-Tinten *et al.*, 1998b). Although the details of the energy deposition may depend on the path from solid to liquid, this is not expected to influence the *nature* of the ablation process occurring on much longer time scales.

As proposed by Perez and Lewis (2002), it is possible to *directly* determine the mechanisms of matter removal by following the time evolution of the system in the ρ-T plane. To this effect, three distinct thermodynamic trajectories are computed: macroscopic (or average), dense (solid and/or liquid), and gas. This approach differs from other MD studies where the ablation mechanisms have been qualitatively assessed from a visual inspection of the plume (Zhigilei *et al.*, 2003a).

A typical trajectory for the 500 fs pulse is given in figure 4.2(a). The starting point is a

crystal at $\rho_0 = 2.33$ g cm^{-3} and $T = 300$ K (marked A). The incoming laser energy is transferred to the ions in about 1 ps. No significant expansion occurs on this time scale and the result is a hot metallic liquid at high pressure and $\rho \approx \rho_0$ (B). The pressure is then released via mechanical expansion and the liquid-gas regime is approached as the system adiabatically *cools*. The rapidly expanding material, eventually entering the metastable region (C), is pushed close to the spinodal limit (dashed line) and homogeneous nucleation of gas bubbles in the superheated liquid takes place. This is indicated by the separation of the dense and macroscopic branches (D) and the concomitant appearance of a gas branch, thus revealing a decomposition of the metastable phase into a mixture of liquid and gas (D→E). Two remarks are in order: (i) the same trajectory can also be plotted in the T-P plane (see inset); this allows a direct comparison with the thermodynamic pathway proposed by Miotello and Kelly whereby the system is pushed into the metastable region at constant pressure *as it is rapidly heated* (Miotello and Kelly, 1995); clearly, this is incorrect. (ii) Although the possibility of a spinodal decomposition — in the mechanically unstable region below the spinodal curve (Sokolowski-Tinten *et al.*, 1998b) — cannot be completely excluded, it is unlikely to be responsible for ablation since the voids grow as highly localized perturbations, i.e., bubbles [figure 4.1(b)].

The above scenario, observed across the whole ablated region, confirms that phase explosion is the primary ejection mechanism under *near-adiabatic cooling conditions close to the threshold energy* (Sokolowski-Tinten *et al.*, 1998b; Perez and Lewis, 2002); we have obtained similar results for a 5 ps pulse. However, as the pulse duration is increased, i.e., under slower heating conditions, slower expansion and significant thermal diffusion are expected. We show below that this has important consequences for matter removal.

Figure 4.2(b) displays a typical trajectory for ablation with a 50 ps pulse slightly above the threshold fluence, $F_{\rm th}^{\rm b} = 0.45$ J cm^{-2}. As in the case of a fs pulse, heating

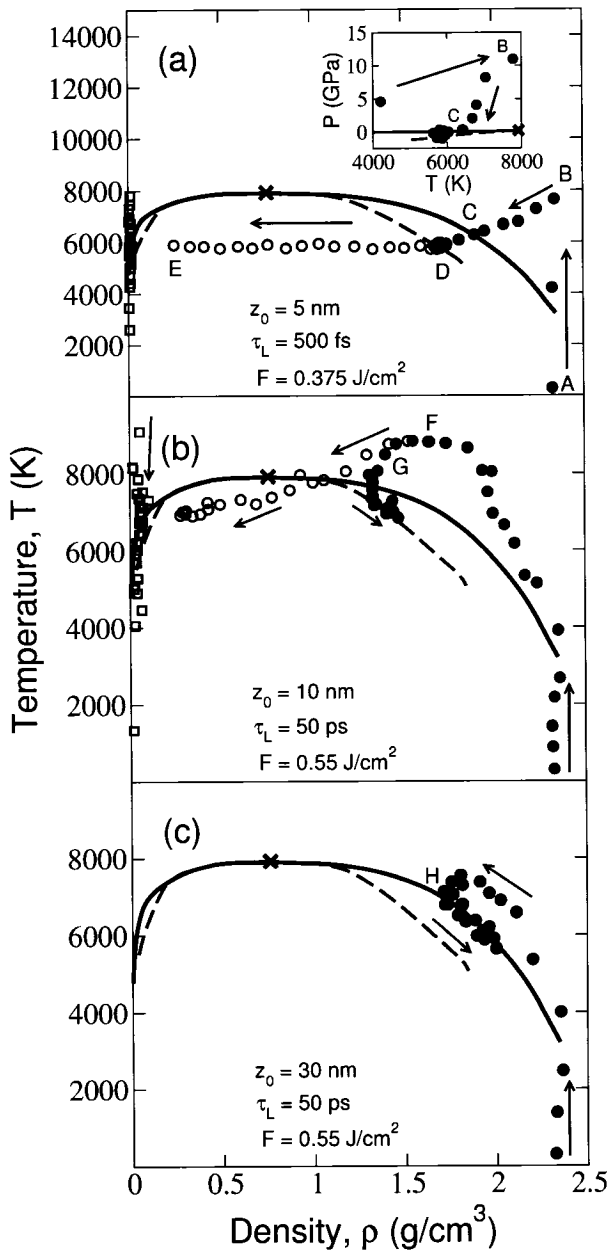

Figure 4.2 Time evolution of the system in the ρ-T plane for different pulse durations, fluences, and depths z_0 below the original surface (as indicated). Full circles: dense branch; open circles: macroscopic branch; squares: gas branch. Solid line: binodal (Honda and Nagasaka, 1999); dashed line: spinodal (Makhov and Lewis, 2003); cross: critical point (Makhov and Lewis, 2003). Arrows indicate the flow of time.

is fast enough to pull the liquid away from the binodal (where it is in equilibrium with the vapor), thus causing the system to initially evolve above the liquid-gas coexistence region and reach a supercritical state (F). In contrast to fs irradiation, however, significant expansion occurs during the pulse, i.e., heating is nonisochoric. Also, the system does not cross the binodal line in a *homogeneous* state: rather, the split of the dense and macroscopic branches, marking the onset of ablation, takes place *outside* of any phase coexistence region (G). Thus, in this case, matter removal cannot be attributed to phase explosion nor spinodal decomposition. The above behavior has been observed over the *entire* ablated volume above F_{th}^{b}: we have *not* found a single case where the metastable region is accessed in a homogeneous state. Simulations using a two-dimensional Lennard-Jones model for pulse durations of a few tens to a few hundreds of ps corroborate these observations.[2]

The breakup of an expanding supercritical fluid during short-pulse laser ablation has recently been attributed to fragmentation (Perez and Lewis, 2002). As discussed below, this is proposed as the primary ablation mechanism under *nonadiabatic cooling conditions.* It can be seen as a structural rearrangement of the system into clusters during the expansion caused by the pressure buildup. Two limits must be considered: (i) under fs irradiation, the rapid expansion of the material can be such that the equilibrium structure can no longer be preserved (e.g., by atomic diffusion); (ii) for significantly longer pulses, the equilibrium structure is likely to be maintained during the (slower) expansion. However, because a fluid at sufficiently low densities is in general not homogeneous, its dissociation into fragments is still possible and is referred to as "trivial" fragmentation (Perez and Lewis, 2003). In any case, fragmentation should not be confused with spallation whereby the material is brought into the solid-gas coexistence region by strong tensile pressure waves (Perez and Lewis, 2003).

[2]PEREZ, D., LEWIS, L. J., unpublished.

The dynamics of a homogeneous system cooling towards the liquid-gas regime depends strongly on the rate at which it expands. This is revealed in figure 4.2(c) for a section of the *unablated* material irradiated by a 50 ps pulse. Heating is nonisochoric and, as it cools, the system reaches the binodal (H). The key point is that, although it does so in the same region as for a 500 fs pulse [point C in figure 4.2(a)], the slower expansion allows significant heat diffusion to take place: the system does not enter the metastable region but, rather, cools along the binodal by thermal diffusion. As detailed below, the absence of explosive boiling for sufficiently long pulses is the result of slow material expansion and efficient heat conduction.

Based on these observations, a schematic overview of the thermodynamic pathways to ablation for pulse durations of $\sim 10^{-13}$ to 10^{-8} s emerges as depicted in figure 4.3 and discussed below:

(i) Miotello and Kelly have argued that, for sufficiently short ($\lesssim$ 1000 ns) pulses, rapid heating pushes the system into the metastable region where homogeneous nucleation of gas bubbles takes place (Miotello and Kelly, 1995); in the ρ-T plane, this can *conceptually* be represented by K$\rightarrow$M. If this were so, explosive boiling would be the only mechanism relevant to short-pulse laser ablation.

(ii) The existence of various ablation mechanisms can be understood if one considers, instead, that rapid heating pulls the system *away* from the metastable region; the rate at which expansion proceeds as the material subsequently *cools* is determinant for the ablation process. This is best viewed by considering an arbitrary point of entry into the metastable region along the binodal (W). Under fs irradiation, isochoric heating leads to the buildup of a strong pressure within the material, later released via mechanical expansion. At high energies, the resulting rapid expansion causes the breakup of the supercritical fluid through fragmentation

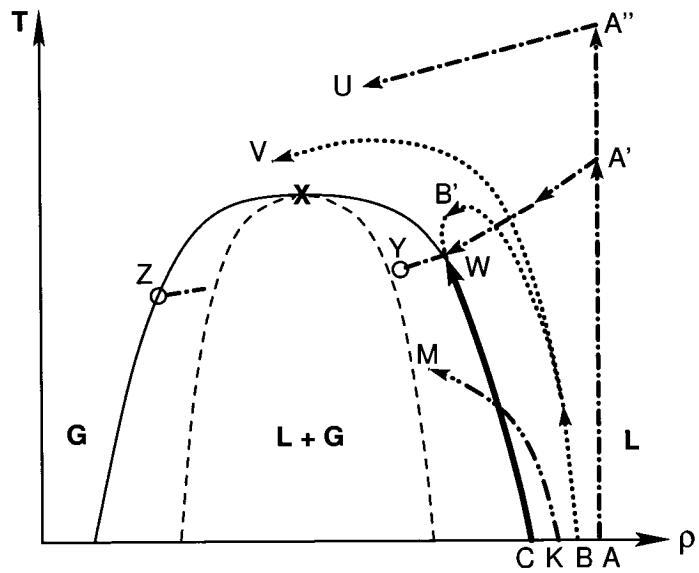

Figure 4.3 Thermodynamic trajectories of a hypothetical semiconductor or metal under fs (dashed-dotted line), ps (dotted line) and ns (thick solid line) laser irradiation. Thin solid line: binodal; dashed line: spinodal; cross: critical point. L: liquid; G: gas. Other capital letters refer to locations in the phase diagram (see text).

(A→A"→U) (Perez and Lewis, 2003). Closer to the threshold energy, however, the expansion is too slow to induce fragmentation. Nevertheless it is sufficiently rapid to push the system into the metastable regime (near the spinodal limit) *before significant thermal diffusion has occurred* (A→A'→W→Y), i.e., cooling is adiabatic. Homogeneous bubble nucleation then sets in, converting the superheated material into a mixture of liquid and gas (Y→Z), a first-order transition. Conversely, under irradiation with long (ns) pulses, the material responds to the slow heating with a slow expansion *along* the binodal (C→W), likely up to the critical point where phase separation proceeds via a second-order transition; for $\tau_L \gtrsim 100$ ns, vaporization may also be important (Kelly and Miotello, 1999).

(iii) Consequently, there must exist a "critical" pulse duration, τ_L^c, beyond which phase explosion is suppressed. This is illustrated by the trajectory B→B'→W for a pulse of intermediate (ps) duration. Following nonisochoric heating the system cools towards the liquid-gas regime. Here, however, expansion occurs in a time of the order of, or greater than, the characteristic time for heat conduction [$\tau_{\rm th} \sim 10^{-11}$ s (von der Linde *et al.*, 1997)]. As a result, the system cools along the binodal by thermal diffusion, i.e., it does not enter the metastable region and phase explosion does not take place. In this case, only those regions associated to an expansion above the critical point contribute to the ablated mass (B→V), here through a fragmentation process ("trivial" or not).

In summary, explosive boiling is particular to ultrashort-pulse laser irradiation where near-isochoric heating conditions lead to a rapid adiabatic cooling of the material. This regime is characterized by (i) the time needed to induce a collective motion of the atoms, $\tau_s = \delta/c_s(\rho)$, where δ $(= 1/\alpha)$ and $c_s(\rho)$ are, respectively, the optical penetration depth and the speed of sound (Zhigilei *et al.*, 2003a); (ii) the time needed to observe significant thermal diffusion, $\tau_{\rm th}$. With $\delta \sim 10^{-8}$ m (as expected for a *metallic liquid* at the surface of a metal or semiconductor) and $c_s(\rho \approx \rho_0) \sim 10^3$ m s^{-1}, this yields a pulse duration upper limit $\tau_L^c \sim \tau_s \sim \tau_{\rm th} \sim 10^{-11}$ s for phase explosion; τ_L^c could be higher in materials where heat diffusion is slower. For $\tau_L > \tau_L^c$, fragmentation remains the only relevant ablation mechanism.

We are most grateful to D. Perez for fruitful discussions. P. L. also wishes to thank K. Sokolowski-Tinten and D. von der Linde for useful insights. This work has been supported by grants from the Canada's NSERC and Québec's FQRNT. We are indebted to the *Réseau québécois de calcul de haute performance* for generous allocations of computer resources.

CHAPITRE 5

THERMODYNAMIC PATHWAYS TO MELTING, ABLATION, AND SOLIDIFICATION IN ABSORBING SOLIDS UNDER PULSED LASER IRRADIATION

Ce chapitre, qui constitue le coeur même de cette thèse, aborde en détail les possibles transformations thermiques induites dans les semi-conducteurs et métaux par de brèves impulsions laser. Ainsi, par le biais de simulations reposant, d'une part, sur un modèle unique décrivant la dynamique aux échelles électronique et atomique dans une cible de silicium soumise à un rayonnement laser et, d'autre part, sur un suivi de l'évolution thermodynamique du matériau irradié, une synthèse des possibles trajets thermodynamiques menant à la fusion, l'ablation et la solidification sous irradiation femtoseconde, picoseconde et nanoseconde est proposée; de plus, une analyse permettant d'éclaircir la nature du seuil d'ablation dans les semi-conducteurs irradiés par des impulsions femtoseconde est également présentée. Ce chapitre est constitué d'un article soumis pour publication à la revue *Physical Review B.*

Thermodynamic pathways to melting, ablation, and solidification in absorbing solids under pulsed laser irradiation

Patrick Lorazo,[1,2,*] Laurent J. Lewis,[2,†] and Michel Meunier[1,‡]

[1] Laboratoire de Procédés par Laser, Département de Génie Physique, École

*Electronic address: patrick.lorazo@UMontreal.CA
†Electronic address: Laurent.Lewis@UMontreal.CA; URL:http://www.esi.umontreal.ca/~grofnum/
‡Electronic address: Michel.Meunier@polymtl.ca; URL:http://lpl.phys.polymtl.ca

Polytechnique de Montréal, C.P. 6079, Succursale Centre-Ville, Montréal (Québec), Canada H3C 3A7

[2] Département de Physique et Regroupement Québécois sur les Matériaux de Pointe (RQMP), Université de Montréal, C.P. 6128, Succursale Centre-Ville, Montréal (Québec), Canada H3C 3J7

The thermodynamic pathways involved in laser irradiation of absorbing solids are investigated in silicon for pulse durations of 500 fs and 100 ps. This is achieved by accounting for carrier and atom dynamics within a combined Monte Carlo and molecular-dynamics scheme and simultaneously tracking the time evolution of the irradiated material in ρ-T-P space. Our simulations reveal thermal *changes in long-range order and state of aggregation driven, in most cases, by* nonequilibrium *states of rapidly heated or promptly cooled matter. Under femtosecond irradiation near the ablation threshold, the system is originally pulled to a near-critical state following rapid* ($\lesssim 10^{-12}$ s) *disordering of the* mechanically unstable *crystal and isochoric heating of the resulting metallic liquid. The latter is then adiabatically* cooled *to the liquid-vapor regime where phase explosion of the subcritical,* superheated *melt is initiated by a direct conversion of translational,* mechanical *energy into surface energy on a* $\sim 10^{-12} - 10^{-11}$ s *time scale. At higher fluences, matter removal involves, instead, the fragmentation of an initially homogeneous fluid subjected to large strain rates upon rapid,* supercritical *expansion in vacuum. Under picosecond irradiation, homogeneous and, at later times, heterogeneous melting of the superheated solid are followed by nonisochoric heating of the molten metal. In this case, the* subcritical *liquid material is subsequently cooled onto the binodal by thermal conduction and explosive boiling does* not *take place; as a result, ablation is associated with a "trivial" fragmentation process, i.e., the relatively slow expansion and dissociation into liquid droplets of* supercritical *matter* near thermodynamic equilibrium. *This implies a liquid-vapor equilibration time of* $\sim 10^{-11} - 10^{-10}$ s *and*

heating along *the binodal under nanosecond irradiation. Solidification of the non-ablated,* supercooled *molten material is eventually observed on a* $\sim 10^{-11} - 10^{-9}$ s *time scale, irrespective of the pulse duration.*

PACS numbers: 79.20.Ds, 79.20.Ap, 61.80.Az

5.1 Introduction

Pulsed laser irradiation of solids, i.e., the interaction of relatively short ($\sim 10^{-13} - 10^{-8}$ s), intense ($\sim 10^{9} - 10^{14}$ W cm^{-2}) bursts of coherent and monochromatic light with surfaces, offers a unique way to perturb materials away from equilibrium (Lindenberg *et al.*, 2005; Sokolowski-Tinten *et al.*, 2003; Rousse *et al.*, 2001; Siwick *et al.*, 2003; Siders *et al.*, 1999; Sundaram and Mazur, 2002; Bloembergen, 1999): here, absorption of the photons by the valence- and conduction-band electrons sets the initial stage for a complex chain of events covering multiple length (electronic to macroscopic) and time (femtosecond to microsecond) scales (von Allmen and Blatter, 1995). In some cases, changes in the long-range order and/or state of aggregation of the material are involved: examples of structural modifications include direct solid-solid (Cavalleri *et al.*, 2001), solid-liquid (Sokolowski-Tinten *et al.*, 2001; Bucksbaum and Bokor, 1984; Thompson *et al.*, 1983), and liquid-gas (Sokolowski-Tinten *et al.*, 1998b; Zhakhovskiĭ *et al.*, 2000; Inogamov *et al.*, 1999a; Liu *et al.*, 1986; Batanov *et al.*, 1973) transitions. These, in turn, have been extensively exploited for laser processing of materials: applications range from surface micromachining (Borowiec *et al.*, 2003), cleaning (Zapka *et al.*, 1991), and annealing (Gillet *et al.*, 2005) to thin-film growth (Shinde *et al.*, 2001; Willmott and Huber, 2000) and the production of nanoparticles in vacuum (Amoruso *et al.*, 2004; Amoruso *et al.*, 2005) and aqueous solutions (Sylvestre *et al.*, 2004); lasers have also found extensive use in medicine and surgery for the manipulation and

destruction of biological tissues (Vogel and Venugopalan, 2003).

The nature of the phenomena induced by laser radiation in transparent (insulators or dielectrics) and absorbing (metals and semiconductors) solids is determined, for the most part, by the coupling of the laser parameters — pulse duration τ_L, wavelength λ_L, and energy per unit area (fluence) F — with the optical, mechanical, and thermal properties of the material. In general, the absorption of a laser pulse gives rise to a gas of hot carriers (electrons or electron-hole pairs at a temperature T_e) which, through repeated emission of phonons, heat the initially cooler ions (at a temperature T) to achieve a common equilibrium after $\tau_E \sim 10^{-12} - 10^{-11}$ s (Siegal *et al.*, 1995). This time scale has far-reaching significance. It sets a boundary between strictly thermal and possible nonthermal routes, a dividing line between "long" and "short" pulses (von der Linde *et al.*, 1997): if $\tau_L \gg \tau_E$, equilibrium between electrons and phonons prevails throughout the heating stage ($T_e \approx T$) and phase change can be regarded as a slow thermal process involving quasiequilibrium thermodynamic states; examples under nanosecond laser irradiation include *heterogeneous* melting (Fabricius *et al.*, 1986; von der Linde, 1991) and, at higher fluences, vaporization (Batanov *et al.*, 1973) at moving solid-liquid and liquid-vacuum boundaries, respectively. Under ultrashort pulses ($\tau_L \lesssim 10^{-12}$ s), however, the material is left in a highly nonequilibrium state following the deposition of the optical energy ($T_e \gg T$) (Anisimov *et al.*, 1974): in this case, the time with which a given structural modification takes place, τ_M, determines whether thermal mechanisms are involved ($\tau_M \gg \tau_E$) or not ($\tau_M < \tau_E$) (von der Linde *et al.*, 1997). In certain circumstances, there may be enough time to establish electron-phonon equilibrium but insufficient time to achieve *phase* equilibrium between the different states of aggregation ($\tau_M \approx \tau_E$) (von der Linde and Sokolowski-Tinten, 2000): here, transient, *nonequilibrium* states associated with the *homogeneous* nucleation of critical nuclei of liquid or gas in a metastable, superheated solid (Rethfeld *et al.*,

2002; Ashitkov *et al.*, 2002; Ivanov and Zhigilei, 2003a; Ivanov and Zhigilei, 2003b) or liquid (Sokolowski-Tinten *et al.*, 1998b; Zhakhovskiĭ *et al.*, 2000; Inogamov *et al.*, 1999a; Anisimov *et al.*, 1999; Cavalleri *et al.*, 1999), respectively, are likely to take part in rapid, thermal phenomena. The occurrence of long-lived, supercooled states in the melt prior to crystallization or amorphization have also been reported for pulses of femtosecond to nanosecond duration (Bucksbaum and Bokor, 1984; Wiggins *et al.*, 2004; Liu *et al.*, 1979b; Stiffler *et al.*, 1988; Larson *et al.*, 1985).

The existence of competing thermal and nonthermal channels in order-to-disorder transitions is exemplified in ultrashort-pulse laser melting of several semiconductors including indium antimonide (Rousse *et al.*, 2001), germanium (Siders *et al.*, 1999; Sokolowski-Tinten *et al.*, 2001), gallium arsenide (Huang *et al.*, 1998; Saeta *et al.*, 1991; Sokolowski-Tinten *et al.*, 1995), and silicon (Shank *et al.*, 1983b; Sokolowski-Tinten *et al.*, 1995; Silvestrelli *et al.*, 1996). On the one hand, if a threshold number of strong, directional, covalent bonds are broken or, equivalently, if the number of electrons that have been promoted from bonding (valence) to antibonding (conduction) states reaches a critical density $N_c \approx 10^{22}$ cm^{-3} (Sokolowski-Tinten and von der Linde, 2000; Stampfli and Bennemann, 1994), the tetravalent lattice collapses to a sixfold-coordinated[1] metallic liquid on a subpicosecond time scale, i.e., *before* carrier-phonon equilibration is achieved. At lower excitations, on the other hand, the path from solid to liquid is presumably a rapid — picosecond — thermal process, i.e., slower than ultrafast nonthermal disordering but significantly faster than heterogeneous, surface-nucleated melting (Rethfeld *et al.*, 2002; Ashitkov *et al.*, 2002). In this case, the transition to the molten state likely proceeds by homogeneous nucleation of liquid inclusions in the strongly superheated, metastable,

[1]In fact, the resulting molten structure is initially characterized by a higher coordination (between 11 and 13) and significantly reduced covalent-bonding attributes. However, this phase is only short-lived and the system rapidly assumes the usual properties of liquid silicon (Silvestrelli *et al.*, 1996).

bulk crystal.[2]

The removal of macroscopic amounts of matter at a laser-irradiated surface, i.e., laser ablation, reveals an additional battleground where thermal and nonthermal pathways collide. In transparent materials, on the one hand, high intensities commonly delivered by femtosecond pulses are normally required to excite electrons across the large band gap (Rethfeld, 2004): here, multiphoton ionization provides the initial seed electrons which later gain kinetic energy from the laser radiation to produce additional free carriers through an impact ionization, avalanche process. At irradiances above a threshold $I_{\text{break}} \sim 10^{13}$ W cm^{-2}, a direct solid-to-plasma transition follows by optical breakdown (von der Linde *et al.*, 1997; von der Linde and Schüler, 1996; Sokolowski-Tinten *et al.*, 1998a; von der Linde, 2001): the dielectric material is fully ionized into a very dense ($N \sim 10^{23}$ cm^{-3}) and hot ($T_e \sim 10^6$ K) plasma which is rapidly carried away with a velocity of $\sim 10^4 - 10^5$ m s^{-1}. Ablation following loss of charge neutrality and ion repulsion at the surface has also been reported (Stoian *et al.*, 2002; Bulgakova *et al.*, 2004; Roeterdink *et al.*, 2003).[3]

In absorbing materials, on the other hand, strong single-photon coupling of the laser field with the solid makes matter removal also achievable with femtosec-

[2]The picture of bond breaking and lattice collapse on ultrashort time scales does not apply to metals where cohesion of the close-packed structure is ensured by delocalized conduction electrons (Siwick *et al.*, 2003). Instead, melting is strictly thermal and whether the liquid phase originates from a heterogeneous or homogeneous nucleation process depends on various parameters such as pulse duration and fluence (Ivanov and Zhigilei, 2003a; Ivanov and Zhigilei, 2003b).

[3]Conflicting views regarding the relevance of Coulomb explosion to semiconductors and metals — where the higher electron mobilities and densities would ensure an effective screening of the net positive charge at the surface — can be found in the literature [STOIAN, R., ROSENFELD, A., HERTEL, I. V., BULGAKOVA, N. M., CAMPBELL, E. E. B. «Comment on "Coulomb explosion in femtosecond laser ablation of Si(111)"». *Applied Physics Letters.* 85:4 (2004). 694-695; ROETERDINK, W. G., BONN, M., KLEYN, A. W. «Response to "Comment on 'Coulomb explosion in femtosecond laser ablation of Si(111)'"». *Applied Physics Letters.* 85:4 (2004). 696-697]. Nevertheless, if nonthermal melting of a highly excited semiconductor lattice (such as silicon) can be triggered *during* the pulse using, e.g., very high intensities, one can envisage that part of the laser radiation may interact with the metallic liquid phase — with significantly lower electron mobility (Glazov and Kol'tsov, 1984) — to induce electrostatic charging and ablation at the surface (Stoian, 2004); this, however, has yet to be confirmed.

ond (Sokolowski-Tinten *et al.*, 1998b; von der Linde *et al.*, 1997; von der Linde and Sokolowski-Tinten, 2000; Cavalleri *et al.*, 1999; Sokolowski-Tinten *et al.*, 1998a; Chichkov *et al.*, 1996), picosecond (Chichkov *et al.*, 1996; Willis and Xu, 2002b; Willis and Xu, 2002a; Jandeleit *et al.*, 1996), and nanosecond (Batanov *et al.*, 1973; Chichkov *et al.*, 1996; Bulgakova and Bulgakov, 2001; Song and Xu, 1998; Yoo *et al.*, 2000) pulses at irradiances well below I_{break}.[4] In this case, significantly lower temperatures ($\sim 10^3 - 10^4$ K) and ejection velocities ($\sim 10^2 - 10^3$ m s^{-1}) reveal a strictly *thermal* ejection pathway belonging to either one or the other of the following two broad classes of mechanisms:[5] (i) *Photothermal* processes in which changes in the state of aggregation of the molten material arise from a first- (or possibly second-) order phase transition to a vapor; possible outcomes include homogeneous nucleation of gas bubbles in a metastable liquid, i.e., phase explosion or explosive boiling (Sokolowski-Tinten *et al.*, 1998b; Inogamov *et al.*, 1999a; Willis and Xu, 2002a; Bulgakova and Bulgakov, 2001; Song and Xu, 1998; Yoo *et al.*, 2000; Martynyuk, 1976; Miotello and Kelly, 1995; Zhigilei and Garrison, 2000; Perez and Lewis, 2002; Perez and Lewis, 2003; Perez and Lewis, 2004; Lorazo *et al.*, 2003; Lorazo *et al.*, 2004), phase separation of a mechanically unstable liquid by spinodal decomposition (Vidal *et al.*, 2001), and normal vaporization at the outer surface (Batanov *et al.*, 1973; Perez and Lewis, 2003; Pronko *et al.*, 1995). (ii) *Photomechanical* processes in which the breakup of the material is assisted by strong, tensile pressure waves — spallation (Zhigilei and Garrison, 2000; Perez and Lewis, 2002; Anisimov *et al.*, 2003) in solids and cavitation (Oraevsky *et al.*, 1995; Yavas *et al.*, 1994) in liquids — or involves the dissociation of a homogeneous, supercritical fluid into clusters upon dilution in vacuum — i.e., fragmentation (Perez

[4]To our knowledge, there has been no report of laser-induced optical breakdown in metals.

[5]Note that photochemical pathways involving the direct photodissociation of molecular bonds have also been proposed in organic solids [YINGLING, Y. G., GARRISON, B. J. «Photochemical induced effects in material ejection in laser ablation». *Chemical Physics Letters.* 364:3-4 (2002). 237-243].

and Lewis, 2002; Perez and Lewis, 2003; Perez and Lewis, 2004; Lorazo *et al.*, 2003; Lorazo *et al.*, 2004; Glover, 2003).

In order to explain ablation in metals irradiated by long (nanosecond) pulses, Miotello and Kelly (Miotello and Kelly, 1995; Miotello and Kelly, 1999), following previous work by Martynyuk (Martynyuk, 1976; Martynyuk, 1983; Martynyuk, 1974), have proposed a picture in which matter removal results from a phase-explosion process. The scenario, further put forward by numerous authors for femtosecond (Chen and Beraun, 2003), picosecond (Willis and Xu, 2002b; Willis and Xu, 2002a; Zhigilei and Garrison, 2000; Zhigilei *et al.*, 2003a), and nanosecond (Bulgakova and Bulgakov, 2001; Song and Xu, 1998; Yoo *et al.*, 2000) pulses, can be outlined as follows: (i) If $\tau_L \gg \tau_{\rm LV}$ — where, according to Bulgakova and Bulgakov (2001), $\tau_{\rm LV} \sim 10^{-9} - 10^{-8}$ s is the time required for a metallic liquid to achieve equilibrium with its vapor — the expanding molten material is stable and heating takes place along the liquid-vapor coexistence (saturation) line, i.e., the binodal. If $\tau_L \lesssim \tau_{\rm LV}$, however, a significant fraction of the energy is stored in the metallic melt before it can be consumed as latent heat of vaporization. In this case, the liquid attempts to equilibrate with its undersaturated vapor and its heating line lies, instead, below the binodal: the liquid is pushed into the liquid-gas regime as it is *rapidly heated* (Willis and Xu, 2002a; Bulgakova and Bulgakov, 2001; Song and Xu, 1998; Martynyuk, 1983; Miotello and Kelly, 1999). (ii) If the fluence is sufficiently high, the molten metal is superheated near the spinodal (Carey, 1992) (the limit of mechanical stability) to a temperature of $\approx 0.9T_c$ (where T_c is the thermodynamic critical temperature) (Bulgakova and Bulgakov, 2001; Song and Xu, 1998; Martynyuk, 1976; Miotello and Kelly, 1995). (iii) Nucleation and growth of gas bubbles sets in on a time scale $\tau_{\rm NUC} \sim 10^{-9} - 10^{-7}$ s (Martynyuk, 1976; Miotello and Kelly, 1995; Martynyuk, 1983; Martynyuk, 1974)[6] and the metastable

[6]In view of a number of experimental and computational studies suggesting the relevance of

mother phase is converted into a heterogeneous mixture of liquid and gas, i.e., explosive boiling occurs. The threshold nature of the ablation process, evidenced by (iv) the sharp increase in the total ablated mass (Cavalleri *et al.*, 1999; Yoo *et al.*, 2000; Cavalleri *et al.*, 1998; Xu, 2002) and (v) the onset of large, nanometer- to micron-sized, liquid-droplet ejection (Yoo *et al.*, 2000)[7] at a well-defined fluence F_{abl}, has often been ascribed to an abrupt rise in the bubble nucleation rate as the metastable liquid is heated toward the spinodal limit (Bulgakova and Bulgakov, 2001; Song and Xu, 1998; Miotello and Kelly, 1995; Zhigilei and Garrison, 2000; Kelly and Miotello, 1999; Lu *et al.*, 2002; Garrison, 2003).

However, ultrafast time-resolved microscopy experiments (Sokolowski-Tinten *et al.*, 1998b; von der Linde and Sokolowski-Tinten, 2000; Cavalleri *et al.*, 1999; Sokolowski-Tinten *et al.*, 1998a) have suggested, and various analytical (Inogamov *et al.*, 1999a; Anisimov *et al.*, 1999; Inogamov *et al.*, 1999b) and molecular-dynamics (Zhakhovskiĭ *et al.*, 2000; Perez and Lewis, 2002; Perez and Lewis, 2003; Perez and Lewis, 2004; Lorazo *et al.*, 2003; Lorazo *et al.*, 2004) calculations confirmed, that the thermal routes to ablation in absorbing solids embrace a fundamentally different, universal behavior under femtosecond laser irradiation: (i) Here, the material is initially pulled *away* from the liquid-vapor regime to a near-critical or supercritical state upon rapid, isochoric heating; the metastable region is approached, instead, as the pressurized matter adiabatically *cools* during its subsequent dilution in vacuum. (ii) In a relatively narrow range of fluences close to the ablation threshold ($1 \leq F/F_{\mathrm{abl}} \lesssim 1.5$ in Si) (Cavalleri *et al.*, 1999; Rethfeld *et al.*, 2003), expansion takes place along subcritical isentropes until the binodal is reached; very near F_{abl}, the latter is crossed at a temperature which may lie significantly below $0.9T_c$ (Lorazo *et al.*, 2003; Lorazo *et al.*, 2004). (iii) As a result of homogeneous

phase explosion to femtosecond (and picosecond) pulses, Miotello and Kelly later discarded the value of τ_{NUC} originally proposed by Martynyuk (Kelly and Miotello, 1999).

[7] See also Kelly and Miotello (1999) and references therein.

nucleation of a stable vapor phase in the metastable liquid phase, on the one hand, and a sharp drop of the sound velocity giving rise to a steep ablation front, on the other hand, the expanding material subsequently develops a bubblelike structure on a $10^{-12} - 10^{-11}$ s time scale (Sokolowski-Tinten *et al.*, 1998b; Perez and Lewis, 2003; Lorazo *et al.*, 2003): a low-density, heterogeneous, two-phase mixture between two optically flat, reflective interfaces — the nonablated matter and a thin, moving liquid shell — is expelled from the surface through a phase-explosion process. The observation of interference fringes (Newton rings) during time-resolved femtosecond laser excitation and imaging of numerous metal and semiconductor surfaces supports this scenario (Sokolowski-Tinten *et al.*, 1998b; von der Linde and Sokolowski-Tinten, 2000; Cavalleri *et al.*, 1999; Sokolowski-Tinten *et al.*, 1998a).

Upon increasing the fluence, before the onset of plasma formation in semiconductors ($1.5 \lesssim F/F_{\mathrm{abl}} \lesssim 3$ in Si) (Cavalleri *et al.*, 1999; Rethfeld *et al.*, 2003), the density profile smooths out and the interference pattern eventually vanishes as the diluting material shifts from a subcritical liquid to a supercritical fluid. In this case, fragmentation gradually takes over explosive boiling as the primary pathway to matter removal (Perez and Lewis, 2002; Perez and Lewis, 2003; Lorazo *et al.*, 2004; Glover, 2003).

Under picosecond laser irradiation, however, expansion is slower and cooling is nonadiabatic (Lorazo *et al.*, 2003; Lorazo *et al.*, 2004; Perez and Lewis, 2004): the expanding subcritical material is efficiently cooled onto the binodal by thermal conduction and phase explosion does not take place; here, the onset of (iv) ablation and (v) droplet ejection is determined, rather, by the breakup of a hot, supercritical fluid near thermodynamic equilibrium, i.e., "trivial" fragmentation. This points to a shorter liquid-vapor equilibration time $\tau_{\mathrm{LV}} \sim 10^{-11} - 10^{-10}$ s and, consequently, a heating process *along* the binodal under nanosecond pulses.

In spite of recent advances, a thorough understanding of the changes in long-range order and state of aggregation induced in solids by laser radiation has yet to come. From a thermodynamic standpoint, the transient, superheated and supercooled states involved in, e.g., the rapid melting and solidification of the irradiated material, respectively, are difficult to assess experimentally. From a kinetic viewpoint, the dynamics of void nucleation and the puzzling nature of the ablation threshold under pulsed laser irradiation can directly be addressed at atomic-to-mesoscopic scales by computational means.

In this paper — which follows preliminary results presented elsewhere (Lorazo *et al.*, 2003; Lorazo *et al.*, 2004) — we report on the structural modifications induced in silicon by 500 fs and 100 ps laser pulses. We explore the *thermal* regime where the laser field acts as a fast heat source and the heated material obeys the laws of thermodynamics and hydrodynamics of fluids. As detailed in section 5.2, this is achieved on a nanosecond time scale by coupling carrier and atom dynamics within a combined Monte Carlo (MC) and molecular-dynamics (MD) scheme, and simultaneously pursuing the time evolution of the irradiated matter in density-temperature-pressure (ρ-T-P) space during heating, expansion, and cooling. The thermal pathways observed in the femtosecond and picosecond regimes are discussed in sections 5.3 and 5.4, respectively: in each case, the routes to melting, ablation, and solidification are identified; in particular, the nature of the ablation threshold under ultrashort-pulse irradiation is carefully examined in section 5.3.3. A unified picture of the thermodynamic pathways available to the irradiated material under femtosecond to nanosecond pulses finally emerges in section 5.4.3.

5.2 Computational scheme

5.2.1 Combined MC and MD model

A schematic illustration of the model is displayed in figure 5.1. We give here a rapid overview of its most important features; full details are provided in sections 5.2.1.1 to 5.2.1.4.

In most cases of interest to the present study, part of the silicon target melts during the pulse. As a result, a significant number of photons (yellow arrows) incident along the z axis (normal to the initial surface) are absorbed by conduction electrons (white disks) in the *metallic* liquid layer (red atoms) at the surface (marked A); if ablation takes place, absorption may also occur in the expanding plume (see section 5.2.1.1). The deposited energy is subsequently shared among other carriers and ions: in accordance with a standard MC procedure, the Drudelike carriers undergo ballistic transport between two successive collisions which instantaneously change their velocity and energy but not their position. Upon emission of a phonon (green wavy arrow), an electron is scattered in a new direction (chosen at random) with a velocity reduced in a way that reflects the corresponding loss of kinetic energy — cf. change in orientation and length of the white arrow (B); other collisions in the melt involve energy exchange upon carrier-carrier scattering (C). In the crystalline, semiconducting bulk (green atoms), the absorption of a photon usually leads to the creation of an electron and hole (black disk) with different initial velocities and energies (D); collisional processes include scattering with carriers and phonons, Auger recombination, and impact ionization (not shown). Atom dynamics are treated using classical MD: depending on the fluence, melting of the silicon crystal, ejection of liquid material, and solidification of the nonablated, molten matter may take place on mesoscopic-length and picosecond-to-nanosecond-time

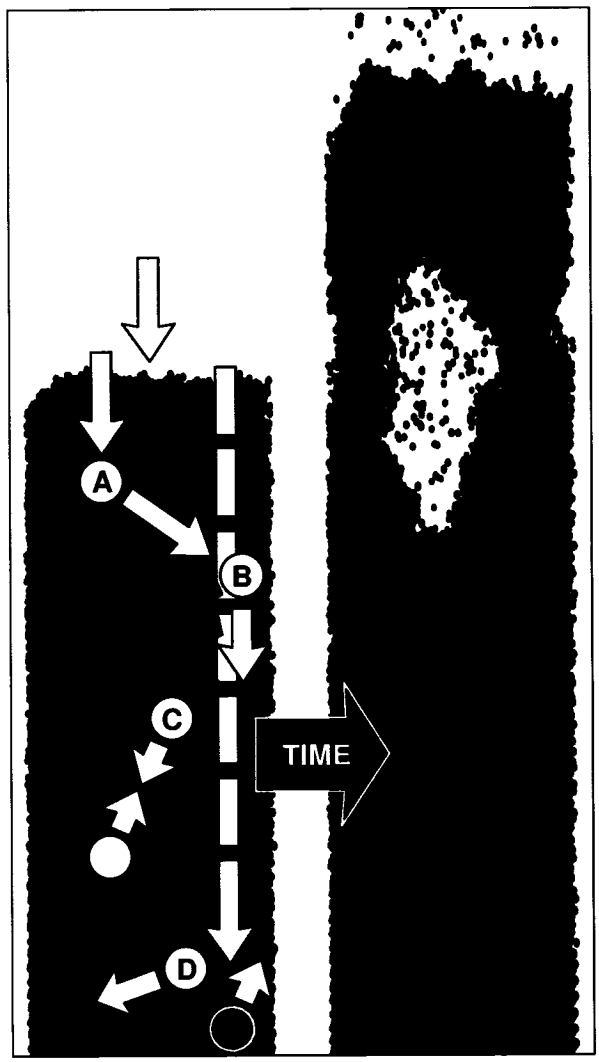

Figure 5.1 Schematic view of the combined MC and MD model for silicon. Left: absorption of the photons and carrier scattering processes. Right: growth of a relatively large cavity prior to the ejection of hot, molten material. Red spheres: atoms belonging to the (metallic) liquid phase; green spheres: atoms belonging to the (semiconducting) crystalline phase; yellow arrows: photons; white disks: conduction electrons; black disk: conduction hole; green wavy arrow: phonon; white arrows: carrier motion (direction and velocity). Capital letters refer to specific absorption and scattering events. See text for full details.

scales. We expect that the general features of our model also apply to other group IV (as well as III-V) semiconductors, also characterized by a metallic liquid phase.

5.2.1.1 Laser pulse and absorption processes

The laser pulse having a duration $\tau_L = 500$ fs or 100 ps (FWHM) and a wavelength $\lambda_L = 266$ nm is Gaussian in time but spatially uniform. It is modeled by successive groups of photons with energy $\hbar\omega_L = 4.66$ eV which couple to "carriers" over a penetration depth of $\approx 5 - 10$ nm (in both c-Si and l-Si). As briefly mentioned above and detailed below, a carrier is a particle (electron or hole) which follows Drude dynamics while undergoing various scattering events, each with its own characteristic collision time.

The photons are absorbed following Beer's law, i.e., with a cumulative probability decreasing exponentially with depth. In practice, we proceed as follows: (i) The supercell (simulation box) is first divided in small cubic cells of side $\ell_c = 5$ Å. (ii) The instantaneous, *local* absorption coefficient $\alpha_i = \alpha(\mathbf{r}_i, t)$ and (normal-incidence) reflectivity $R_i = R(\mathbf{r}_i, t)$ in each cell i (centered at $\mathbf{r}_i$) are then defined as (Bassani and Pastori Parravicini, 1975)

$$\alpha_i = \alpha_{\rm vc}(\epsilon_i^*) + \alpha_{\rm fcr}(\epsilon_i^*) = \frac{2\pi}{n(\epsilon_i^*)\lambda_L}{\rm Im}\{\epsilon_i^*\} \tag{5.1}$$

and

$$R_i = \frac{[n(\epsilon_i^*) - 1]^2 + k^2(\epsilon_i^*)}{[n(\epsilon_i^*) + 1]^2 + k^2(\epsilon_i^*)}, \tag{5.2}$$

where the *total* refractive index $n(\epsilon_i^*)$ and extinction coefficient $k(\epsilon_i^*)$ of the excited material are obtained from the instantaneous, *local*, complex permittivity (Sokolowski-

Tinten and von der Linde, 2000)

$$\epsilon_i^* = \epsilon_{\rm vc}^*(T_i) + \epsilon_{\rm fcr}^*(N_i). \tag{5.3}$$

Here, the first term accounts for the single-photon,[8] valence-to-conduction (interband) transitions in the unexcited semiconducting crystal at a temperature $T_i = T(\mathbf{r}_i, t)$[9] and with band-gap energy $E_{g,i} = E_g(T_i, N_i) \lesssim 1.12$ eV (van Driel, 1987). The second term describes the changes to ϵ_i^* resulting from the free-carrier (intraband) transitions taking place in the Drude electron gas with density $N_i = N(\mathbf{r}_i, t)$ (Sokolowski-Tinten and von der Linde, 2000).[10,11] In the solid, the latter contribution becomes significant at electron densities exceeding the critical plasma density $N_{\rm cr}$ ($\approx 5.9 \times 10^{21}$ cm^{-3} in c-Si at 266 nm) (Sokolowski-Tinten and von der Linde, 2000); in the metallic liquid, $\epsilon_{\rm fcr}^*$ represents the *total* optical response which is assumed to be purely Drudelike (Li and Fauchet, 1987; Gantner *et al.*, 1995). (iii) The in-plane x and y coordinates of each photon are subsequently chosen at random; in each case, this determines a column of cells along the z axis which are successively visited starting from the top of the supercell. (iv) In a cell i at an interface separating a gaseous phase from a dense, solid or liquid material — such as the surface of the target or of a cluster in the plume (see below for a definition

[8] In the present study, the optical response of the irradiated material is dominated by linear processes and multiphoton transitions are ignored. This can be justified by estimating the value of $G_{12}(\mathbf{r}_i, t) = (1 - R_i) I(\mathbf{r}_i, t) \beta(\mathbf{r}_i, t) / (2\alpha_i)$ which expresses the local ratio of the two-photon to the one-photon interband transition rates in the crystalline, semiconducting phase (van Driel, 1987). With $R_i \approx 0.7$ and $\alpha_i \approx 2 \times 10^6$ cm^{-1} (Sun *et al.*, 1997), $\beta(\mathbf{r}_i, t) \lesssim 40$ cm GW^{-1} the two-photon absorption coefficient (Murayama and Nakayama, 1995), and an irradiance $I(\mathbf{r}_i, t) \lesssim 10^{12}$ W cm^{-2} (see section 5.3), we have that $G_{12} \lesssim 10^{-3}$.

[9] The temperature dependence of $\epsilon_{\rm vc}^*$ has been obtained from a fit to the experimental data by Sun *et al.* (1997).

[10] The overall changes to the dielectric constant due to state-and-band filling and band-structure renormalization are relatively small and are consequently neglected (Sokolowski-Tinten and von der Linde, 2000).

[11] A Drude damping time $\tau_D = 10$ fs and an optical effective mass $m_{\rm opt}^* = (m_e^{*-1} + m_h^{*-1})^{-1} = 0.375 m_e$ [where the electron and hole mobility effective masses m_e^* and m_h^* are equal to $0.75 m_e$ (see section 5.2.1.1)] are used in the solid phase, irrespective of the pulse duration; the values of τ_D and $m_{\rm opt}^*$ in the liquid phase have been taken from Li and Fauchet (1987).

of the gaseous and dense phases), the photon is reflected (and afterwards ignored) with a probability R_i. However, it is absorbed with a probability $1 - \exp(-\alpha_i \ell_c)$ if the material is locally dense: in the crystal, interband and intraband transitions take place with relative probabilities proportional to the ratio of the respective absorption coefficients $\alpha_{\rm vc}/\alpha_{\rm fcr}$; in the liquid, photons couple to conduction electrons via intraband transitions (inverse bremsstrahlung). Photoelectric emission is neglected.[12]

As suggested above, this approach relies on the *local* properties of the material; among other benefits, it allows to directly account for the screening of the laser radiation by the plume produced by relatively long, picosecond pulses (see section 5.4).

Upon interband excitation of one of the (originally four) valence electrons of the atom with position $\mathbf{r}_0$ nearest to $\mathbf{r}_i$, an electron-hole pair is created with total kinetic energy $\hbar\omega_L - E_{g,i}$: each carrier is initially assigned position $\mathbf{r}_0$, velocity $\mathbf{v}_0$ (in a random direction), and kinetic energy $E_k(v_0) = m^* v_0^2/2$, where the effective mass $m^* = 0.75 m_e$ (the only free parameter in the model) is chosen so as to reproduce the experimental threshold fluence for melting under a laser pulse with $\lambda_L = 266$ nm and $\tau_L = 15$ ps (Malvezzi *et al.*, 1984); in the liquid, an effective mass $m^* = 1.75 m_e$ is used (m_e is the free-electron mass) (Glazov and Kol'tsov,

[12]This is based upon the following two observations: (i) Because single-photon processes govern the optical response of the material (see footnote 8), conduction-band electrons are initially generated in the crystal with a maximum kinetic energy $\hbar\omega_L - E_g \approx 3.5$ eV which is below the minimum energy required to escape the solid — as given by the electron affinity $\chi \approx 3.7$ eV [GOLDMAN, J. R., PRYBYLA, J. A. «Ultrafast dynamics of laser-excited electron distributions in silicon». *Physical Review Letters.* 72:9 (1994). 1363-1367]. (ii) A photon may excite a *conduction* electron above the vacuum level (since $\hbar\omega_L > \chi$), thus leaving the surface with a net positive charge; at sufficiently high irradiances, this could lead to space-charge effects which are not accounted for by our model. However, recent experiments and calculations have shown that such a positive charge would be rapidly balanced out by the diffusion of electrons from the bulk (Stoian *et al.*, 2002; Bulgakova *et al.*, 2004). The same reasoning applies to thermionic emission which is also neglected.

1984). In the case of an intraband transition, the energy of the carrier closest to $\mathbf{r}_i$ is increased by an amount $\hbar\omega_L$. Note that carriers may absorb more than one photon during their lifetime.

5.2.1.2 Carrier dynamics

The hot electrons and holes subsequently relax through a cascade of collisional events involving multiple scattering processes (Sundaram and Mazur, 2002; von Allmen and Blatter, 1995; Siegal *et al.*, 1995; van Driel, 1987). This is simulated using a standard MC approach (Lundstrom, 2000; Jacoboni and Reggiani, 1983). At every MC (or equivalently MD) time step of duration $\Delta t = 1$ fs, a carrier, after traveling a distance $v\Delta t$, has a probability $1 - \exp(-\Gamma_0 \Delta t)$ of suffering a collision which instantaneously changes its velocity and energy but not its position. Here, $\Gamma_0 = 1/\tau_0 = (1 \text{ fs})^{-1}$ is chosen so that, at all times,

$$\Gamma(E_k) = \sum_j \Gamma_j(E_k) = \sum_j 1/\tau_j(E_k) \leq \Gamma_0, \tag{5.4}$$

where the carrier instantaneous (and energy-dependent) collisional rate $\Gamma(E_k)$ involves a sum over all physically relevant scattering mechanisms, each characterized by a collision time τ_j. (A fictitious self-scattering mechanism is added to ensure a fixed total scattering rate equal to Γ_0). Upon the occurrence of a collision, a scattering event j with probability τ_0/τ_j is chosen at random: if appropriate, the carrier kinetic energy is updated and its velocity adjusted accordingly [in both magnitude and (randomly chosen) direction]; in certain circumstances, the carrier may, instead, annihilate (Auger recombination) or new particles may additionally be created (impact ionization). Table 5.1 summarizes the various collisional processes and respective scattering times used.

Tableau 5.1 Carrier scattering processes and related collision times in solid and liquid silicon; when τ is a function of the carrier energy, references are given instead.

Scattering mechanism	τ (c-Si)	τ (l-Si)
Carrier-carrier[13]	10 fs	10 fs
Carrier-phonon	(see references)[14]	10 fs[15]
Auger recombination	≥ 6 ps[16]	...
Impact ionization	(see references)[17]	...

Carrier-carrier scattering allows electrons and holes to exchange energy over a radius of 5 Å. Heating, and eventually local thermal equilibrium at a common electron [$T_{e,i} = T_e(\mathbf{r}_i, t)$] and ion temperature, is achieved through scattering of carriers with (longitudinal-optical) phonons: if $T_{e,i} > T_i$, a quantum of energy of 62.6 meV (Lundstrom, 2000) (c-Si) or 50 meV (l-Si) is given to the nearest atom by adding an appropriate component to its velocity in a random direction.[18] In the crystal, additional collisional processes include Auger recombination and impact ionization: in the former case, the sum of $E_{g,i}$ and the kinetic energy of the recombining electron and hole (near an atom with at least one missing valence electron) is transferred to a neighboring carrier; in the latter case, the energy of the secondary electron and hole generated at $\mathbf{r}_0$ (where $\mathbf{r}_0$ is the position of the impacted atom with at least one valence electron) is computed from the primary carrier energy (Kamakura *et al.*, 1994; Kunikiyo *et al.*, 1996). Thermionic emission

[13]See von Allmen and Blatter (1995) and Siegal *et al.* (1995).

[14]FISCHETTI, M. V., LAUX, S. E. «Monte carlo analysis of electron transport in small semiconductor devices including band-structure and space-charge effects». *Physical Review B.* 38:14 (1988). 9721-9745; FISCHETTI, M. V., LAUX, S. E., CRABBÉ, E. «Understanding hot-electron transport in silicon devices: Is there a shortcut?». *Journal of Applied Physics.* 78:2 (1995). 1058-1087.

[15]Typical value for metals [EESLEY, G. L. «Generation of nonequilibrium electron and lattice temperatures in copper by picosecond laser pulses». *Physical Review B.* 33:4 (1986). 2144-2151].

[16]YOFFA, E. J. «Dynamics of dense laser-induced plasmas». *Physical Review B.* 21:6 (1980). 2415-2425; DZIEWIOR, J., SCHMID, W. «Auger coefficients for highly doped and highly excited silicon». *Applied Physics Letters.* 31:5 (1977). 346-348.

[17]See Kamakura *et al.* (1994) and Kunikiyo *et al.* (1996).

[18]In the present model, carriers are not allowed to absorb phonons.

is neglected.[19,20]

As pointed out earlier, silicon, like other group IV and III-V semiconductors, is metallic in the liquid state (Li and Fauchet, 1987; Gantner *et al.*, 1995; Godlevsky *et al.*, 1998): upon melting, the average coordination increases from 4 to 6 (and the density from 2.30 to 2.53 g cm^{-3}) (Glazov *et al.*, 1969) while the electron density jumps to $\approx 2 \times 10^{23}$ cm^{-3}. In our model, the transition from the solid semiconductor to the liquid metal is simulated by locally promoting to the conduction band (with zero initial kinetic energy) the remaining valence electrons of each and every atom which has migrated to the liquid phase; the reverse procedure is carried out upon crystallization. An approach based on a topological analysis of the structure, whereby the diamond elementary building blocks of the silicon crystal are identified, is used to distinguish the periodic solid from the disordered melt (Beaucage and Mousseau, 2005a). Finally, note that the difference in band-gap energy between the solid and liquid phases acts as a potential barrier which prevents the carriers from diffusing from the latter to the former.

5.2.1.3 Atom dynamics

The motion of the atoms is described using standard MD methodology, excellent accounts of which can be found in the literature (Allen and Tildesley, 1987). The

[19] See footnote 12.

[20] Other phenomena, such as possible screening of the electron-phonon interaction [YOFFA, E. J. «Screening of hot-carrier relaxation in highly photoexcited semiconductors». *Physical Review B.* 23:4 (1981). 1909-1919; SJODIN, T., PETEK, H., DAI, H.-L. «Ultrafast Carrier Dynamics in Silicon: A Two-Color Transient Reflection Grating Study on a (111) Surface». *Physical Review Letters.* 81:25 (1998). 5664-5667], recombination at surface trap states [HALAS, N. J., BOKOR, J. «Surface Recombination on the Si(111) 2 x 1 Surface». *Physical Review Letters.* 62:14 (1989). 1679-1682], many-body effects [YOUNG, J. F., VAN DRIEL, H. M. «Ambipolar diffusion of high-density electrons and holes in Ge, Si, and GaAs: Many-body effects». *Physical Review B.* 26:4 (1982). 2147-2158], electron confinement due to band-gap shrinkage (Siegal *et al.*, 1995), and scattering by ionized impurities or plasmons (Lundstrom, 2000), are ignored for simplicity.

silicon ions interact via the Stillinger-Weber (SW) potential (Stillinger and Weber, 1985) which exhibits elastic (Noya *et al.*, 1996; Cowley, 1988), vibrational (Noya *et al.*, 1996; Broughton and Li, 1987), triple-point (Broughton and Li, 1987; Abraham and Broughton, 1986), and liquid (Stillinger and Weber, 1985; Balamane *et al.*, 1992) properties in good agreement with experiment. It also predicts a first-order transition from a fragile, dense liquid to a strong, low-density and near-tetrahedral, supercooled liquid which could act as a precursor to the ubiquitous solid, amorphous phase in a subsequent glass transition (Sastry and Angell, 2003; Beaucage and Mousseau, 2005b). Note, however, that the liquid-liquid transition is observed at a temperature of $\approx$ 1060 K, i.e., significantly below that at which the "liquid-amorphous" transition is usually assumed to occur ($\approx$ 1450 K) (Luedtke and Landman, 1989); possible consequences of a lower liquid-to-amorphous transition temperature on the solidification dynamics are discussed in section 5.3.1.3.

Note also that the empirical SW potential cannot account for ultrafast, nonthermal phenomena induced in silicon by ultrashort pulses. In the present study, all simulations are carried out well below the threshold for plasma formation but, in some cases, above that for electronically induced melting of a strongly excited covalent solid. However, it should be pointed out that: (i) The "cold" liquid thus obtained is only short-lived and rapidly assumes the usual properties of molten silicon; in this context, it is not likely to influence the ablation and solidification processes taking place on longer time scales. (ii) The observed characteristic time for *thermal* melting under femtosecond irradiation (sufficiently far from the melting threshold) being comparable — albeit slightly longer — to that anticipated for a nonthermal disordering process (see section 5.3.1.1), coupling of the laser energy with the irradiated material is not expected to differ significantly in the two cases. Consequently, we expect our simulations to provide a complete, valid picture of the possible thermal routes and related time scales.

5.2.1.4 Simulation setup

Two Si(100) slabs, consisting of 142560 ($10\times10\times30$ nm^3) and 165600 ($8\times8\times50$ nm^3) atoms embedded into a much larger supercell, are used for pulse durations of 500 fs and 100 ps, respectively. Periodic boundary conditions are applied in the x and y directions. In the z direction, normal to the surface, we proceed as follows: (i) To simulate heat diffusion into an infinite bulk, the crystal is terminated by a Langevin heat bath (Allen and Tildesley, 1987). (ii) To mimic the propagation of pressure waves beyond the bottom of the supercell, a single atomic layer, to which an appropriate set of forces are applied, is added (Zhigilei and Garrison, 2000). The originally crystalline substrates are initially equilibrated at $\rho = 2.33$ g cm^{-3}, $T = 300$ K, and zero pressure.

5.2.2 Thermodynamic-analysis method

Insight into the *thermal* pathways to melting, ablation, and solidification under pulsed laser irradiation can be obtained provided the following two conditions are met: (i) The elementary features of the silicon phase diagram are adequately described by the SW potential (see section 5.2.2.2). (ii) The structural modifications take place under *local* equilibrium between electrons and ions: apart from the possible nonthermal disordering of covalent semiconducting crystals by ultrashort pulses, recent experiments (Sokolowski-Tinten *et al.*, 1998b; von der Linde and Sokolowski-Tinten, 2000; Cavalleri *et al.*, 1999) confirm that, below the threshold for plasma formation, absorbing solids evolve thermally on picosecond and longer time scales.

The fulfillment of a local (thermal) equilibrium does not imply, however, that equilibrium between the different — solid, liquid, and gaseous — states of aggregation

has been achieved on mesoscopic and macroscopic length scales (von der Linde and Sokolowski-Tinten, 2000); in fact, highly transient, nonequilibrium states of matter may develop under femtosecond and picosecond laser irradiation (Rethfeld *et al.*, 2002; Sokolowski-Tinten *et al.*, 1998b; Wiggins *et al.*, 2004). In this regard, we show in sections 5.3 and 5.4 that, by judiciously combining a visual analysis with a thermodynamic description of the irradiated material, metastable states, such as superheated solids or liquids and supercooled melts, can be identified; by further ascertaining where, in the phase diagram, voids begin to develop in the expanding material, we demonstrate that the mechanisms of matter removal can also be determined. This is accomplished using a method first introduced by Perez and Lewis (2002) and discussed at length elsewhere (Perez and Lewis, 2003).

5.2.2.1 Computation of local thermodynamic states

As noted above, it is reasonable to assume that most of the system evolution occurs under conditions of local equilibrium between electrons and phonons. In this context, the different routes to changes in long-range order and state of aggregation may be described — provided the system is not too far from thermodynamic equilibrium — as a succession of states in ρ-T-P space; this sequence of states will be referred to as the "trajectory" of the system.

In the present study, the density, temperature, and pressure for various sections of the target are obtained at regular intervals in time and the result mapped onto the equilibrium phase diagram of the material (see below). In practice, the target is initially divided (along the z axis) into five-atomic-layer-thick "slices". The following procedure is subsequently carried out at selected points in time: (i) The atoms belonging to the dense (solid or liquid) and gaseous phases — where the latter includes all clusters consisting of 10 atoms or less — are first identified using

the Hoshen-Kopelman algorithm (Hoshen and Kopelman, 1976); here, the clustering radius is chosen as the mean interatomic distance in a *homogeneous* system with critical-point density $\rho_c = 0.76$ g cm^{-3}, i.e., 3.45 Å. (ii) The supercell is then divided into small cells of side $\ell_c \approx 0.5$ Å, for each of which the closest atom is identified: by summing the volumes of all cells associated with a given atom, an atomic "volume" may, in this way, be defined; in the limit $\ell_c \to 0$, this is equivalent to a tessellation of space into Voronoi polyhedra (Perez and Lewis, 2003). (iii) In the specific case of the dense phase, the *surface* atoms, i.e., located in the vicinity of voids, are further distinguished from *volumic*, bulk atoms by having at least one cell distant by more than $r_c = 3.77$ Å, where r_c is the SW potential cutoff radius (Stillinger and Weber, 1985); the latter value ensures that no voids are detected in a *homogeneous* system with density $\rho \leq \rho_c$. (iv) A cell belonging to an atom in the gas phase, or distant from an atom in the dense material by more than r_c, is attributed to voids: by later making use of the Hoshen-Kopelman algorithm, the number of internal voids, as well as their respective volumes, can be assessed. (Two cells are assumed to be connected if adjacent to one another). An example of nucleation of a large cavity in a superheated liquid below the ablation threshold under femtosecond irradiation (see section 5.3.3) is depicted in figure 5.2: surface atoms surrounding the void (in green) are shown in red; gas-phase atoms — above the outer surface atoms also in red — are displayed in yellow. (v) The density, temperature, and pressure associated with the condensed and gaseous phases are finally obtained in each slice as detailed by Perez and Lewis (2003), and the result assigned to dense and gas "branches", respectively; a third, macroscopic branch providing an overall — averaged over the slice — view of the local thermodynamic state of the system is also computed.

In principle, a thermodynamic picture involving the phase diagram is strictly valid for processes taking place at or very near equilibrium. As mentioned earlier, how-

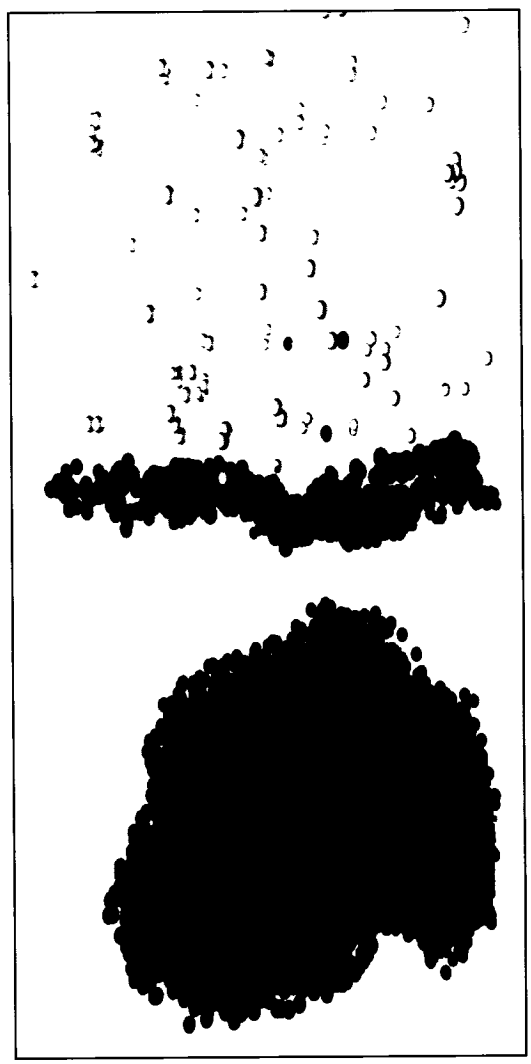

Figure 5.2 Identification of surface atoms (red), gas-phase atoms (yellow), and internal voids (green). Atoms belonging to the dense, volumic phase are not shown for clarity. See text for details.

ever, transient, metastable states of matter may be identified by combining a visual analysis with the computed local thermodynamic states of the system: e.g., a perfectly ordered crystal above the equilibrium melting temperature T_m and a *homogeneous* liquid below the binodal (see below) indicate superheated solid and liquid states, respectively; similarly, a disordered, liquid structure at a temperature below T_m is associated with nonequilibrium, supercooled states of rapidly cooled matter. In addition, the mechanisms leading to ablation can be inferred by determining where, in the phase diagram, void nucleation — which causes the average and condensed branches to split — takes place.

As shown in sections 5.3 and 5.4, this method constitutes a simple, yet powerful, tool for probing the thermodynamic states induced in a solid by laser irradiation.

5.2.2.2 Phase diagram of silicon

The phase diagram of SW silicon is shown in figure 5.3. The binodal has been taken from Broughton and Li (1987) and Honda and Nagasaka (1999). The triple line at the equilibrium melting temperature $T_m = 1691$ K (near the experimental value of 1683 K) and the solid-vapor coexistence curve have been obtained from Broughton and Li (1987). The solid-liquid coexistence regime is bounded by a low- and a high-density branch (which meet the triple line at 2.28 and 2.45 g cm^{-3}) (Abraham and Broughton, 1986): while the latter could be deduced from the difference in coordination with the neighboring (sixfold-coordinated) liquid region, the former has been approximated by a line parallel to the high-density boundary (Moran and Shapiro, 2000). The critical isobar and isotherm have been inferred from isochoric-isothermal and isochoric-isobaric MD simulations, respectively. The spinodal and the critical point at $\rho_c = 0.76$ g cm^{-3}, $T_c = 7925$ K, and $P_c = 185$ MPa have been reproduced from Makhov and Lewis (2003).

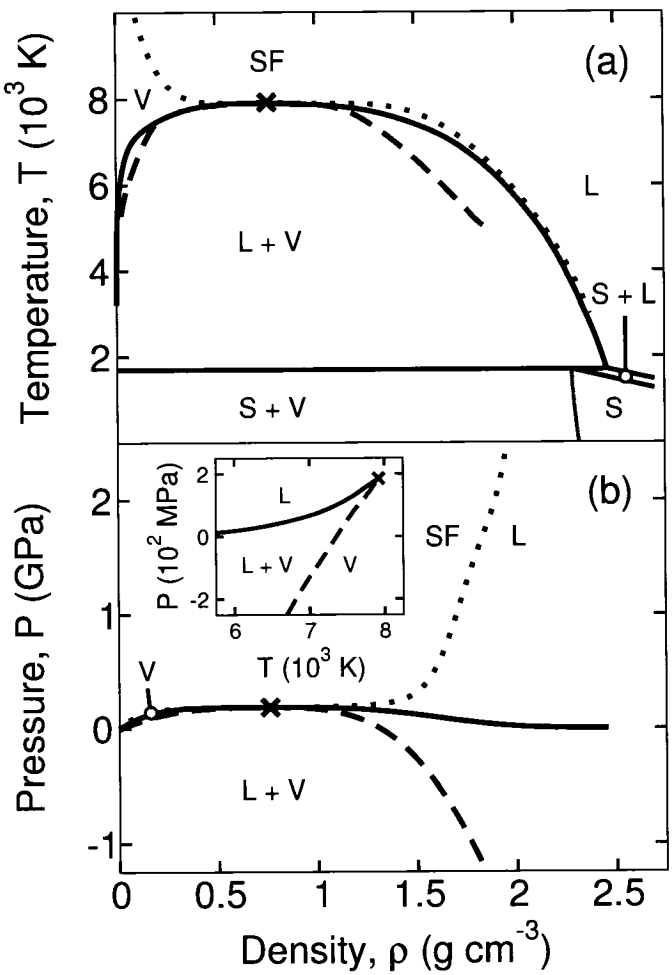

Figure 5.3 Phase diagram of silicon: (a) ρ-T plane; (b) ρ-P plane; inset: T-P plane. Black solid line: binodal (liquid-vapor coexistence); blue: triple line (solid-liquid-vapor coexistence); green: solid-vapor coexistence line; red: solid-liquid coexistence lines; dotted line: critical isobar and isotherm; dashed line: spinodal; cross: critical point. S: solid; L: liquid; V: vapor; SF: supercritical fluid ($T > T_c$ and $P > P_c$). See text for details.

Note that: (i) A liquid undergoing expansion may transiently penetrate into the metastable region (between the binodal and the spinodal) in a homogeneous state; from a thermodynamic standpoint, large, localized, thermal fluctuations — or, as shown in section 5.3.3, the direct conversion of mechanical energy into surface energy — will then favor the widespread, simultaneous nucleation of gas bubbles in the metastable liquid phase, i.e., explosive boiling, on a time scale which varies strongly with the degree of superheating (Sokolowski-Tinten *et al.*, 1998b). (ii) In the region below the spinodal, a homogeneous system is mechanically unstable against small perturbations $[(\partial P/\partial \rho)_T > 0]$: here, the liquid-to-gas transition is described, rather, by a spinodal decomposition process (Koch *et al.*, 1983). (iii) Upon entrance into the liquid-vapor (and solid-vapor) regime, the sound velocity $[c^2 = (\partial P/\partial \rho)_S$ where S denotes the entropy] decreases sharply (typically down to a few meters per second) (Sokolowski-Tinten *et al.*, 1998b; Perez and Lewis, 2003); as discussed in section 5.3, this is of great significance for the mechanisms of matter removal. (iv) The above phase diagram possesses the essential features which are relevant to a satisfactory qualitative description of group IV and III-V semiconducting materials (Moran and Shapiro, 2000). In particular, it correctly accounts for the increase in density upon melting (provided heating is carried out at a sufficiently slow rate); this is distinct from the case of, e.g., metals (Moran and Shapiro, 2000; Lorazo *et al.*, 2004). In this view, we expect that the general conclusions drawn in this study also apply to other covalent semiconductors.

5.3 Thermodynamics under femtosecond laser irradiation

The modifications to long-range order and state of aggregation observed in this study for both femtosecond and picosecond pulses are summarized in figure 5.4 and discussed at length in the following sections: (i) Under femtosecond irradi-

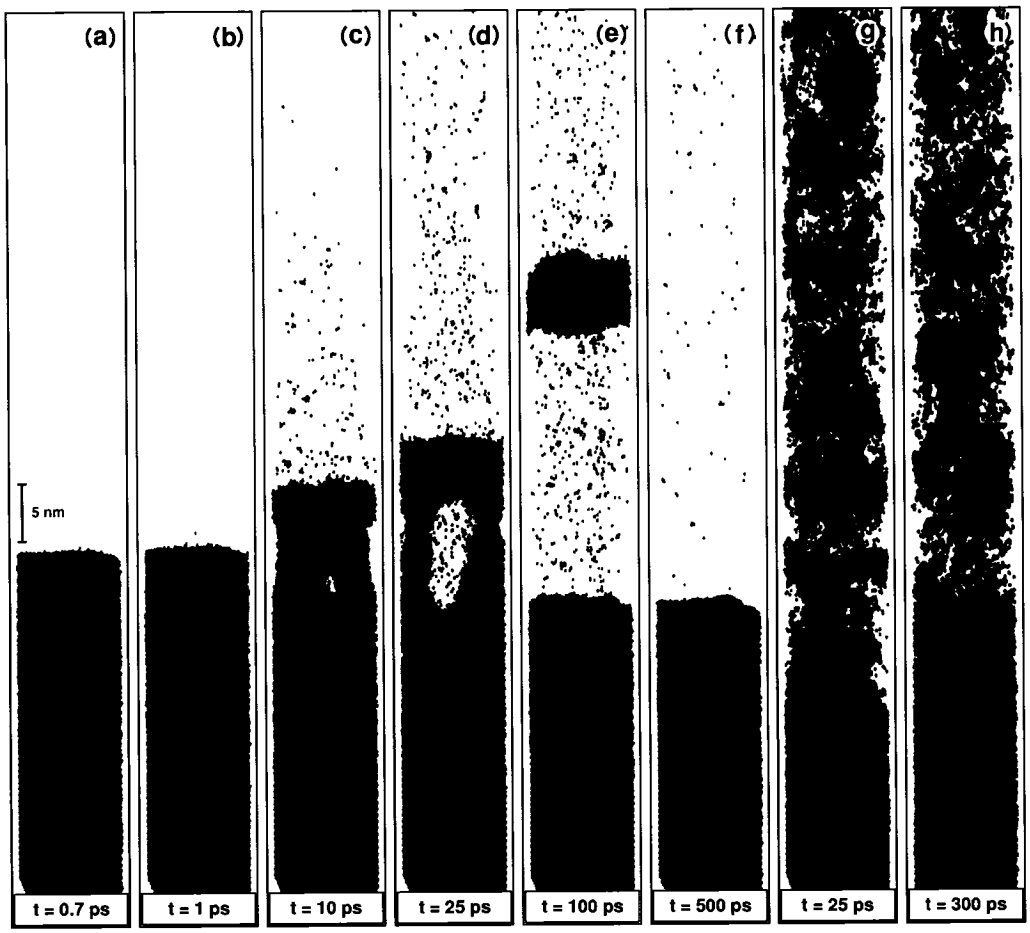

Figure 5.4 Snapshots revealing the structural changes induced in a Si(100) substrate by 500 fs and 100 ps pulses at 266 nm: (a)-(f) 500 fs pulse at a fluence $F = F_{\rm th}^{\rm fs} = 0.225$ J cm^{-2}; (g) 500 fs pulse at a fluence $F = 2.2F_{\rm th}^{\rm fs} = 0.50$ J cm^{-2}; (h) 100 ps pulse at a fluence $F = 1.1F_{\rm th}^{\rm ps} = 0.45$ J cm^{-2}; $F_{\rm th}^{\rm fs}$ and $F_{\rm th}^{\rm ps}$ are the ablation thresholds under femtosecond and picosecond irradiation, respectively. Green: (semiconducting) crystalline silicon; red: (metallic) liquid silicon. Each pulse begins at $t = 0$.

ation near the ablation threshold, on the one hand, rapid ($\lesssim 10^{-12}$ s), thermal melting of the excited semiconducting crystal is followed by the expansion of an inhomogeneous, bubble-filled, metallic melt between two well-defined interfaces and the expulsion of a few-nanometer-thick liquid shell, i.e., phase explosion, in a time of $\sim 10^{-12} - 10^{-10}$ s [figures 5.4(a)-5.4(e)]; solidification of the nonablated molten material subsequently takes place on a $10^{-11} - 10^{-9}$ s time scale [figure 5.4(f)]. (ii) At higher fluences or longer (picosecond) pulse durations, on the other hand, the ejected matter exhibits, instead, a diffuse, clusterlike structure [figures 5.4(g) and 5.4(h)]: here, the breakup of the expanding liquid metal follows, rather, from a fragmentation process.

The remainder of this paper is devoted to a thorough analysis of the transient thermodynamic states available to the irradiated material under femtosecond and picosecond pulses. We begin with the thermal routes to melting, ablation, and solidification under ultrashort-pulse laser irradiation.

5.3.1 Near-threshold ablation

Figures 5.4(a)-5.4(f) portray the various morphological changes taking place during and after irradiation with a 500 fs pulse at the threshold fluence for ablation $F_{\text{th}}^{\text{fs}} = 0.225$ J cm^{-2}. The average irradiance is 5×10^{11} W cm^{-2}, i.e., well below I_{break}. The threshold fluence for melting is equal to 0.05 J cm^{-2}.

5.3.1.1 Heating and melting

A typical thermodynamic trajectory for a region of the target originally near the surface is depicted in figure 5.5. The starting point is a crystal at $\rho_0 = 2.33$ g cm^{-3}, $T = 300$ K, and zero pressure (marked A). The photons initially generate electron-

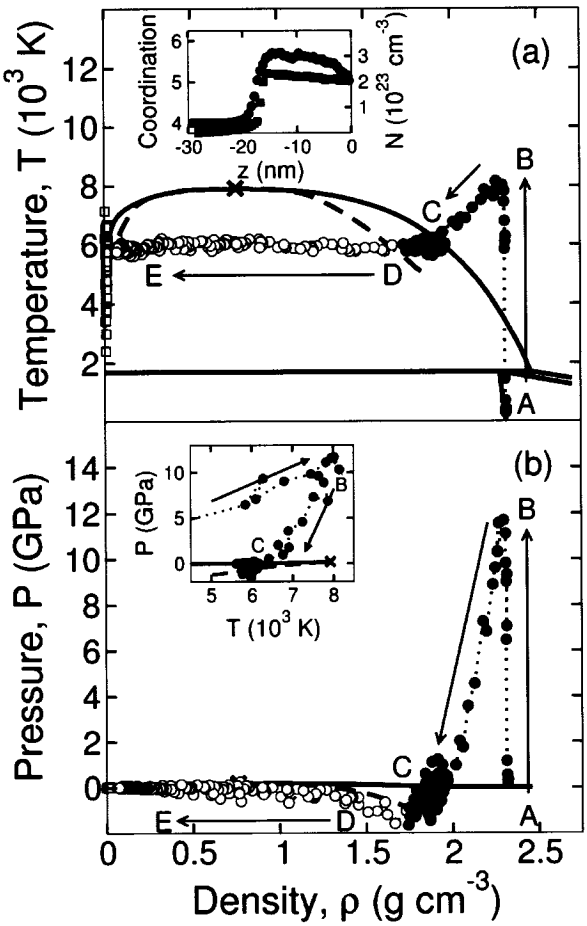

Figure 5.5 Time evolution of the system in the (a) ρ-T and (b) ρ-P planes for a 500 fs pulse at a fluence $F = F_{\rm th}^{\rm fs} = 0.225$ J cm^{-2}; the trajectory is for a region of the target initially at a depth of 4 nm below the surface. White circles and dotted line: macroscopic branch; red circles: dense branch; yellow squares: gas branch. Arrows indicate the flow of time. Capital letters refer to locations in the phase diagram (see text). Insets: (a) coordination (green circles) and electron density N (red squares) as a function of distance from the surface z at $t = 1$ ps (note the change in properties across the solid-liquid interface at $z \approx -18$ nm); (b) view of the trajectory in the T-P plane.

hole pairs in the unexcited silicon substrate via interband transitions over a penetration depth of $\approx 5 - 10$ nm; the carrier density eventually increases beyond $N_{\rm cr} \approx 5.9 \times 10^{21}$ cm^{-3} and intraband transitions also occur in the dense, overcritical electron gas. The carriers subsequently reach a common equilibrium state at a temperature $T_e \approx 8000 - 10000$ K through mutual collisions and impact ionization in a time of $\sim 10^{-13}$ s; Auger recombination is not significant on this time scale (see Table 5.1).

The hot electrons and holes simultaneously attempt to equilibrate with the ions by emitting phonons. The heated solid ultimately melts at the surface and the incoming photons thereafter interact primarily with the growing layer of liquid metal via inverse bremsstrahlung [figure 5.4(a)].

The laser energy is converted into lattice vibrational energy in roughly a picosecond (Sokolowski-Tinten *et al.*, 1998b). Mechanical expansion is negligible on this time scale and the system is pulled *away* from the liquid-vapor regime at nearly constant volume ($\rho \approx \rho_0$) to a high-temperature ($T \approx 8000$ K) and high-pressure ($P \approx 12$ GPa) supercritical state (B): at the end of the pulse, i.e., after a time $t_{\rm liq} \approx 1$ ps, the surface is covered by a hot and highly pressurized liquid layer of thickness $d_{\rm liq} \approx 20$ nm and having metallic properties [see inset in figure 5.5(a)]; below the molten layer lies an intact, semiconducting, bulk crystal at much lower temperature and pressure [figure 5.4(b)].

The following remarks are in order at this point: (i) The system is transiently heated *above* the triple line in a nonequilibrium *crystalline* — *not* the corresponding *equilibrium* liquid-vapor — state, i.e., the solid becomes superheated; this is further supported by an apparent "melt-front" velocity $d_{\rm liq}/t_{\rm liq} \approx 2 \times 10^4$ m s^{-1} well above the (longitudinal) speed of sound $\sqrt{c_{11}/\rho_0} \approx 8020$ m s^{-1} (where $c_{11} \approx 1.5 \times 10^{11}$ N m^{-2} is the appropriate elastic stiffness constant of c-Si) (Kittel, 2005;

Cowley, 1988). In this context, melting of the metastable crystal is expected to proceed by homogeneous nucleation of liquid nuclei whose size decreases with superheating $\theta = T/T_m$ (Rethfeld *et al.*, 2002). In figure 5.4(a), the relatively small liquid inclusions ahead of the "melt front" could indicate a very high degree of superheating or that the material has been heated beyond its limit of mechanical stability at $T_{\mathrm{mec}} \approx 2600$ K ($\theta_{\mathrm{mec}} \approx 1.54$) (Stillinger and Weber, 1985). Because of the large computational effort involved in the determination of the material thermodynamic trajectory, the same conditions have been simulated in smaller systems but with increased time resolution; results indicate that the solid may be heated to a temperature of ≈ 3000 K before it starts to melt, thus suggesting a disordering process driven by a mechanical instability in the irradiated crystal; similar conclusions have recently been reported in a MD study of short-pulse laser melting of metal films (Ivanov and Zhigilei, 2003a; Ivanov and Zhigilei, 2003b). In contrast, a maximum superheating $\theta \approx 1.45 < \theta_{\mathrm{mec}}$ is observed under picosecond irradiation (see section 5.4). (ii) In certain circumstances, the solid may (locally) be superheated without melting (not shown); this is consistent with the experimental observations presented by Cavalleri *et al.* (1999). (iii) As noted earlier, the empirical SW potential cannot account for the ultrafast, nonthermal melting of silicon at carrier densities in excess of $N_c \approx 10^{22}$ cm^{-3} (Sokolowski-Tinten *et al.*, 1995); computation of the electron density indicates that the latter value is indeed reached in the present case. Nevertheless, our simulations provide a realistic picture of the possible *thermal* processes and related time scales; in particular, the observed time for thermal melting under femtosecond irradiation, $\sim 10^{-12}$ s, agrees well with recent theoretical estimates (Rethfeld *et al.*, 2002).

5.3.1.2 Cooling I: expansion and ablation

In order to release the pressure and mechanically equilibrate with the ambient medium, the molten layer subsequently undergoes expansion in vacuum; at the same time, a compressive strain wave ($\approx$ 5 GPa) is launched from the highly pressurized liquid into the cold, crystalline bulk. A relatively weak tensile pressure wave is also emitted from the latter into the melt; however, the resulting acoustic perturbation is later damped in the expanding liquid-gas mixture characterized by a vanishing sound velocity (see below) (Sokolowski-Tinten *et al.*, 2001). In the present context, the strong initial surface pressure gradient leads to the rapid, adiabatic — and consequently isentropic — cooling of the liquid (B→C): through a conversion of thermal energy into potential and translational energy, the diluting material with flow velocity of ≈ 500 m s^{-1} enters the liquid-vapor regime (C) where the superheated molten matter is partially transformed into gas on a $10^{-12}-10^{-11}$ s time scale (D→E).

Three remarks are in order: (i) From a visual standpoint, the growth of a large, localized cavity in the expanding liquid strongly suggests an explosive-boiling — *not* a spinodal-decomposition — scenario [figures 5.4(c) and 5.4(d)]. (ii) From a thermodynamic viewpoint, the separation of the dense and macroscopic branches in the metastable region, and the concomitant appearance of a gas branch, confirms a phase-explosion process; inspection of the trajectory in the T-P plane further supports the above observations [see inset in figure 5.5(b)]. (iii) Explosive boiling takes place at a temperature of $\approx 0.75T_c$, i.e., significantly below $0.9T_c$. A detailed analysis of the nucleation process in relation with the nature of the ablation threshold will be given in section 5.3.3.

The growing cavity eventually percolates through the slab and a few-nanometer-thick liquid shell is removed from the target after a few tens of picoseconds [fig-

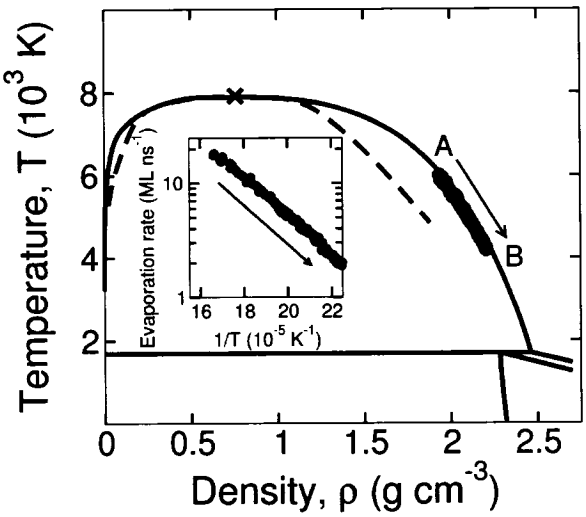

Figure 5.6 Thermodynamic evolution of the ejected liquid shell in figure 5.4(e). Inset: evaporation rate of the ablated layer as a function of inverse temperature. Capital letters refer to locations in the phase diagram (see text). See figure 5.5 for the definition of symbols and lines.

ure 5.4(e)]. The thermodynamic evolution of the ablated layer on a 10^{-10} s time scale is displayed in figure 5.6: as it moves further away from the surface with a (constant) velocity of ≈ 250 m s^{-1}, the molten material cools by evaporating (marked A$\rightarrow$B); in this regard, the computed evaporation rate (expressed in monolayers per nanosecond) exhibits a clear Arrhenius dependence as a function of inverse temperature, with a corresponding activation energy of ≈ 3.21 eV (see inset). More importantly, the ejected layer (whose thickness is on the order of the optical penetration depth in the initially solid material) evolves *along* the binodal throughout the cooling stage, thus suggesting that a liquid metal achieves equilibrium with its vapor in a time of $\sim 10^{-11} - 10^{-10}$ s. As discussed below, this is of great significance for the physical pathways to ablation under picosecond and nanosecond pulses.

Hence, near the threshold fluence for matter removal, our results confirm that an inhomogeneous mixture of liquid and gas expands between two optically flat,

reflective interfaces — the ablation front and the boundary separating the nonablated matter from the ejected material; similar conclusions have been obtained in other MD simulations (Zhakhovskiĭ *et al.*, 2000; Perez and Lewis, 2003). This is also consistent with the observation of optical interference patterns (Newton rings) in time-resolved microscopy experiments on numerous metals and semiconductors (Sokolowski-Tinten *et al.*, 1998b).

As the fluence is increased, however, the expanding matter shifts from a subcritical liquid to a supercritical fluid. As will be shown in section 5.3.2, this has important consequences for the mechanisms of matter removal.

5.3.1.3 Cooling II: solidification and final structure

Thermal diffusion into the solid bulk (and evaporation at the outer surface to a lesser extent) is responsible for the cooling and solidification of the nonablated molten material on a $10^{-11} - 10^{-10}$ s time scale [figure 5.4(f)]. As shown in figure 5.7, two distinct physical pathways are observed: (i) Deep into the metallic liquid layer [figure 5.7(a)], the neighboring crystalline phase acts as a seed for *heterogeneous* crystallization from the melt (marked A→B→C→D); the transition from a disordered liquid with average coordination of ≈ 6 to a fourfold-coordinated, ordered structure confirms this (see inset). (ii) Closer to the surface [figure 5.7(b)], the material is initially heated to a higher temperature (E); the resulting liquid subsequently expands toward the binodal (E→F). As a result of insufficient translational energy (see section 5.3.3), homogeneous nucleation of gas does not take place in the superheated melt (F) and the system is later slowly cooled under liquid-vapor coexistence (F→G). The triple line is eventually crossed and the liquid becomes *supercooled* (G); visual inspection of the nonablated material confirms that (locally) the (equilibrium) solid-liquid and solid regions of the phase diagram

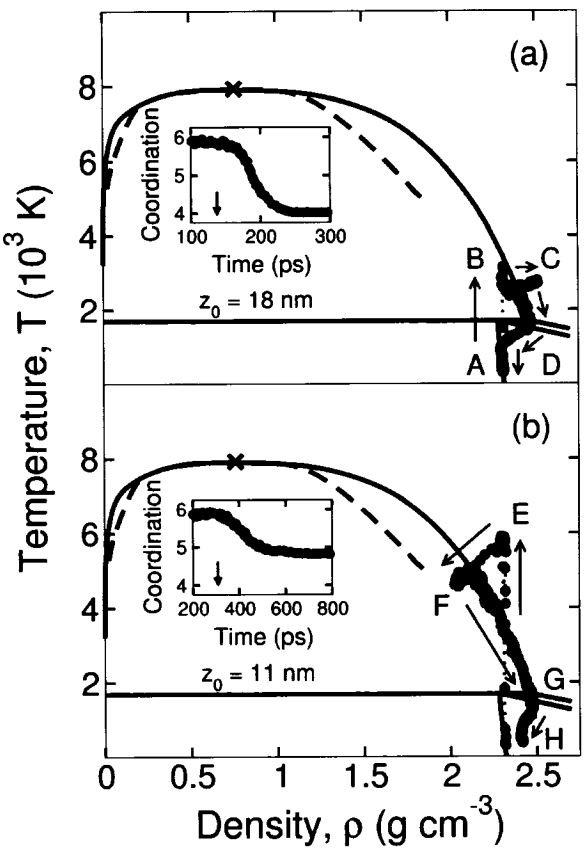

Figure 5.7 Time evolution of the system in the ρ-T plane for a 500 fs pulse at a fluence $F = F_{\text{th}}^{\text{fs}} = 0.225$ J cm^{-2} and two different depths z_0 below the original surface (as indicated): (a) solidification to a crystalline state; (b) solidification to a glassy state. Insets: local coordination as a function of time (arrows indicate the time at which the equilibrium melting temperature $T_m = 1691$ K is reached upon cooling). Capital letters refer to locations in the phase diagram (see text). See figure 5.5 for the definition of symbols and lines.

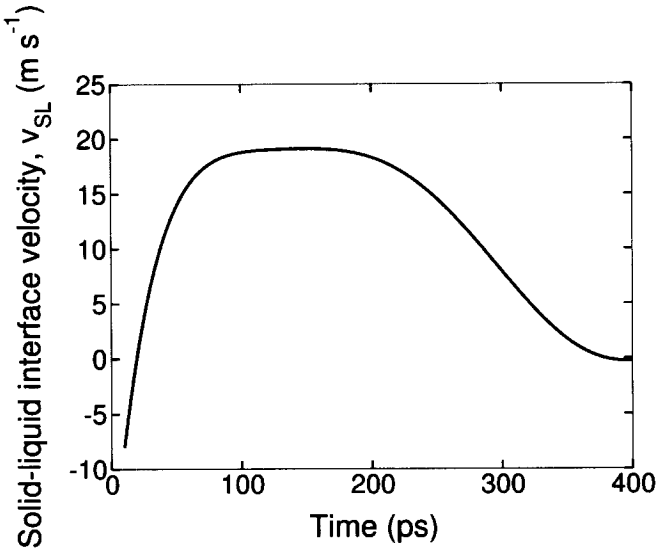

Figure 5.8 Velocity of the interface between the solid (crystal) and liquid phases as a function of time following irradiation with a 500 fs pulse at a fluence $F = F_{\rm th}^{\rm fs} = 0.225$ J cm^{-2}; negative and positive values indicate melting and solidification (crystallization), respectively.

are accessed in a disordered — metastable — state. However, crystallization does not occur for the following reasons: (a) The system standing relatively far from the solid-liquid interface, a heterogeneous liquid-to-crystal transition is not possible. (b) The energy required to *homogeneously* nucleate critical nuclei of the stable crystalline phase into the supercooled melt decreases with temperature, i.e., with increased supercooling; however, this also translates into a significant decrease of the atomic mobility and a corresponding increase of the liquid-to-crystal relaxation time. Consequently, the structure — several hundred degrees below T_m — is ultimately "frozen" into an intermediate state with coordination between that of the liquid and the crystal (see inset): the molten material transforms into a *glass* (at $\approx$ 900 K) which subsequently cools to 300 K (H).

Figure 5.8 displays the solid-liquid interface velocity $v_{\rm SL}$ as a function of time. As

can be seen, the solidification process begins after a few tens of picoseconds and is complete after a few hundreds of picoseconds, in good agreement with experimental data (von der Linde, 1991); the observed regrowth velocity of $\approx 10 - 20$ m s^{-1} also compares favorably with experiment (Bucksbaum and Bokor, 1984; Thompson *et al.*, 1983) and other MD studies (Kluge and Ray, 1989).

Three distinct stages can be identified: (i) Efficient heat conduction into the solid initially gives rise to an increase of the regrowth velocity ($t \lesssim 100$ ps). (ii) This takes place until heat flow is balanced out by the rate of latent heat release (which increases as more liquid is converted into a crystal), at which point a steady-state regime is achieved at $v_{\mathrm{SL}} = 18$ m s^{-1} ($100 \lesssim t \lesssim 200$ ps). (iii) As noted above, however, the atomic mobility decreases and the liquid-to-crystal relaxation time eventually increases as the supercooled molten material further cools ($t \gtrsim 200$ ps): v_{SL} decreases and crystallization of the melt stops on a 10^{-10} s time scale; as a result, a layer of "frozen", uncrystallized liquid with thickness of ≈ 10 nm is left at the surface [figure 5.4(f)].

Note that a transition from a disordered liquid to a near-fourfold-coordinated, short-range-ordered *amorphous* phase above a threshold regrowth velocity of ≈ 15 m s^{-1} has been discussed in several experimental investigations of laser-induced melting and solidification of silicon (Bucksbaum and Bokor, 1984; Thompson *et al.*, 1983; Liu *et al.*, 1979b; Tsu *et al.*, 1979; Cullis *et al.*, 1982). However, this is not seen in the present study; similar conclusions have also been reported in other MD simulations involving the SW potential (Kluge and Ray, 1989). Two reasons could explain the observed discrepancy: (i) From a thermodynamic standpoint, the predicted liquid-to-amorphous temperature (slightly under 1060 K), below which the melt needs to be supercooled for the transition to take place, is significantly lower than the experimentally derived value of ≈ 1450 K (Luedtke and Landman, 1989). (ii) From a kinetic viewpoint, a possible explanation could be a higher

threshold regrowth velocity in SW silicon (Wood, 1983).

5.3.2 Ablation at higher fluences

As suggested by figure 5.4(g), far-from-threshold femtosecond irradiation involves different pathways to ablation. In this respect, two observations can be drawn from a comparison with figures 5.4(d) and 5.4(e): (i) The removal of molten material does *not* take place by the growth of a highly localized cavity between two sharp interfaces and the subsequent ejection of a liquid shell; instead, the expanding plume displays a diffuse, clusterlike structure without a well-defined ablation front. (ii) The ejected liquid expands noticeably faster. As shown below, such differences are associated with expansion in a different region of the phase diagram.

Figure 5.9 illustrates the transition to a new regime. The scenario is as follows: (i) Similarly to near-threshold irradiation, the system is pulled *away* from the region of metastable states upon near-isochoric heating of the material; in figure 5.9(a) — which is for the maximum average irradiance of 1×10^{12} W cm^{-2} investigated in this work — the result is a hot ($T \approx 16000$ K), highly pressurized ($P \approx 28$ GPa) supercritical fluid at near-solid density (marked A). (ii) The liquid-vapor regime is subsequently approached upon rapid, adiabatic cooling of the expanding matter with maximum flow velocity of ≈ 800 m s^{-1} (A→B); a strong (≈ 14 GPa) compressive strain wave is also emitted from the molten layer into the solid bulk. (iii) However, the binodal is *not* reached in a homogeneous state: instead, the split of the dense and macroscopic branches — which indicates the onset of ablation — takes place in the supercritical regime, i.e., *outside* of any phase coexistence region (B); the same conclusions emerge from inspection of the trajectory in the ρ-P plane (see inset). In regions standing further from the surface, the molten material — following a short incursion into the metastable region — is cooled along the binodal

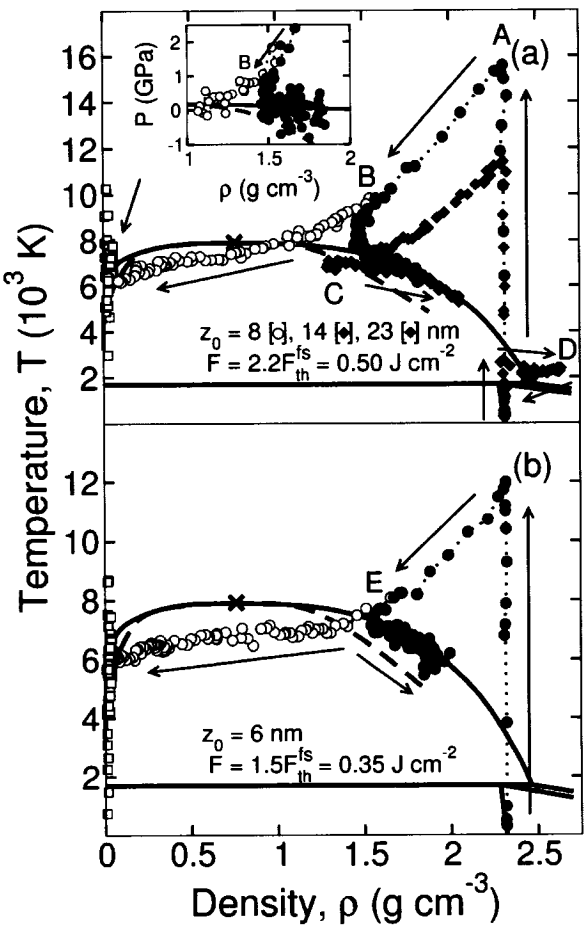

Figure 5.9 Time evolution of the system in the ρ-T plane for a 500 fs pulse at two different fluences F and various depths z_0 below the original surface (as indicated). Inset: zoom on the trajectory for $z_0 = 8$ nm in the ρ-P plane. White circles and dotted line: macroscopic branch; red circles: dense branch; yellow squares: gas branch; green and orange diamonds: additional macroscopic branches. Arrows indicate the flow of time. Capital letters refer to locations in the phase diagram (see text).

and matter removal is not observed (C).

Undoubtedly, ablation cannot be attributed, in the present case, to a phase transition such as, e.g., explosive boiling or spinodal decomposition; vaporization is also excluded since fairly large clusters are produced in the dissociation process.

The above picture is analogous to that recently reported in a MD study of femtosecond irradiation and ablation of a two-dimensional Lennard-Jones system (Perez and Lewis, 2002; Perez and Lewis, 2003). At fluences relatively far from the threshold for matter removal, the rapid expansion is such that the equilibrium structure of the *supercritical* material can no longer be preserved by atomic diffusion: the expanding matter undergoes a *nonequilibrium* transition from a homogeneous fluid to a heterogeneous, clustered phase through a "nontrivial" *fragmentation* process; in this case, the average fragment size depends upon the local strain rate, i.e., the translational velocity *gradient* normal to the surface. Note that: (i) This phenomenon is qualitatively different from spallation or cavitation whereby the breakup of the material is assisted by tensile strain waves. (ii) As discussed in section 5.4, matter removal under picosecond pulses is also driven by a fragmentation process; however, the latter takes place *near thermodynamic equilibrium* and is said, instead, to be "trivial" (Perez and Lewis, 2003; Lorazo *et al.*, 2004).

The differences in expansion dynamics between near- and far-from-threshold femtosecond irradiation are best understood within a one-dimensional self-similar rarefaction-wave (SSRW) model (Sokolowski-Tinten *et al.*, 1998b; Inogamov *et al.*, 1999a; Sokolowski-Tinten *et al.*, 1998a; Perez and Lewis, 2003); the latter describes the propagation of the rarefaction (density-decrease) wave into the bulk molten material as the heated liquid layer expands in vacuum. In principle, the SSRW model is strictly valid for an instantaneously and homogeneously heated solid at uniform density ρ_i; however, we show below that it is also suitable for a qualitative under-

standing of the ablation process taking place in the present "real" conditions.

According to this model, the increase in translational (flow) velocity $\mathrm{d}u$, for an infinitesimal increase in density $\mathrm{d}\rho$, is proportional to the sound velocity $c(\rho)$; the translational velocity at density ρ_f reads

$$u_f(\rho_f, S) = -\int_{\rho_i}^{\rho_f} \left(\frac{c(\rho)}{\rho}\right)_S d\rho, \tag{5.5}$$

where S denotes the entropy (a "-" sign is added to ensure that expansion in vacuum is described by *positive* velocities). The strong dependence of the speed of sound on density is of great significance here: as detailed by Perez and Lewis (2003), the sharp drop of $c(\rho)$ in the liquid-vapor coexistence regime implies a subcritical, metastable material with flow velocity u_f nearly *independent* on ρ_f and S; upon supercritical expansion, however, the drastic decrease of the sound velocity is not observed and the expanding fluid is expected to be characterized by significantly higher, density- and entropy-dependent translational velocities.

This has the following consequences: (i) Near the ablation threshold, the system enters the metastable region upon cooling and the various sections of the superheated material (which follow different subcritical isentropes) possess similar translational velocities; as depicted in figure 5.4(d), this leads to a heterogeneous mixture of liquid and gas with a steplike density profile — the sharp ablation front — giving rise to the optical interference patterns observed in time-resolved microscopy experiments (Sokolowski-Tinten *et al.*, 1998b). (ii) At higher fluences, however, the flow-velocity *gradient* across the supercritical diluting fluid is significantly higher. In this case, it is expected that: (a) The density drops smoothly across the ablating material which, consequently, does not exhibit a steep liquid-vacuum boundary. (b) The breakup of the rapidly expanding matter results from a ("nontrivial") fragmentation process. Both a visual inspection of the system in figure 5.4(g) and the

disappearance of the Newton rings at relatively high fluences (but before the onset of plasma formation) support the above conclusions (Cavalleri *et al.*, 1999; Perez and Lewis, 2003; Rethfeld *et al.*, 2003); in particular, the transition between the two regimes in silicon [marked E in figure 5.9(b)] occurs at a predicted fluence of $\approx 1.5F_{\text{th}}^{\text{fs}}$ which agrees remarkably well with experiment (Rethfeld *et al.*, 2003).

Metals — which *expand* upon melting and whose thermodynamic properties can be *qualitatively* described by, e.g., the Lennard-Jones phase diagram (Perez and Lewis, 2003) — and semiconductors exhibit different solid-liquid features (Lorazo *et al.*, 2004; Moran and Shapiro, 2000). This translates into the following differences under femtosecond irradiation: (i) Unlike semiconducting materials, metals — for which the initial state does *not* lie below the triple line — can remain *solid* at temperatures significantly above T_c (Perez and Lewis, 2003); as a result, melting can also be observed upon *cooling* to the solid-liquid (or liquid) region. (ii) In a very narrow range of fluences near the ablation threshold, the *cooling* metallic system can be pulled by tensile strain waves toward the *solid*-vapor coexistence regime where the breakup of the mechanically unstable *solid* material is described by a spallation process (Perez and Lewis, 2003); this is unlikely to take place in semiconductors such as silicon where melting occurs at relatively low temperatures ($T \ll T_c$) upon *heating*, and where ablation therefore involves the ejection of *liquid* matter upon rapid cooling to the *liquid*-vapor regime. (iii) As a result of a liquid phase with higher density than the solid in group IV and III-V covalent materials, melting of the superheated crystal can be assisted by a *compressive* strain wave emitted from the upper, highly pressurized liquid layer [marked D in figure 5.9(a)].

However, in view of phase diagrams with similar liquid-vapor and supercritical features (Lorazo *et al.*, 2004; Moran and Shapiro, 2000), metals and semiconductors display common thermal routes to matter removal under near- and far-from-threshold femtosecond irradiation; as noted earlier, this is confirmed by both

experiment (Sokolowski-Tinten *et al.*, 1998b; Cavalleri *et al.*, 1999) and numerous MD studies (Zhakhovskiĭ *et al.*, 2000; Perez and Lewis, 2002; Perez and Lewis, 2003; Lorazo *et al.*, 2003; Lorazo *et al.*, 2004). In section 5.4, we present results which strongly suggest that this universal behavior may be extended to longer, picosecond (and possibly nanosecond) pulses.

5.3.3 Nature of the ablation threshold

Evidence for a well-defined threshold fluence — below which matter removal is driven by evaporation and above which large, macroscopic amounts of material are ejected from the irradiated surface — has been reported under femtosecond (Sokolowski-Tinten *et al.*, 1998b; Cavalleri *et al.*, 1999; Cavalleri *et al.*, 1998), picosecond (Willis and Xu, 2002a), and nanosecond (Bulgakova and Bulgakov, 2001; Song and Xu, 1998; Yoo *et al.*, 2000) irradiation of metals and semiconductors. This has also been observed in several MD investigations of laser ablation (Zhigilei and Garrison, 2000; Perez and Lewis, 2003; Lorazo *et al.*, 2003; Anisimov *et al.*, 2003; Schäfer *et al.*, 2002; Ivanov and Zhigilei, 2003b; Nedialkov *et al.*, 2004); in the present study, an increase of the fluence by only a few percent (under both femtosecond and picosecond pulses) is sufficient to cause sudden, massive ejection of molten material.

In spite of its ubiquitous nature, the origin of the threshold behavior has, to date, remained unclear. In general, it is postulated that the onset of ablation results from the strong increase with temperature of the bubble nucleation rate in a strongly superheated melt (Sokolowski-Tinten *et al.*, 1998b; Garrison, 2003; Zhigilei *et al.*, 1997): i.e., near-threshold matter removal is described as a nonequilibrium process driven by large, localized, *thermal* fluctuations in a metastable liquid. In the work by Garrison *et al.*, in particular, the relatively high flow velocities characterizing

the expanding material upon entrance into the liquid-vapor regime have not been taken into account.

At fluences near the ablation threshold, we find that the initial increase in translational energy of the expanding molten matter is followed by a rapid decrease of the flow velocity and the *concomitant* growth of a large cavity within the diluting material; this suggests that the rapid expansion of the liquid may play a role in the bubble nucleation process.

In the following discussion, we give strong evidence that the threshold behavior is, to a significant extent, *mechanical* in nature; more specifically, it is shown that bubble nucleation in the metastable liquid is initiated by the conversion of *translational* energy into surface energy, *not* by highly localized thermal fluctuations. Note that the analysis given below applies only to covalent semiconductors under femtosecond irradiation where near-threshold ablation is governed by explosive boiling; it does not describe the case of metallic systems (Perez and Lewis, 2003; Schäfer *et al.*, 2002) and organic solids (Zhigilei and Garrison, 2000) where the threshold dynamics are likely to be determined, rather, by spallation.[21]

Figure 5.10 portrays the bubble nucleation process near — but *below* — the threshold fluence for matter removal; the corresponding thermodynamic trajectory is displayed in figure 5.11. In addition, figure 5.12 provides information on the time dependence of various quantities of interest in the initially expanding and subsequently contracting molten layer: (i) The total volume occupied by cavities V_c and their total number in the liquid (as obtained following the method presented in section 5.2.2.1) are first shown in figure 5.12(a). (ii) The molten layer is divided into thin (≈ 5 Å) slices at various points in time. In each slice containing N_a atoms

[21] In metallic systems, *near*-threshold ablation is driven by spallation; at higher fluences, phase explosion and, eventually, fragmentation are responsible for matter removal (Perez and Lewis, 2003).

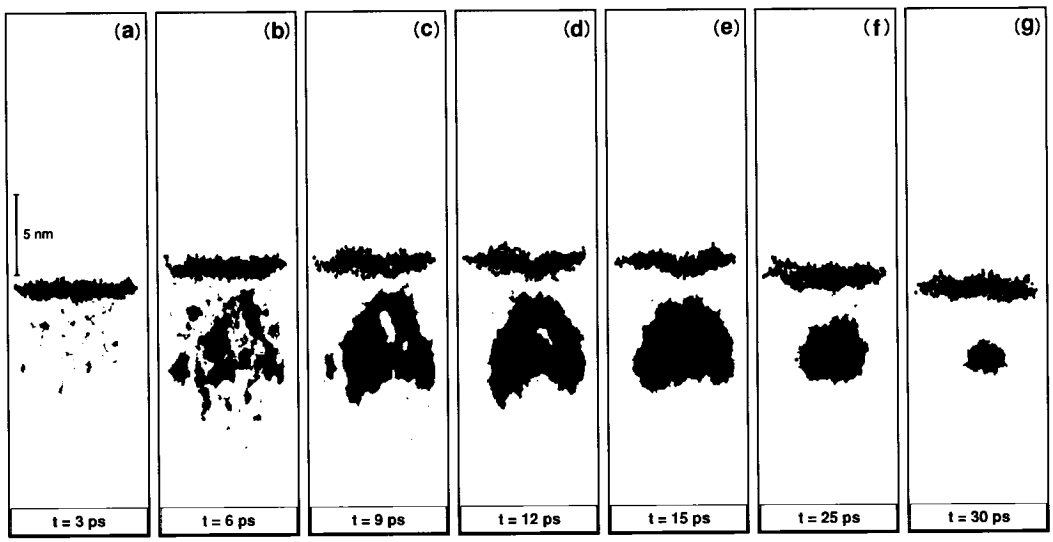

Figure 5.10 Snapshots illustrating the growth and subsequent collapse of a cavity (green) below the surface (red) following irradiation with a 500 fs pulse at a (subthreshold) fluence $F = 0.9F_{\text{th}}^{\text{fs}} = 0.20$ J cm^{-2}; gas-phase atoms are not shown. The pulse begins at $t = 0$.

of equal mass m, we proceed as follows: (a) The center-of-mass velocity v_{cm} (in the z direction) is computed and the local *translational* energy defined as $N_a m v_{\text{cm}}^2/2$. (b) The N_s atoms in the vicinity of internal voids — but *not* at the outer surface — and N_v atoms in the dense, volumic material are identified as described in section 5.2.2.1; the local *surface* energy is then defined as $N_s(E_s - E_v)$, where E_s and E_v are the average potential energies of the surface and volumic atoms, respectively. The liquid *total* translational and surface energies in figure 5.12(b) are finally obtained by summing over all slices. (We have verified that, within a satisfactory range, the result does not depend on the thickness of the slices).

The evolution of the system under *subthreshold* femtosecond irradiation can be divided into five successive stages:

(i) The laser energy is first converted into heat in about a picosecond, which is too

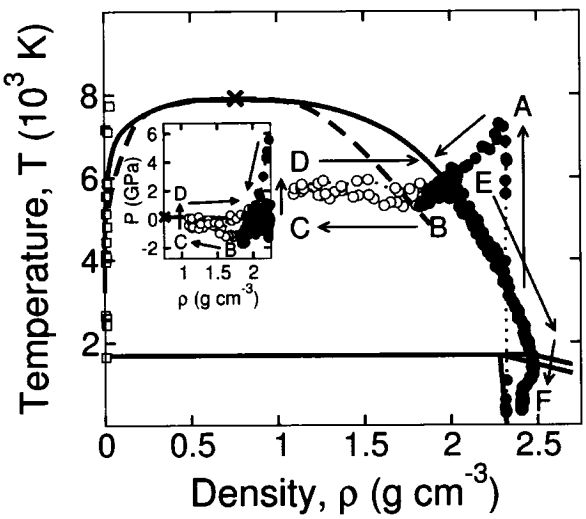

Figure 5.11 Typical thermodynamic trajectory for the region where nucleation of the large cavity takes place in figures 5.10(a)-5.10(g). Inset: view of the trajectory in the ρ-P plane. Capital letters refer to locations in the phase diagram (see text). See figure 5.5 for the definition of symbols and lines.

short for significant expansion to occur; here, the resulting state corresponds to a *subcritical* liquid at $\rho \approx 2.33$ g cm^{-3}, $T \approx 7200$ K, and $P \approx 10$ GPa (marked A in figure 5.11).

(ii) The liquid-vapor regime is then approached upon rapid, adiabatic cooling (A→B): the molten layer expands and its translational energy increases until the metastable region is reached at $t \approx 3$ ps (B). The consequences of the subsequent abrupt drop of the sound velocity are twofold: (a) The flow velocity stops increasing (see Eq. 5.5); as a result, the translational energy reaches its maximum value [figure 5.12(b)]. (b) The superheated material is thereafter characterized by a well-defined liquid-vacuum boundary; as can also be appreciated from figure 5.10(a), the metastable liquid is still rather homogeneous at this point.

(iii) In the following few picoseconds ($3 \lesssim t \lesssim 5$ ps), the *translational* energy

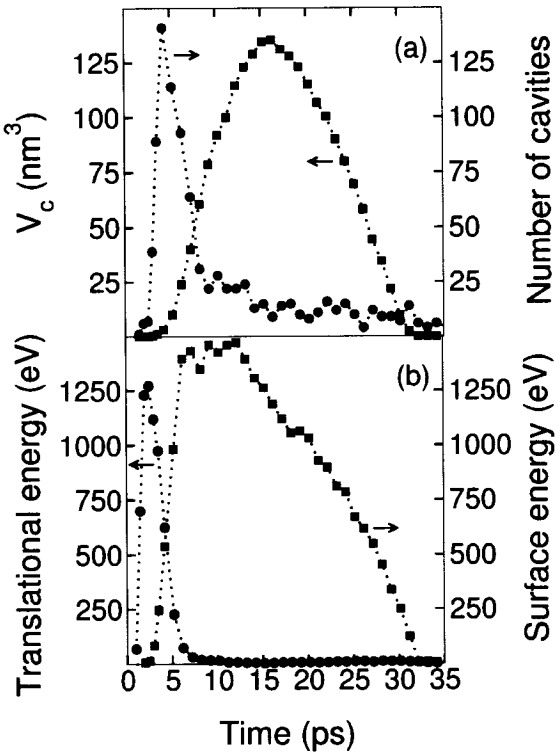

Figure 5.12 Time dependence of various quantities characterizing the molten layer produced upon irradiation with a 500 fs pulse at a (subthreshold) fluence $F = 0.9F_{\rm th}^{\rm fs} = 0.20$ J cm^{-2}: (a) total volume occupied by cavities V_c (red squares) and total number of cavities (green circles) in the liquid; (b) total translational (green circles) and surface (red squares) energies of the liquid.

gained upon cooling is rapidly converted into *surface* energy and expansion slows down. This can be seen from the steep rise in the number of independent cavities in figure 5.12(a); visual inspection of the system confirms that small, subnanometer-sized voids have been created in the metastable liquid [figure 5.10(b)]. Note also that the total decrease in translational energy agrees closely (in absolute value) with the *simultaneous* total increase in surface energy [figure 5.12(b)].

(iv) At later times ($5 \lesssim t \lesssim 15$ ps), during which the total *surface* — but not the volume — is conserved, the further expansion of the liquid is driven by the growth

of a cavity below the surface. This occurs in two distinct steps: (a) As can be seen from the decrease in the number of cavities in figure 5.12(a) and a comparison of figures 5.10(b) and 5.10(c), void coalescence first takes place in the superheated liquid ($5 \lesssim t \lesssim 10$ ps). (b) The resulting single, large cavity later grows to reach a maximum volume of ≈ 135 nm^3 at $t \approx 15$ ps and expansion of the molten layer stops [figures 5.10(d), 5.10(e), and 5.12(a)]; this can also be inferred from the split of the dense and macroscopic branches in figure 5.11 (B→C). Note that the total surface energy remains *constant* during coalescence and growth [figure 5.12(b)]: it is easy to show that, for equal surfaces, the total volume occupied by two (or more) voids is smaller than that occupied by a single cavity; in other words, bubble nucleation in the superheated melt can be seen as a rapid rearrangement of the total surface initially created by conversion of translational energy into surface energy.

As a result of insufficient translational energy to grow a critically-sized nucleus of the stable vapor phase into the metastable liquid phase, the cavity subsequently collapses [figures 5.10(f) and 5.10(g)]; this is also apparent from the corresponding decrease of V_c [figure 5.12(a)]. The temperature increase in figure 5.11 (C→D→E) and simultaneous decrease of the total surface energy in figure 5.12(b) indicate that the latter is dissipated into heat. The material is then cooled by thermal conduction along the binodal and eventually solidifies (to a glass in this case) on a 10^{-10} s time scale (E→F).

The following remarks are in order: (i) As mentioned earlier, the threshold behavior governing the onset of explosive boiling in covalent semiconductors is, to a significant extent, *mechanical* in nature: here, the relatively high translational energy gained upon cooling to the liquid-vapor regime — *not* large, localized, thermal fluctuations — provides the energy required to grow critically-sized nuclei of gas in the superheated liquid; the remaining translational energy is carried away by the ejected liquid shell moving with constant velocity. (ii) As a result of the rather

small lateral dimensions of the system in the present study, the threshold behavior is determined, instead, by the minimum translational energy needed to grow a nucleus that will percolate through the slab; it is therefore likely that the "true" threshold fluence for matter removal is somewhat underestimated. (iii) In a study by Sokolowski-Tinten *et al.* (1998b), the flow velocity at the liquid-vacuum boundary is approximated as $u_\ell \approx c_0 \ln(\rho_0/\rho_b)$ (see Eq. 5.5), where ρ_0 and ρ_b are the solid density and liquid density at the binodal (marked B in figure 5.11), respectively; c_0 is the sound velocity of the unperturbed material. In view of the above discussion, however, it is clear that u_ℓ (≈ 1000 m s^{-1} at the threshold fluence) significantly overestimates the velocity of the layer ejected upon near-threshold femtosecond irradiation [≈ 250 m s^{-1} in figure 5.4(e)].

5.4 Thermodynamics under picosecond laser irradiation

The thermodynamic pathways observed under femtosecond laser irradiation have revealed phase-change phenomena driven by metastable states of rapidly heated or promptly cooled matter: upon thermal melting (see note concerning possible nonthermal effects in section 5.3.1.1), on the one hand, the transient, superheated solid presumably crosses the limit of mechanical stability before disordering to a metallic melt; upon solidification, on the other hand, long-lived, supercooled liquid states are involved in a direct liquid-to-glass transition.

In the vicinity of the threshold fluence for matter removal, the phase-explosion-like transition from a homogeneous, aggregated, and disordered state to a heterogeneous mixture of liquid and gas is associated with short-lived, metastable states of matter: the molten material is *cooled* to the two-phase regime before liquid-vapor equilibrium is achieved and, consequently, becomes *superheated.* At higher fluences, however, ablation does not result from a phase transition and high strain

rates — not highly superheated states — are responsible for the nonequilibrium fragmentation process.

In all phase transitions observed under femtosecond irradiation, equilibrium is locally achieved between electrons and ions, but *not* among the different — solid, liquid, and vapor — states of aggregation on larger — mesoscopic — length scales. Hence, phase change can be regarded as a *nonequilibrium* thermal process involving transient, superheated or supercooled, thermodynamic states.

As noted in section 5.3, the material ejected under picosecond pulses exhibits a diffuse, clusterlike structure very different from that observed under near-threshold femtosecond irradiation but, however, remarkably similar to that obtained following (nonequilibrium) fragmentation of an expanding fluid with ultrashort pulses at higher fluences [see figures 5.4(d), 5.4(g), and 5.4(h)]. We show below that matter removal under picosecond irradiation can also be described by a fragmentation process; in particular, significantly slower expansion allows liquid-vapor equilibrium to take place — and explosive boiling to be suppressed — on a $\sim 10^{-11} - 10^{-10}$ s time scale.

5.4.1 Dynamics under subcritical expansion

Figure 5.13 displays the various morphological changes taking place during and after irradiation with a 100 ps pulse slightly above the threshold fluence for matter removal $F_{\rm th}^{\rm ps} = 0.40$ J cm^{-2}; the average irradiance is equal to 5×10^9 W cm^{-2}. The corresponding thermodynamic trajectories are depicted in figure 5.14.

A typical pathway under *subcritical* expansion is shown in figure 5.14(a); the initial depth corresponds to a section of the *nonablated* matter slightly below the boundary separating the ablating, volatile plume from the subthreshold material. The laser

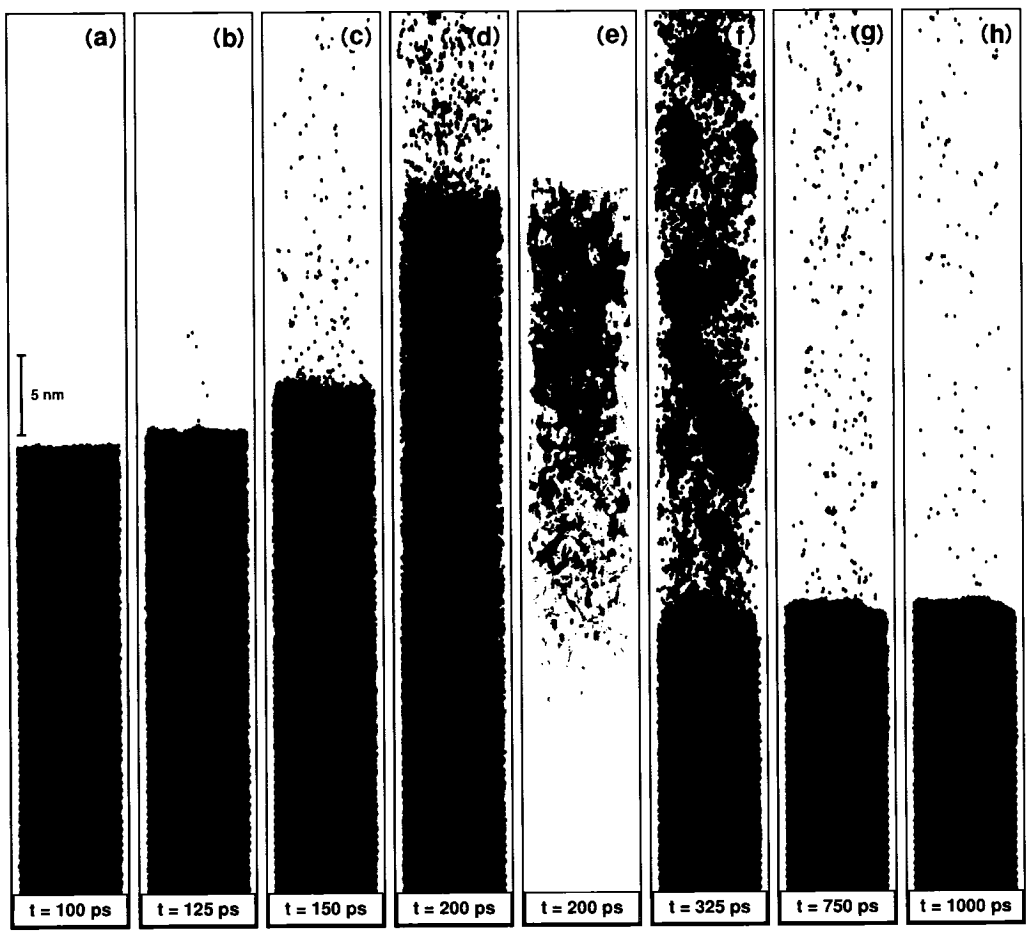

Figure 5.13 Snapshots revealing the structural changes induced in a Si(100) substrate by a 266 nm, 100 ps pulse at a fluence $F = 1.1F_{\text{th}}^{\text{ps}} = 0.45$ J cm^{-2}: (a)-(d) and (f)-(h) green: (semiconducting) crystalline silicon; red: (metallic) liquid silicon; (e) view of the voids in the expanding molten layer. The pulse begins at $t = 0$.

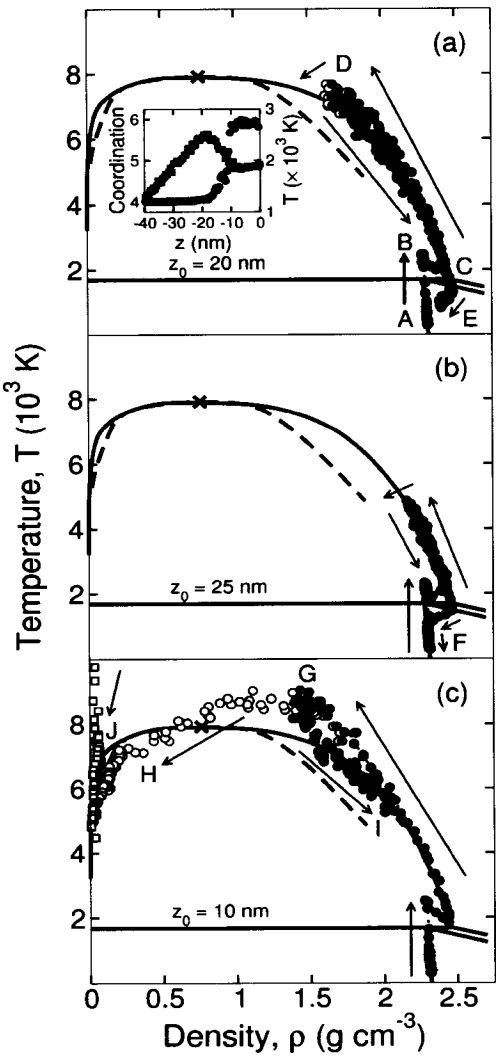

Figure 5.14 Time evolution of the system in the ρ-T plane for a 266 nm, 100 ps pulse at a fluence $F = 1.1F_{\text{th}}^{\text{ps}} = 0.45$ J cm^{-2} and various depths z_0 below the original surface (as indicated). Inset: coordination (green circles) and temperature T (red squares) as a function of distance from the surface z shortly after the onset of melting; the solid-liquid interface is at $z \approx -12$ nm. Capital letters refer to locations in the phase diagram (see text). See figure 5.5 for the definition of symbols and lines.

pulse originally gives rise to interband transitions in the initially unexcited solid at $\rho = 2.33$ g cm^{-3} and $T = 300$ K (marked A). Upon absorption of additional photons in the crystal, more electron-hole pairs are created and the carrier density increases to reach a maximum value of $\approx 3 \times 10^{21}$ cm^{-3} after a few tens of picoseconds.[22] In the present case, intraband absorption is negligible in the undercritical electron gas ($N < N_{\rm cr}$); however, carrier diffusion, impact ionization, and Auger recombination are all significant on a $10^{-11} - 10^{-10}$ s time scale.

The deposited energy is simultaneously transferred to the ions through scattering of the carriers with phonons. The solid is rapidly heated ($\sim 10^{13}$ K s^{-1}) and a maximum superheating $\theta \approx 1.45$ ($T \approx 2450$ K) is achieved in the perfectly ordered, metastable crystal (B). This corresponds to a temperature ≈ 750 K above T_m but, nevertheless, *below* the limit of mechanical stability at ≈ 2600 K (see section 5.3.1.1); reports of semiconducting materials superheated by several hundred degrees above their equilibrium melting temperature under picosecond pulses can be found elsewhere (Bucksbaum and Bokor, 1984; Fabricius *et al.*, 1986; von der Linde, 1991).

The metastable crystalline state is only short-lived and *homogeneous* nucleation of liquid nuclei in the strongly heated solid takes place in a time of $\sim 10^{-12} - 10^{-11}$ s [figure 5.13(a)]: these grow ahead of the apparent "melt front" characterized by a maximum velocity of $\sim 10^3$ m s^{-1}; at later times — upon slower heating and reduced superheating — the solid-liquid interface propagates *heterogeneously* into the bulk crystal with a velocity of $\sim 10^2$ m s^{-1} [figures 5.13(b)-5.13(d)].[23] Note that competing heterogeneous and homogeneous melting mechanisms have also been reported in a recent MD study of short-pulse laser irradiation of metallic

[22] As expected for a picosecond pulse, this is strictly below the critical electron density $N_c \approx 10^{22}$ cm^{-3} for nonthermal melting.

[23] See, e.g., Rethfeld *et al.* (2002) and references therein.

films (Ivanov and Zhigilei, 2003b).

The irradiated solid *cools* (due to the consumption of latent heat) and densifies to a sixfold-coordinated structure upon disordering to a liquid (B→C); the resulting molten material is momentarily at a *lower* temperature than the superheated bulk crystal, and the corresponding *negative*[24] ($\partial T/\partial z < 0$) temperature gradient gives rise to a temporary reversal of the direction of heat flow at the surface [see inset in figure 5.14(a)] (Sokolowski-Tinten *et al.*, 1998c). The liquid subsequently couples with the incoming photons through inverse bremsstrahlung and heating of the metallic melt takes place (C→D). The system (locally) is eventually left (at the end of the pulse) in a *subcritical* state at near-critical temperature $T \approx 0.95T_c$ ($\approx$ 7500 K) and pressure $P \approx 1.35P_c$ ($\approx$ 250 MPa), and with *nearly zero flow velocity* (D).

Two differences readily emerge from a comparison with near-threshold femtosecond irradiation [figures 5.4(a)-5.4(f) and 5.5]: (i) In light of the much longer pulse duration, significant expansion and surface evaporation occur during the slower heating of the melt [figures 5.13(a)-5.13(d) and 5.14(a)]; in the present case, about 3% of the incident laser radiation is screened by the plume (see section 5.2.1.1). (ii) More importantly, the subsequently cooling liquid — at a relatively low pressure — expands very slowly. This has the following two consequences: (a) The penetration into the liquid-vapor regime — if any — is small and the corresponding size of the critical nucleus of gas therefore large; consequently, too little translational energy is available to initiate bubble nucleation in the metastable region (see section 5.3.3). (b) In this context, explosive boiling can only follow from highly localized *thermal* fluctuations in the superheated melt. Here, however, *thermal conduction* takes place on a shorter time scale and the system (locally) is, rather, efficiently cooled

[24] In a related study by Sokolowski-Tinten *et al.* (1998c), z takes positive values and the temperature gradient is, instead, *positive*.

along the binodal: i.e., *phase explosion does not take place.* This strongly suggests equilibration of metallic liquids with their vapor in a time of $\sim 10^{-11} - 10^{-10}$ s, with equally important consequences for the mechanisms of matter removal under nanosecond irradiation (see section 5.4.3).

Solidification of the nonablated molten material to a glass is eventually observed near the surface on a 10^{-10} s time scale (D→E); closer to the solid-liquid interface [figure 5.14(b)], the metallic melt solidifies, instead, to a crystal (F) with a corresponding maximum regrowth velocity of ≈ 15 m s^{-1} (see section 5.3.1.3).

5.4.2 Dynamics under supercritical expansion

As shown in figure 5.14(c), only those regions of the target expanding *above* the critical point contribute to the ablated mass. This is indicated by the split of the dense and macroscopic branches in the *single-phase*, supercritical region of the phase diagram (G); evaporation from the surface of the clusters produced in the dissociation process is responsible for the concomitant appearance of a gas branch. The further separation of the dense and macroscopic branches (G→H), on the one hand, and the cooling of the condensed (G→I) and gaseous (J) phases toward the binodal, on the other hand, are associated at later times with expansion and liquid-vapor equilibration within the plume, respectively.

In the present case, material removal does not result from the nucleation of a large, localized cavity in a subcritical, superheated liquid. Instead, ablation follows from the breakup of *supercritical* matter whereby voids initially develop *homogeneously* across the expanding material [figure 5.13(e)]; consequently, the ablating fluid does *not* exhibit a bubblelike character but, rather, a clusterlike, diffuse structure [figures 5.4(h) and 5.13(f)] very similar to that observed under far-from-threshold

femtosecond irradiation [figure 5.4(g)].

Unquestionably, matter removal — which takes place *outside* of any phase coexistence region — cannot be ascribed to a phase transition such as, e.g., phase explosion or spinodal decomposition; "nontrivial" fragmentation of the irradiated material is also excluded in view of the relatively low expansion rate involved in the ejection process. However, it is well established that a supercritical fluid at *equilibrium* and moderately low densities is *not* homogeneous (Perez and Lewis, 2003). In this regard, ablation under long, picosecond (and possibly nanosecond) pulses can be described by a "trivial" fragmentation process (Perez and Lewis, 2004; Lorazo *et al.*, 2003; Lorazo *et al.*, 2004): the system — locally near thermodynamic equilibrium — undergoing slow expansion in vacuum reaches a region of the phase diagram [marked G in figure 5.14(c)] where the corresponding (equilibrium) structure is *not* that of a homogeneous fluid but, instead, corresponds to a collection of disconnected liquid droplets.

The nonablated molten matter solidifies at later times and the final structure is characterized by a ten-nanometer-thick layer of "frozen" liquid (glass) on top of a crystalline bulk material [figures 5.13(g) and 5.13(h)].

Note finally that: (i) The above behavior under picosecond irradiation has been observed at *all* fluences and for *each* of the pulse durations (ranging from 25 to 100 ps) investigated in this work (Lorazo *et al.*, 2003; Lorazo *et al.*, 2004);[25] similar conclusions have also been reported in metallic systems (Perez and Lewis, 2004). This suggests common pathways to matter removal in absorbing solids extending to picosecond and, possibly, nanosecond pulses. (ii) As mentioned earlier, the liquid-vapor region is *not* accessed in the picosecond regime; this implies a pulse

[25] In the case of a 5 ps pulse, near-threshold ablation involves, rather, a phase-explosion scenario (Lorazo *et al.*, 2003).

duration upper limit for phase explosion of $\sim 10^{-11} - 10^{-10}$ s. (iii) In view of the above discussion, the threshold for matter removal under picosecond pulses is determined by the minimum fluence at which *supercritical* expansion takes place. (iv) The ablation threshold *irradiance* for a 100 ps pulse is about 100 times *lower* than that observed for a 500 fs pulse; this can be explained by a significantly larger proportion of the laser energy which is absorbed via inverse bremsstrahlung (whereby the photon energy is entirely converted into kinetic energy of the carriers) in the metallic melt under picosecond irradiation.

5.4.3 Thermodynamics under nanosecond laser irradiation

In a paper published some thirty years ago (Martynyuk, 1976), Martynyuk pointed out that the total ablated mass and the liquid (not gaseous) character of the ejected material under relatively long ($\sim 10^{-7} - 10^{-5}$ s) laser pulses cannot be explained by a simple evaporation model; prompted by this question, Martynyuk proposed a picture whereby the metallic liquid at undersaturated pressure undergoes a phase-explosion process as it is *rapidly heated into the liquid-vapor regime* (Martynyuk, 1976; Martynyuk, 1983; Martynyuk, 1974). The model — reintroduced a decade ago by Miotello and Kelly (Miotello and Kelly, 1995) for nanosecond pulses (and discussed at length in section 5.1) — has since been put forward by numerous other authors for femtosecond to nanosecond pulses (Chen and Beraun, 2003; Willis and Xu, 2002b; Willis and Xu, 2002a; Zhigilei and Garrison, 2000; Zhigilei *et al.*, 2003a; Bulgakova and Bulgakov, 2001; Song and Xu, 1998; Yoo *et al.*, 2000).

However, the above (hypothetical) scenario is not supported by the thermodynamic pathways presented in sections 5.3 and 5.4. In this respect, figure 5.15 summarizes the thermodynamic routes observed in silicon under femtosecond and picosecond laser irradiation and illustrates the expected trajectory under longer, nanosecond

pulses:

(i) Under femtosecond irradiation above the threshold fluence for ablation [figure 5.15(a)], the material is initially pulled *away* from the liquid-vapor regime to a near-critical (marked A→B) or supercritical (A→C) state following mechanical instability in the strongly superheated solid and subsequent isochoric heating of the liquid: (a) In the former case, rapid adiabatic *cooling* of the system into the metastable region gives rise to a phase explosion of the subcritical, *superheated* liquid at a temperature significantly below $0.9T_c$ and in a time $\tau_{\rm NUC} \sim 10^{-12} - 10^{-11}$ s (B→Y→E→F). (b) In the latter case, the higher pressure gradient at the surface results in a faster, *supercritical* expansion of the initially homogeneous material which undergoes a *nonequilibrium* transition to a heterogeneous, clustered fluid through a "nontrivial" fragmentation process (C→D).

(ii) Under picosecond irradiation, homogeneous and, at later times, heterogeneous melting of the superheated crystal (A→G→I) is followed by nonisochoric heating of the metallic melt. Here, the *subcritical* liquid material is eventually cooled along the binodal by heat conduction on a $10^{-11} - 10^{-10}$ s time scale and phase explosion does *not* take place (I→J→Y); as a result, matter removal is associated with the *near-equilibrium* expansion and dissociation into liquid droplets of *supercritical* matter undergoing a "trivial" fragmentation process (I→K).

(iii) As the pulse duration τ_L is further increased, the solid-to-liquid transition is eventually expected to occur at the equilibrium melting temperature (A→H→I) (Fabricius *et al.*, 1986; von der Linde, 1991). If $\tau_L \lesssim \tau_{\rm LV}$, where it is usually assumed that the liquid-vapor equilibration time $\tau_{\rm LV} \sim 10^{-9} - 10^{-8}$ s (Bulgakova and Bulgakov, 2001), the resulting heated liquid metal at undersaturated pressure will enter the metastable region [dashed-dotted line in figure 5.15(b)] where explosive boiling may subsequently occur near the spinodal. However, the absence of

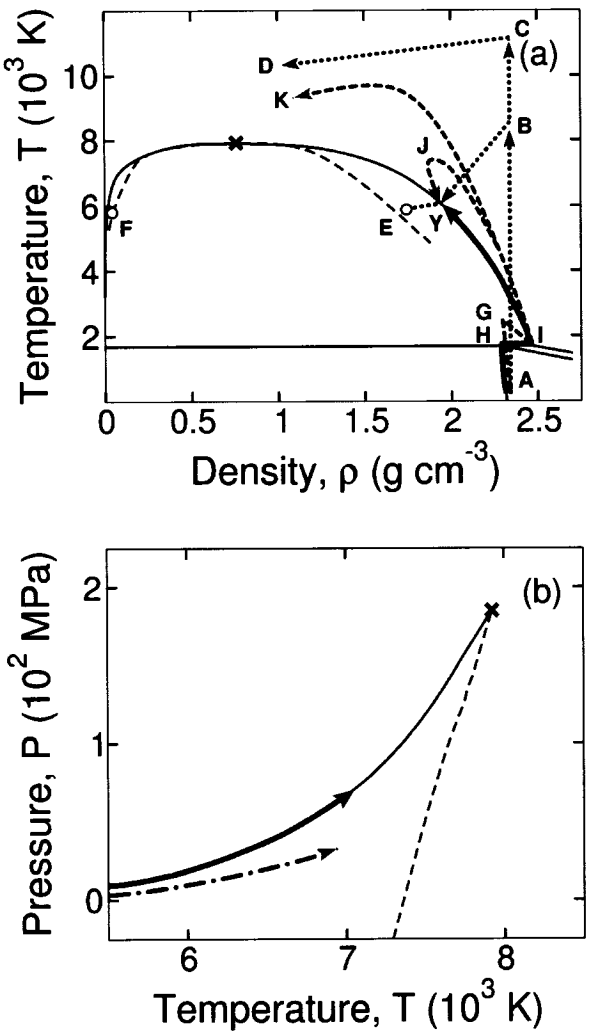

Figure 5.15 Schematic illustration of the thermodynamic pathways in silicon under femtosecond (blue dotted line), picosecond (red dashed line), and nanosecond (thick green solid line) irradiation: (a) ρ-T plane; (b) T-P plane. Capital letters refer to locations in the phase diagram (see text).

metastable *liquid* states observed under picosecond irradiation suggests, rather, that $\tau_{LV} \sim 10^{-11} - 10^{-10}$ s. Consequently, it is more likely that heating takes place *along* the binodal under nanosecond pulses (I→Y).

In this case, the presence of large, micron-sized liquid droplets (Kelly and Miotello, 1999) in the plume could be explained by a second-order phase transition at the critical point near which the metallic melt is expected to transform into a dielectric (Batanov *et al.*, 1973); hydrodynamic mechanisms could also account for the massive matter removal observed in the nanosecond regime (Zhigilei, 2003b).

5.5 Summary and conclusions

In summary, we have explored the thermodynamics involved in laser irradiation of silicon by 500 fs to 100 ps laser pulses. Our combined Monte Carlo and molecular-dynamics simulations reveal thermal transitions taking place between order and disorder and among different states of aggregation on mesoscopic-length and picosecond-to-nanosecond-time scales.

Upon femtosecond irradiation relatively far from the melting threshold, we observe the thermal disordering of a mechanically unstable solid in a time of $\sim 10^{-12}$ s. Under lower superheating with picosecond pulses, rapid homogeneous nucleation of liquid in the metastable solid is followed by slower, heterogeneous melting of the crystal. In contrast, solidification of the nonablated, supercooled melt to a crystal or a glass is a relatively slow process occurring on a $\sim 10^{-11} - 10^{-9}$ s time scale, independent of the pulse duration.

At fluences above a well-defined threshold, hot, liquid material is ejected from the surface with a velocity of $\sim 10^2 - 10^3$ m s^{-1}. Under near-threshold irradiation with femtosecond pulses, the subcritical material undergoes rapid adiabatic cool-

ing to the liquid-gas regime where a phase-explosion-like process takes place on a $10^{-12} - 10^{-11}$ s time scale: here, the onset of ablation — determined by the growth of critical nuclei of the stable vapor phase in the metastable liquid phase — is *not* initiated by large, localized, thermal fluctuations but, rather, by a direct conversion of translational, *mechanical* energy into surface energy. At higher fluences, however, a *nonequilibrium* transition from a homogeneous supercritical fluid to a heterogeneous, clustered phase upon rapid expansion in vacuum, i.e., "nontrivial" fragmentation, determines the early stages of matter removal; recent experimental investigation of silicon nanoparticle generation via femtosecond laser ablation in vacuum supports this scenario (Amoruso *et al.*, 2004).

Under slower expansion with picosecond pulses, liquid-vapor equilibrium is achieved through efficient, nonadiabatic cooling of the *subcritical* liquid material onto the binodal: in this case, the system does *not* access the region of metastable states and phase explosion does *not* occur; as a result, ablation is associated with a "trivial" fragmentation process, i.e., a *near-equilibrium* transition from a homogeneous *supercritical* state to a heterogeneous, fragmented fluid upon relatively slow dilution in vacuum. This implies the equilibration of the metallic liquid with its vapor on a $\sim 10^{-11} - 10^{-10}$ s time scale, thereby indicating a heating process *along* the binodal under nanosecond irradiation.

In view of similar conclusions for metallic systems (Lorazo *et al.*, 2004; Perez and Lewis, 2003; Perez and Lewis, 2004), this suggests universal routes to matter removal extending to pulse durations far beyond the femtosecond regime in absorbing solids (Sokolowski-Tinten *et al.*, 1998b; Rethfeld *et al.*, 2003); in particular, the irrelevance of explosive boiling to picosecond and nanosecond laser irradiation should manifest itself by the absence of interference fringes (Newton rings) in ultrafast time-resolved optical-microscopy experiments (Anisimov *et al.*, 2003).

As a final note, the recent emergence of attosecond pulses is likely to push laser material processing toward new frontiers and horizons in the years to come (Papadogiannis *et al.*, 1999; Paul *et al.*, 2001; Hentschel *et al.*, 2001): in the same way that femtosecond lasers have revealed the existence of ultrafast, nonthermal phenomena following their advent in the early 1980s, the availability of attosecond pulses may unveil unexplored pathways where nonthermal effects are expected to play a greater role. In this regard, ultrashort electron and free-electron-laser x-ray pulses appear as promising candidates to probe new, extreme states of matter (von der Linde, 2003).

5.6 Acknowledgments

We are greatly indebted to Danny Perez for numerous fruitful discussions. P. L. also wishes to thank Philippe Beaucage, Paul Callan, Massimo V. Fischetti, Richard Leonelli, Ralf Meyer, Pier Luigi Silvestrelli, Klaus Sokolowski-Tinten, Frank H. Stillinger, Razvan Stoian, Henry M. van Driel, Dietrich von der Linde, and Leonid V. Zhigilei for their help and useful insights. This work has been supported by grants from the Natural Sciences and Engineering Research Council of Canada (NSERC), the Canada Research Chair on Laser Micro/Nano-engineering of Materials, and the *Fonds Québécois de la Recherche sur la Nature et les Technologies* (FQRNT). We are grateful to the *Réseau Québécois de Calcul de Haute Performance* (RQCHP) for generous allocations of computer resources.

CHAPITRE 6

DISCUSSION GÉNÉRALE ET SYNTHÈSE

Les trajectoires thermodynamiques présentées aux chapitres précédents mettent en évidence des modifications structurales thermiques impliquant, dans la plupart des cas, des états métastables ou instables associés à un rapide chauffage ou refroidissement de la cible de silicium irradiée par des impulsions laser dont la durée varie de 500 fs à 100 ps.

En régime femtoseconde, au voisinage du seuil d'ablation, les simulations confirment — et complémentent — le scénario formulé par Sokolowski-Tinten *et al.* (1998a, 1998b): à la suite d'un chauffage isochore, le matériau à très hautes température et pression entreprend un rapide refroidissement adiabatique vers la région de coexistence liquide-vapeur où survient l'explosion de phase du liquide surchauffé entre deux interfaces nettes en un temps $\tau_{\mathrm{NUC}} \sim 10^{-12} - 10^{-11}$ s et à une température notablement en deçà de $0.9T_c$, et ce, non pas suite à d'importantes fluctuations thermiques mais, plutôt, à une conversion directe de l'énergie de translation (c'est-à-dire mécanique) en énergie de surface.

À des fluences plus élevées, les résultats soutiennent les observations faites pour des systèmes métalliques par Perez et Lewis (2002, 2003): le fluide homogène en rapide expansion supercritique se dissocie en une multitude d'agrégats suivant un processus de fragmentation hors équilibre.

Il est à noter qu'aucune dissociation par décomposition spinodale [tel que tout récemment rapporté par Cheng et Xu (2005)] n'a été observée.

Ainsi, les simulations sont en accord avec l'apparition et la disparition d'anneaux d'interférence observées par Sokolowski-Tinten *et al.* (1998a, 1998b) subséquemment à l'irradiation femtoseconde de semi-conducteurs (et de métaux) à des fluences, respectivement, au voisinage et "loin" du seuil d'ablation.

En régime picoseconde, le liquide dont l'expansion, relativement lente, est sous-critique, est refroidi le long de la binodale (où il parvient à l'équilibre avec sa vapeur saturée) sous l'action de la diffusion de la chaleur sur une échelle de temps de l'ordre de 10^{-11} à 10^{-10} s; autrement dit, le système n'a pas accès à la région métastable et aucune explosion de phase n'a lieu. Conséquemment, seules les régions de la cible dont l'expansion est supercritique contribuent au phénomène d'ablation par l'intermédiaire d'un processus de fragmentation qui, cette fois, se produit au voisinage de l'équilibre thermodynamique.

L'analyse thermodynamique effectuée dans le cadre de cette étude confirme aussi la présence d'une phase cristalline surchauffée dans le matériau irradié. En régime femtoseconde, le solide covalent, rapidement chauffé au-delà de sa limite de stabilité, effectue une transition vers un liquide métallique en un temps $\lesssim 10^{-12}$ s. En régime picoseconde, la fusion du cristal, qui a d'abord lieu par germination homogène d'embryons liquides dans le solide métastable sur une échelle de temps de 10^{-12} à 10^{-11} s, est suivie d'une fusion hétérogène par la propagation d'une interface solide-liquide en volume.

Ainsi, les résultats étayent les calculs théoriques de Rethfeld *et al.* (2002) en confirmant la possibilité d'une germination homogène de liquide dans le cristal surchauffé à l'échelle de la picoseconde.

Enfin, la solidification du liquide non ablaté et surfondu vers un cristal ou un verre est observée en un temps de l'ordre de 10^{-9} s, et ce, indépendamment de la durée

de l'impulsion.

De manière générale, les simulations dévoilent des mécanismes d'ablation mettant en lumière un comportement universel dans les semi-conducteurs s'étendant aux impulsions picoseconde et, possiblement, nanoseconde. Les résultats, dont une illustration schématique est présentée à la figure 5.15, conduisent aussi à une représentation unifiée des possibles trajets thermodynamiques (et modifications structurales associées) résultant d'une irradiation par une brève impulsion laser.

CONCLUSION

La contribution de cette thèse à la modélisation et la compréhension des possibles modifications structurales *thermiques* induites dans les semi-conducteurs par un rayonnement laser est importante et novatrice à plusieurs égards.

Tout d'abord, cette étude a permis la conception d'un modèle unique capable de rendre compte de la vaste majorité des processus et phénomènes aux échelles électronique à mésoscopique qui découlent (sur des périodes de temps allant jusqu'à la nanoseconde) de l'interaction de brèves impulsions laser avec la matière. Bien que ce travail ait porté sur le silicium, le modèle peut aisément être modifié afin d'étudier l'irradiation d'autres semi-conducteurs ainsi que de métaux.

À un niveau plus fondamental, les simulations ont permis de mettre en évidence un temps d'équilibration du liquide métallique avec sa vapeur $\tau_{\mathrm{LV}} \sim 10^{-11} - 10^{-10}$ s notablement inférieur à la valeur couramment admise. Conséquemment, l'explosion de phase, qui n'est possible que si $\tau_L < \tau_{\mathrm{LV}}$, est un phénomène essentiellement propre aux impulsions *femtoseconde*, et non aux impulsions nanoseconde comme le laissent entendre de nombreux travaux.

Les recherches ont aussi conduit à une meilleure compréhension de la *nature* du seuil d'ablation sous irradiation femtoseconde. À cet effet, la germination de bulles de gaz dans le liquide métastable et surchauffé n'est pas la conséquence de fluctuations thermiques locales mais, plutôt, le résultat d'une conversion directe de l'énergie de translation du liquide (acquise lors de son refroidissement vers la région de coexistence liquide-vapeur) en énergie de surface. Cette observation, contraire aux conceptions généralement entretenues, met en exergue l'origine en partie *mécanique* du phénomène.

Enfin, si l'étude a permis de répondre à plusieurs questions, elle en a, en revanche, soulevé de nouvelles.

L'une d'entre elles concerne les mécanismes d'ablation sous irradiation par des impulsions nanoseconde. En effet, celles-ci, d'une durée supérieure à τ_{LV}, doivent — en principe — donner lieu à un chauffage *le long* de la binodale. Dans ce contexte, la dissociation du matériau pourrait survenir au voisinage du point critique suivant une transition de phase du deuxième ordre; de possibles processus *hydrodynamiques* (Zhigilei, 2003b) faisant intervenir la relaxation de forts gradients de pression pourraient aussi expliquer l'éjection de gouttelettes micrométriques en régime nanoseconde.

Une autre question concerne la nature du seuil d'ablation sous irradiation *picoseconde*: si les simulations mettent en lumière une éjection restreinte à la matière supercritique, le détail du processus menant à la rupture du fluide en expansion n'est toujours pas compris.

Finalement, dans les solides organiques caractérisés par une portée de la lumière laser pouvant atteindre un micromètre, d'importants effets inertiels restreignant la libre expansion de la matière située loin de la surface sont anticipés; à cet égard, des simulations pour un système de Lennard-Jones bidimensionnel soumis à une impulsion de plusieurs centaines de picosecondes suggèrent la croissance de cavités par un processus d'explosion de phase similaire à celui observé dans les semi-conducteurs et métaux irradiés par un rayonnement laser femtoseconde.[1]

[1]PEREZ, D., LEWIS, LAURENT J., non publié.

RÉFÉRENCES

ABRAHAM, F. F., BROUGHTON, J. Q. «Pulsed melting of silicon (111) and (100) surfaces simulated by molecular dynamics». *Physical Review Letters.* 56:7 (1986). 734-737.

AGASSI, D. «Phenomenological model for picosecond-pulse laser annealing of semiconductors». *Journal of Applied Physics.* 55:12 (1984). 4376-4383.

ALLEN, M. P., TILDESLEY, D. J. *Computer Simulation of Liquids.* Oxford: Oxford University Press, 1987.

AMORUSO, S., AUSANIO, G., BRUZZESE, R., VITIELLO, M., WANG, X. «Femtosecond laser pulse irradiation of solid targets as a general route to nanoparticle generation in a vacuum». *Physical Review B.* 71:3 (2005). 033406.

AMORUSO, S., BRUZZESE, R., SPINELLI, N., VELOTTA, R., VITIELLO, M., WANG, X., AUSANIO, G., IANNOTTI, V., LANOTTE, L. «Generation of silicon nanoparticles via femtosecond laser ablation in vacuum». *Applied Physics Letters.* 84:22 (2004). 4502-4504.

ANISIMOV, S. I., INOGAMOV, N. A., OPARIN, A. M., RETHFELD, B., YABE, T., OGAWA, M., FORTOV, V. E. «Pulsed laser evaporation: equation-of-state effects». *Applied Physics A.* 69:6 (1999). 617-620.

ANISIMOV, S. I., KAPELIOVICH, B. L., PEREL'MAN, T. L. «Electron emission from metal surfaces exposed to ultrashort laser pulses». *Soviet Physics - JETP.* 39 (1974). 375-377.

ANISIMOV, S. I., ZHAKHOVSKIĬ, V. V., INOGAMOV, N. A., NISHIHARA, K., OPARIN, A. M., PETROV, YU. V. «Destruction of a Solid Film under the Action of Ultrashort Laser Pulse». *JETP Letters.* 77:11 (2003). 606-610.

ASHITKOV, S. I., AGRANAT, M. B., KONDRATENKO, P. S., ANISIMOV, S. I., FORTOV, V. E., TEMNOV, V. V., SOKOLOWSKI-TINTEN, K., RETHFELD, B., ZHOU, P., VON DER LINDE, D. «Ultrafast Laser-Induced Phase Transitions in Tellurium». *JETP Letters.* 76:7 (2002). 461-464.

AUSTON, D. H., SURKO, C. M., VENKATESAN, T. N. C., SLUSHER, R. E., GOLOVCHENKO, J. A. «Time-resolved reflectivity of ion-implanted silicon during laser annealing». *Applied Physics Letters.* 33:5 (1978). 437-440.

BAERI, P., CAMPISANO, S. U., FOTI, G., RIMINI, E. «A melting model for pulsing-laser annealing of implanted semiconductors». *Journal of Applied Physics.* 50:2 (1979). 788-797.

BAERI, P., CAMPISANO, S. U., FOTI, G., RIMINI, E. «Arsenic diffusion in silicon melted by high-power nanosecond laser pulsing». *Applied Physics Letters.* 33:2 (1978). 137-140.

BALAMANE, H., HALICIOGLU, T., TILLER, W. A. «Comparative study of silicon empirical interatomic potentials». *Physical Review B.* 46:4 (1992). 2250-2279.

BASSANI, F., PASTORI PARRAVICINI, G. *Electronic States and Optical Transitions in Solids.* Oxford: Pergamon Press, 1975.

BATANOV, V. A., BUNKIN, F. V., PROKHOROV, A. M., FEDOROV, V. B. «Evaporation of metallic targets caused by intense optical radiation». *Soviet Physics - JETP.* 36:2 (1973). 311-322.

BEAUCAGE, P., MOUSSEAU, N. «Nucleation and crystallization process of silicon using the Stillinger-Weber potential». *Physical Review B.* 71:9 (2005a). 094102.

BEAUCAGE, P., MOUSSEAU, N. «Liquid-liquid phase transition in Stillinger-Weber silicon». *Journal of Physics: Condensed Matter.* 17:15 (2005b). 2269-2279.

BLINOV, L. M., VAVILOV, V. S., GALKIN, G. N. «Changes in optical properties and in charge carrier concentration in silicon and gallium arsenide at an intensive photoexcitation by a ruby laser». *Soviet Physics - Semiconductors.* 1 (1967). 1124-1129.

BLOEMBERGEN, N. «Pulsed laser interactions with condensed matter». *Materials Research Society Symposia Proceedings.* 51 (1985). 3-13.

BLOEMBERGEN, N. «From nanosecond to femtosecond science». *Reviews of Modern Physics.* 71:2 (1999). S283-S287.

BOROWIEC, A., BRUCE, D. M., CASSIDY, D. T., HAUGEN, H. K. «Imaging the strain fields resulting from laser micromachining of semiconductors». *Applied Physics Letters.* 83:2 (2003). 225-227.

BROUGHTON, J. Q., LI, X. P. «Phase diagram of silicon by molecular dynamics». *Physical Review B.* 35:17 (1987). 9120-9127.

BUCKSBAUM, P. H., BOKOR, J. «Rapid Melting and Regrowth Velocities in Silicon Heated by Ultraviolet Picosecond Laser Pulses». *Physical Review Letters.* 53:2 (1984). 182-185.

BULGAKOVA, N. M, BULGAKOV, A. V. «Pulsed laser ablation of solids: transition from normal vaporization to phase explosion». *Applied Physics A.* 73:2 (2001). 199-208.

BULGAKOVA, N. M, STOIAN, R., ROSENFELD, A., HERTEL, I. V., CAMPBELL, E. E. B. «Electronic transport and consequences for material removal in ultrafast pulsed laser ablation of materials». *Physical Review B.* 69:5 (2004). 054102.

CAREY, V. P. *Liquid-Vapor Phase-Change Phenomena.* New York: Hemisphere, 1992.

CAVALLERI, A., SOKOLOWSKI-TINTEN, K., BIALKOWSKI, J., SCHREINER, M., VON DER LINDE, D. «Femtosecond melting and ablation of semiconductors studied with time of flight mass spectroscopy». *Journal of Applied Physics.* 85:6 (1999). 3301-3309.

CAVALLERI, A., SOKOLOWSKI-TINTEN, K., BIALKOWSKI, J., VON DER LINDE, D. «Femtosecond laser ablation of gallium arsenide investigated with time-of-flight mass spectroscopy». *Applied Physics Letters.* 72:19 (1998). 2385-2387.

CAVALLERI, A., TÓTH, CS., SIDERS, C. W., SQUIER, J. A., RÁKSI, F., FORGET, P., KIEFFER, J. C. «Femtosecond Structural Dynamics in VO_2 during an Ultrafast Solid-Solid Phase Transition». *Physical Review Letters.* 87:23 (2001). 237401.

CELLER, G. K., POATE, J. M., KIMERLING, L. C. «Spatially controlled crystal regrowth of ion-implanted silicon by laser irradiation». *Applied Physics Letters.* 32:8 (1978). 464-466.

CHEN, J. K., BERAUN, J. E. «Modelling of ultrashort laser ablation of gold films in vacuum». *Journal of Optics A.* 5:3 (2003). 168-173.

CHENG, C., XU, X. «Mechanisms of decomposition of metal during femtosecond laser ablation». *Physical Review B.* 72:16 (2005). 165415.

CHICHKOV, B. N., MOMMA, C., NOLTE, S., VON ALVENSLEBEN, F., TÜNNERMANN, A. «Femtosecond, picosecond and nanosecond laser ablation of solids». *Applied Physics A.* 63 (1996). 109-115.

CHRISEY, D. B., HUBLER, G. K. *Pulsed Laser Deposition of Thin films.* New York: John Wiley and Sons, 1994.

COWLEY, E. R. «Lattice Dynamics of Silicon with Empirical Many-Body Potentials». *Physical Review Letters.* 60:23 (1988). 2379-2381.

CULLIS, A. G., WEBBER, H. C., CHEW, N. G., POATE, J. M., BAERI, P. «Transitions to Defective Crystal and the Amorphous State Induced in Elemental Si by Laser Quenching». *Physical Review Letters.* 49:3 (1982). 219-222.

DOWNER, M. C., FORK, R. L., SHANK, C. V. «Femtosecond imaging of melting and evaporation at a photoexcited silicon surface». *Journal of the Optical Society of America B.* 2:4 (1985). 595-599.

EESLEY, G. L. «Generation of nonequilibrium electron and lattice temperatures in copper by picosecond laser pulses». *Physical Review B.* 33:4 (1986). 2144-2151.

FABRICIUS, N., HERMES, P., VON DER LINDE, D., POSPIESZCZYK, A., STRITZKER, B. «Observation of superheating during picosecond laser melting». *Solid State Communications.* 58:4 (1986). 239-242.

FISCHETTI, M. V., LAUX, S. E. «Monte carlo analysis of electron transport in small semiconductor devices including band-structure and space-charge effects». *Physical Review B.* 38:14 (1988). 9721-9745.

FISCHETTI, M. V., LAUX, S. E., CRABBÉ, E. «Understanding hot-electron transport in silicon devices: Is there a shortcut?». *Journal of Applied Physics.* 78:2 (1995). 1058-1087.

GANTNER, G., BOYEN, H. G., OELHAFEN, P. «Valence band photoelectron spectroscopy of liquid silicon». *Europhysics Letters.* 31:3 (1995). 163-168.

GARRISON, B. J., ITINA, T. E., ZHIGILEI, L. V. «Limit of overheating and the threshold behavior in laser ablation». *Physical Review E.* 68:4 (2003). 041501.

GILLET, J.-N., DEGORCE, J.-Y., MEUNIER, M. «General model and segregation coefficient measurement for ultrashallow doping by excimer laser annealing». *Applied Physics Letters.* 86:22 (2005). 222104.

GLAZOV, V. M., CHIZHEVSKAYA, S. N., GLAGOLEVA, N. N. *Liquid Semiconductors.* New York: Plenum Press, 1969.

GLAZOV, V. M., KOL'TSOV, V. B. «Changes in the effective mass and mobility of electrons as a result of melting of germanium and silicon». *Soviet Physics - Semiconductors.* 18:10 (1984). 1153-1156.

GLOVER, T. E. «Hydrodynamics of particle formation following femtosecond laser ablation». *Journal of the Optical Society of America B.* 20:1 (2003). 125-131.

GODLEVSKY, V. V., DERBY, J. J., CHELIKOWSKY, J. R. «*Ab Initio* Molecular Dynamics Simulation of Liquid CdTe and GaAs: Semiconducting versus Metallic Behavior». *Physical Review Letters.* 81:22 (1998). 4959-4962.

HENTSCHEL, M., KIENBERGER, R., SPIELMANN, CH., REIDER, G. A., MILOSEVIC, N., BRABEC, T., CORKUM, P., HEINZMANN, U., DRESCHER, M., KRAUSZ, F. «Attosecond metrology». *Nature (London).* 414:6863 (2001). 509-513.

HONDA, N., NAGASAKA, Y. «Vapor-Liquid Equilibria of Silicon by the Gibbs Ensemble Simulation». *International Journal of Thermophysics.* 20:3 (1999). 837-846.

HOSHEN, J., KOPELMAN, R. «Percolation and cluster distribution. I. Cluster multiple labeling technique and critical concentration algorithm». *Physical Review B.* 14:8 (1976). 3438-3445.

HUANG, L., CALLAN, J. P., GLEZER, E. N., MAZUR, E. «GaAs under Intense Ultrafast Excitation: Response of the Dielectric Function». *Physical Review Letters.* 80:1 (1998). 185-188.

INOGAMOV, N. A., PETROV, YU. V., ANISIMOV, S. I., OPARIN, A. M., SHAPOSHNIKOV, N. V., VON DER LINDE, D., MEYER-TER-VEHN, J. «Expansion of matter heated by an ultrashort laser pulse». *JETP Letters.* 69:4 (1999a). 310-316.

INOGAMOV, N. A., ANISIMOV, S. I., RETFELD, B. «Rarefaction wave and gravitational equilibrium in a two-phase liquid-vapor medium». *Journal of Experimental and Theoretical Physics.* 88:6 (1999b). 1143-1150.

IVANOV, D. S., ZHIGILEI, L. V. «Effect of Pressure Relaxation on the Mechanisms of Short-Pulse Laser Melting». *Physical Review Letters.* 91:10 (2003a). 105701.

IVANOV, D. S., ZHIGILEI, L. V. «Combined atomistic-continuum modeling of short-pulse laser melting and disintegration of metal films». *Physical Review B.* 68:6 (2003b). 064114.

JACOBONI, C., REGGIANI, L. «The Monte Carlo method for the solution of charge transport in semiconductors with applications to covalent materials». *Reviews of Modern Physics.* 55:3 (1983). 645-705.

JANDELEIT, J., URBASCH, G., HOFFMANN, H. D., TREUSCH, H.-G., KREUTZ, E. W. «Picosecond laser ablation of thin copper films». *Applied Physics A.* 63 (1996). 117-121.

KACHURIN, G. A., PRIDACHIN, N. B., SMIRNOV, L. S. «Annealing of radiation-induced defects by pulsed laser irradiation». *Soviet Physics - Semiconductors.* 9 (1976). 946.

KAMAKURA, Y., MIZUNO, H., YAMAJI, M., MORIFUJI, M., TANIGUCHI, K., HAMAGUCHI, C., KUNIKIYO, T., TAKENAKA, M. «Impact ionization model for full band Monte Carlo simulation». *Journal of Applied Physics.* 75:7 (1994). 3500-3506.

KELLY, R., MIOTELLO, A. «Contribution of vaporization and boiling to thermal-spike sputtering by ions or laser pulses». *Physical Review E.* 60:3 (1999). 2616-2625.

KHAIBULLIN, I. B., SHTYRKOV, E. I., ZARIPOV, M. M., BAYAZITOV, R. M., GALYATUDINOV, M. F. «Some features of laser annealing of implanted silicon layers». *Radiation Effects.* 36:3-4 (1978). 225-233.

KHAIBULLIN, I. B., SHTYRKOV, E. I., ZARIPOV, M. M., GALYATUDINOV, M. F., ZAKIROV, G. G. «Utilization coefficient of implanted impurities in silicon layers subjected to subsequent laser annealing». *Soviet Physics - Semiconductors.* 11:2 (1977). 190.

KITTEL, C. *Introduction to Solid State Physics.* 8th ed. New York: John Wiley and Sons, 2005.

KLUGE, M. D., RAY, J. R. «Velocity versus temperature relation for solidification and melting of silicon: A molecular-dynamics study». *Physical Review B.* 39:3 (1989). 1738-1746.

KOCH, S. W., DESAI, R. C., ABRAHAM, F. F. «Dynamics of phase separation in two-dimensional fluids: Spinodal decomposition». *Physical Review A.* 27:4 (1983). 2152-2167.

KUNIKIYO, T., TAKENAKA, M., MORIFUJI, M., TANIGUCHI, K., HAMAGUCHI, C. «A model of impact ionization due to the primary hole in silicon for

a full band Monte Carlo simulation». *Journal of Applied Physics.* 79:10 (1996). 7718-7725.

LANDSBERG, P. T. *Recombination in Semiconductors.* Cambridge: Cambridge University Press, 1991.

LARSON, B. C., TISCHLER, J. Z., MILLS, D. M. *Materials Research Society Symposia Proceedings.* 51 (1985). 113.

LARSON, B. C., WHITE, C. W., NOGGLE, T. S., MILLS, D. «Synchrotron X-Ray Diffraction Study of Silicon during Pulsed-Laser Annealing». *Physical Review Letters.* 48:5 (1982). 337-340.

LI, K. D., FAUCHET, P. M. «Drude parameters of liquid silicon at the melting temperature». *Applied Physics Letters.* 51:21 (1987). 1747-1749.

LIETOILA, A., GIBBONS, J. F. «Computer modeling of the temperature rise and carrier concentration induced in silicon by nanosecond laser pulses». *Journal of Applied Physics.* 53:4 (1982). 3207-3213.

LINDENBERG, A. M., LARSSON, J., SOKOLOWSKI-TINTEN, K., GAFFNEY, K. J., BLOME, C., SYNNERGREN, O., SHEPPARD, J., CALEMAN, C., MACPHEE, A. G., WEINSTEIN, D., LOWNEY, D. P., ALLISON, T. K., MATTHEWS, T., FALCONE, R. W., CAVALIERI, A. L., FRITZ, D. M., LEE, S. H., BUCKSBAUM, P. H., REIS, D. A., RUDATI, J., FUOSS, P. H., KAO, C. C., SIDDONS, D. P., PAHL, R., ALS-NIELSEN, J., DUESTERER, S., ISCHEBECK, R., SCHLARB, H., SCHULTE-SCHREPPING, H., TSCHENTSCHER, TH., SCHNEIDER, J., VON DER LINDE, D., HIGNETTE, O., SETTE, F., CHAPMAN, H. N., LEE, R. W., HANSEN, T. N., TECHERT, S., WARK, J. S., BERGH, M., HULDT, G., VAN DER SPOEL, D., TIMNEANU, N., HAJDU, J., AKRE, R. A., BONG, E., KREJCIK, P.,

ARTHUR, J., BRENNAN, S., LUENING, K., HASTINGS, J. B. «Atomic-Scale Visualization of Inertial Dynamics». *Science.* 308:5720 (2005). 392-395.

LIU, Y. S., WANG, K. L. «A transient optical reflectivity study of laser annealing of ion-implanted silicon: Thresholds and kinetics». *Applied Physics Letters.* 34:6 (1979a). 363-365.

LIU, J. M., YEN, R., KURZ, H., BLOEMBERGEN, N. «Phase transformation on and charged particle emission from a silicon crystal surface, induced by picosecond laser pulses». *Applied Physics Letters.* 39:9 (1981). 755-757.

LIU, J. M., KURZ, H., BLOEMBERGEN, N. «Picosecond time-resolved plasma and temperature-induced changes of reflectivity and transmission in silicon». *Applied Physics Letters.* 41:7 (1982). 643-646.

LIU, J. M., MALVEZZI, A. M., BLOEMBERGEN, N. «Picosecond laser melting and evaporation of GaAs surfaces». *Applied Physics Letters.* 49:11 (1986). 622-624.

LIU, P. L., YEN, R., BLOEMBERGEN, N., HODGSON, R. T. «Picosecond laser-induced melting and resolidification morphology on Si». *Applied Physics Letters.* 34:12 (1979b). 864-866.

LO, H. W., COMPAAN, A. «Raman Measurement of Lattice Temperature during Pulsed Laser Heating of Silicon». *Physical Review Letters.* 44:24 (1980). 1604-1607.

LOMPRÉ, L. A., LIU, J. M., KURZ, H., BLOEMBERGEN, N. «Time-resolved temperature measurement of picosecond laser irradiated silicon» *Applied Physics Letters.* 43:2 (1983). 168-170.

LORAZO, P., LEWIS, L. J., MEUNIER, M. «Short-Pulse Laser Ablation of Solids: From Phase Explosion to Fragmentation». *Physical Review Letters.* 91:22 (2003). 225502.

LORAZO, P., PEREZ, D., LEWIS, L. J., MEUNIER, M. «Thermodynamics of absorbing solids during short-pulse laser ablation». *Proceedings of the SPIE: High-Power Laser Ablation V.* Bellingham, WA: Edited by PHIPPS, C. R. 2004. Vol. 5448, P. 520-531.

LOWNDES, D. H., WOOD, R. F. «Time-resolved reflectivity during pulsed-laser irradiation of GaAs». *Applied Physics Letters.* 38:12 (1981). 971-973.

LU, Q., MAO, S. S., MAO, X., RUSSO, R. E. «Delayed phase explosion during high-power nanosecond laser ablation of silicon». *Applied Physics Letters.* 80:17 (2002). 3072-3074.

LUEDTKE, W. D., LANDMAN, U. «Preparation, structure, dynamics, and energetics of amorphous silicon: A molecular-dynamics study». *Physical Review B.* 40:2 (1989). 1164-1174.

LUNDSTROM, M. *Fundamentals of Carrier Transport.* Reading, MA: Addison-Wesley, 1990.

LUNDSTROM, M. *Fundamentals of Carrier Transport.* 2nd ed. Cambridge: Cambridge University Press, 2000.

MAIMAN, T. H. «Stimulated Optical Radiation in Ruby». *Nature (London).* 187:4736 (1960). 493-494.

MAKHOV, D. V., LEWIS, L. J. «Isotherms for the liquid-gas phase transition in silicon from NPT Monte Carlo simulations». *Physical Review B.* 67:15 (2003). 153202.

MALVEZZI, A. M., LIU, J. M., BLOEMBERGEN, N. «Photoelectric emission studies from crystalline silicon at 266 nm». *Materials Research Society Symposia Proceedings.* 23 (1984). 135-139.

MARTYNYUK, M. M. «Mechanism for metal damage by intense electromagnetic radiation». *Soviet Physics - Technical Physics.* 21:4 (1976). 430-433.

MARTYNYUK, M. M. «Critical constants of metals». *Russian Journal of Physical Chemistry.* 57:4 (1983). 494-501.

MARTYNYUK, M. M. «Vaporization and boiling of liquid metal in an explosive wire». *Soviet Physics - Technical Physics.* 19:6 (1974). 793-797.

MIOTELLO, A., KELLY, R. «Critical assessment of thermal models for laser sputtering at high fluences». *Applied Physics Letters.* 67:24 (1995). 3535-3537.

MIOTELLO, A., KELLY, R. «Laser-induced phase explosion: new physical problems when a condensed phase approaches the thermodynamic critical temperature». *Applied Physics A.* 69 (1999). S67-S73.

MORAN, M. J., SHAPIRO, H. N. *Fundamentals of Engineering Thermodynamics.* 4th ed. New York: John Wiley and Sons, 2000.

MURAYAMA, M., NAKAYAMA, T. «*Ab initio* calculations of two-photon absorption spectra in semiconductors». *Physical Review B.* 52:7 (1995). 4986-4997.

NEDIALKOV, N. N., IMAMOVA, S. E., ATANASOV, P. A. «Ablation of metals by ultrashort laser pulses». *Journal of Physics D: Applied Physics.* 37:4 (2004). 638-643.

NOYA, J. C., HERRERO, C. P., RAMÍREZ, R. «Thermodynamic properties of c-Si derived by quantum path-integral Monte Carlo simulations». *Physical Review B.* 53:15 (1996). 9869-9875.

ORAEVSKY, A. A., JACQUES, S. L., TITTEL, F. K. «Mechanism of laser ablation for aqueous media irradiated under confined-stress conditions». *Journal of Applied Physics.* 78:2 (1995). 1281-1290.

PAPADOGIANNIS, N. A., WITZEL, B., KALPOUZOS, C., CHARALAMBIDIS, D. «Observation of Attosecond Light Localization in Higher Order Harmonic Generation». *Physical Review Letters.* 83:21 (1999). 4289-4292.

PAUL, P. M., TOMA, E. S., BREGER, P., MULLOT, G., AUGÉ, F., BALCOU, PH., MULLER, H. G., AGOSTINI, P. «Observation of a Train of Attosecond Pulses from High Harmonic Generation». *Science.* 292:5522 (2001). 1689-1692.

PEREZ, D., LEWIS, L. J. «Ablation of Solids under Femtosecond Laser Pulses». *Physical Review Letters.* 89:25 (2002). 255504.

PEREZ, D., LEWIS, L. J. «Molecular-dynamics study of ablation of solids under femtosecond laser pulses». *Physical Review B.* 67:18 (2003). 184102.

PEREZ, D., LEWIS, L. J. «Thermodynamic evolution of materials during laser ablation under pico and femtosecond pulses». *Applied Physics A.* 79:4-6 (2004). 987-990.

PRONKO, P. P., DUTTA, S. K., DU, D., SINGH, R. K. «Thermophysical effects in laser processing of materials with picosecond and femtosecond pulses». *Journal of Applied Physics.* 78:10 (1995). 6233-6240.

RETHFELD, B. «Unified Model for the Free-Electron Avalanche in Laser-Irradiated Dielectrics». *Physical Review Letters.* 92:18 (2004). 187401.

RETHFELD, B., SOKOLOWSKI-TINTEN, K., VON DER LINDE, D. «Ultrafast thermal melting of laser-excited solids by homogeneous nucleation». *Physical Review B.* 65:9 (2002). 092103.

RETHFELD, B., TEMNOV, V. V., SOKOLOWSKI-TINTEN, K., ANISIMOV, S. I., VON DER LINDE, D. «Dynamics of ultrashort pulse-laser ablation: equation-of-state considerations». *Proceedings of the SPIE: High-Power Laser Ablation IV.* Bellingham, WA: Edited by PHIPPS, C. R. 2002. Vol. 4760, P. 72-80.

ROETERDINK, W. G., JUURLINK, L. B. F., VAUGHAN, O. P. H., DURA DIEZ, J., BONN, M., KLEYN, A. W. «Coulomb explosion in femtosecond laser ablation of Si(111)». *Applied Physics Letters.* 82:23 (2003). 4190-4192.

ROUSSE, A., RISCHEL, C., FOURMAUX, S., USCHMANN, I., SEBBAN, S., GRILLON, G., BALCOU, PH., FÖRSTER, E., GEINDRE, J. P., AUDEBERT, P., GAUTHIER, J. C., HULIN, D. «Non-thermal melting in semiconductors measured at femtosecond resolution». *Nature (London).* 410:6824 (2001). 65-68.

SAETA, P., WANG, J.-K., SIEGAL, Y., BLOEMBERGEN, N., MAZUR, E. «Ultrafast electronic disordering during femtosecond laser melting of GaAs». *Physical Review Letters.* 67:8 (1991). 1023-1026.

SASTRY, S., ANGELL, C. A. «Liquid-liquid phase transition in supercooled silicon». *Nature Materials.* 2:11 (2003). 739-743.

SCHÄFER, C., URBASSEK, H. M., ZHIGILEI, L. V. «Metal ablation by picosecond laser pulses: A hybrid simulation». *Physical Review B.* 66:11 (2002). 115404.

SHANK, C. V., YEN, R., HIRLIMANN, C. «Femtosecond-Time-Resolved Surface Structural Dynamics of Optically Excited Silicon». *Physical Review Letters.* 51:10 (1983a). 900-902.

SHANK, C. V., YEN, R., HIRLIMANN, C. «Time-Resolved Reflectivity Measurements of Femtosecond-Optical-Pulse-Induced Phase Transitions in Silicon». *Physical Review Letters.* 50:6 (1983b). 454-457.

SHINDE, S. R., OGALE, S. B., GREENE, R. L., VENKATESAN, T., CANFIELD, P. C., BUD'KO, S. L., LAPERTOT, G., PETROVIC, C. «Superconducting MgB_2 thin films by pulsed laser deposition». *Applied Physics Letters.* 79:2 (2001). 227-229.

SHTYRKOV, E. I., KHAIBULLIN, I. B., ZARIPOV, M. M., GALYATUDINOV, M. F., BAYAZITOV, R. M. «Local laser annealing of ion-doped semiconductor layers». *Soviet Physics - Semiconductors.* 9:10 (1976). 1309-1310.

SIDERS, C. W., CAVALLERI, A., SOKOLOWSKI-TINTEN, K., TÓTH, CS., GUO, T., KAMMLER, M., HORN VON HOEGEN, M., WILSON, K. R., VON DER LINDE, D., BARTY, C. P. J. «Detection of Nonthermal Melting by Ultrafast X-ray Diffraction». *Science.* 286:5443 (1999). 1340-1342.

SIEGAL, Y., GLEZER, E. N., HUANG, L., MAZUR, E. «Laser-Induced Phase Transitions in Semiconductors». *Annual Review of Materials Science.* 25 (1995). 223-247.

SILVESTRELLI, P. L., ALAVI, A., PARRINELLO, M., FRENKEL, D. «*Ab initio* Molecular Dynamics Simulation of Laser Melting of Silicon». *Physical Review Letters.* 77:15 (1996). 3149-3152.

SIWICK, B. J., DWYER, J. R., JORDAN, R. E., MILLER, R. J. D. «An Atomic-Level View of Melting Using Femtosecond Electron Diffraction». *Science.* 302:5649 (2003). 1382-1385.

SOKOLOWSKI-TINTEN, K., BIALKOWSKI, J., VON DER LINDE, D. «Ultrafast laser-induced order-disorder transitions in semiconductors». *Physical Review B.* 51:20 (1995). 14186-14198.

SOKOLOWSKI-TINTEN, K., BIALKOWSKI, J., CAVALLERI, A., BOING, M., SCHÜLER, H., VON DER LINDE, D. «Dynamics of femtosecond laser induced ablation from solid surfaces». *Proceedings of the SPIE: High-Power Laser Ablation.* Bellingham, WA: Edited by PHIPPS, C. R. 1998a. Vol. 3343, P. 46-57.

SOKOLOWSKI-TINTEN, K., BIALKOWSKI, J., CAVALLERI, A., VON DER LINDE, D., OPARIN, A., MEYER-TER-VEHN, J., ANISIMOV, S. I. «Transient

States of Matter during Short Pulse Laser Ablation». *Physical Review Letters.* 81:1 (1998b). 224-227.

SOKOLOWSKI-TINTEN, K., BIALKOWSKI, J., BOING, M., CAVALLERI, A., VON DER LINDE, D. «Thermal and nonthermal melting of gallium arsenide after femtosecond laser excitation». *Physical Review B.* 58:18 (1998c). R11805-R11808.

SOKOLOWSKI-TINTEN, K., BLOME, C., BLUMS, J., CAVALLERI, A., DIETRICH, C., TARASEVITCH, A., USCHMANN, I., FÖRSTER, E., KAMMLER, M., HORN-VON-HOEGEN, M., VON DER LINDE, D. «Femtosecond X-ray measurement of coherent lattice vibrations near the Lindemann stability limit». *Nature (London).* 422:6929 (2003). 287-289.

SOKOLOWSKI-TINTEN, K., BLOME, C., DIETRICH, C., TARASEVITCH, A., HORN VON HOEGEN, M., VON DER LINDE, D., CAVALLERI, A., SQUIER, J., KAMMLER, M. «Femtosecond X-Ray Measurement of Ultrafast Melting and Large Acoustic Transients». *Physical Review Letters.* 87:22 (2001). 225701.

SOKOLOWSKI-TINTEN, VON DER LINDE, D. «Generation of dense electron-hole plasmas in silicon». *Physical Review B.* 61:4 (2000). 2643-2650.

SONG, K. H., XU, X. «Explosive phase transformation in excimer laser ablation». *Applied Surface Science.* 127-129 (1998). 111-116.

SOOY, W. R., GELLER, M., BORTFELD, D. P. «Switching of semiconductor reflectivity by a giant pulse laser». *Applied Physics Letters.* 5:3 (1964). 54-56.

STAMPFLI, P., BENNEMANN, K. H. «Time dependence of the laser-induced femtosecond lattice instability of Si and GaAs: Role of longitudinal optical distorsions». *Physical Review B.* 49:11 (1994). 7299-7305.

STIFFLER, S. R., THOMPSON, M. O., PEERCY, P. S. «Supercooling and Nucleation of Silicon after Laser Melting». *Physical Review Letters.* 60:24 (1988). 2519-2522.

STILLINGER, F. H., WEBER, T. A. «Computer simulation of local order in condensed phases of silicon». *Physical Review B.* 31:8 (1985). 5262-5271.

STOIAN, R., ROSENFELD, A., ASHKENASI, D., HERTEL, I. V., BULGAKOVA, N. M., CAMPBELL, E. E. B. «Surface Charging and Impulsive Ion Ejection during Ultrashort Pulsed Laser Ablation». *Physical Review Letters.* 88:9 (2002). 097603.

STOIAN, R., private communication (2004).

STRITZKER, B., POSPIESZCZYK, A., TAGLE, J. A. «Measurement of Lattice Temperature of Silicon during Pulsed Laser Annealing». *Physical Review Letters.* 47:5 (1981). 356-358.

SUN, B. K., ZHANG, X., GRIGOROPOULOS, C. P. «Spectral optical functions of silicon in the range of 1.13-4.96 eV at elevated temperatures». *International Journal of Heat and Mass Transfer.* 40:7 (1997). 1591-1600.

SUNDARAM, S. K., MAZUR, E. «Inducing and probing non-thermal transitions in semiconductors using femtosecond laser pulses». *Nature Materials.* 1:4 (2002). 217-224.

SURKO, C. M., SIMONS, A. L., AUSTON, D. H., GOLOVCHENKO, J. A., SLUSHER, R. E., VENKATESAN, T. N. C. «Calculation of the dynamics of surface melting during laser annealing». *Applied Physics Letters.* 34:10 (1979). 635-637.

SVANTESSON, K. G., NILSSON, N. G., HULDT, L. «Recombination in strongly excited silicon». *Solid State Communications.* 9:3 (1971). 213-216.

SYLVESTRE, J.-P., KABASHIN, A. V., SACHER, E., MEUNIER, M., LUONG, J. H. T. «Stabilization and Size Control of Gold Nanoparticles during Laser Ablation in Aqueous Cyclodextrins». *Journal of the American Chemical Society.* 126:23 (2004). 7176-7177.

THOMPSON, M. O., MAYER, J. W., CULLIS, A. G., WEBBER, H. C., CHEW, N. G., POATE, J. M., JACOBSON, D. C. «Silicon Melt, Regrowth, and Amorphization Velocities During Pulsed Laser Irradiation». *Physical Review Letters.* 50:12 (1983). 896-899.

TSU, R., HODGSON, R. T., TAN, T. Y., BAGLIN, J. E. «Order-Disorder Transition in Single-Crystal Silicon Induced by Pulsed uv Laser Irradiation». *Physical Review Letters.* 42:20 (1979). 1356-1358.

VAN DRIEL, H. M. «Kinetics of high-density plasmas generated in Si by 1.06- and 0.53-μm picosecond laser pulses». *Physical Review B.* 35:15 (1987). 8166-8176.

VAN VECHTEN, J. A., TSU, R., SARIS, F. W. «Nonthermal pulsed laser annealing of Si; plasma annealing». *Physics Letters A.* 74:6 (1979). 422-426.

VIDAL, F., JOHNSTON, T. W., LAVILLE, S., BARTHÉLEMY, O., CHAKER, M., LE DROGOFF, B., MARGOT, J., SABSABI, M. «Critical-Point Phase Separation in Laser Ablation of Conductors». *Physical Review Letters.* 86:12 (2001). 2573-2576.

VINK, R. L. C., BARKEMA, G. T., VAN DER WEG, W. F., MOUSSEAU, N. «Fitting the Stillinger-Weber potential to amorphous silicon». *Journal of Non-Crystalline Solids.* 282:2-3 (2001). 248-255.

VOGEL, A., VENUGOPALAN, V. «Mechanisms of Pulsed Laser Ablation of Biological Tissues». *Chemical Reviews.* 103:2 (2003). 577-644.

VON ALLMEN, M., BLATTER, A. *Laser-Beam Interactions with Materials.* 2nd ed. Berlin: Springer, 1995.

VON DER LINDE, D., private communication (2001).

VON DER LINDE, D. «A Picosecond View of Melting». *Science.* 302:5649 (2003). 1345-1346.

VON DER LINDE, D. 1991. «Solid-liquid phase transformations induced by ultrashort laser pulses». *Resonances: A Volume in Honor of the 70th Birthday of Nicolaas Bloembergen.* Singapore: Edited by LEVENSON, M. D., MAZUR, E., PERSHAN, P. S., SHEN, Y. R. P. 337-347.

VON DER LINDE, D., SCHÜLER, H. «Breakdown threshold and plasma formation in femtosecond laser-solid interaction». *Journal of the Optical Society of America B.* 13:1 (1996). 216-222.

VON DER LINDE, D., SOKOLOWSKI-TINTEN, K. «The physical mechanisms of short-pulse laser ablation». *Applied Surface Science.* 154-155 (2000). 1-10.

VON DER LINDE, D., SOKOLOWSKI-TINTEN, K., BIALKOWSKI, J. «Laser-solid interaction in the femtosecond time regime». *Applied Surface Science.* 109-110 (1997). 1-10.

VON DER LINDE, D., WARTMANN, G. «Raman scattering with nanosecond resolution during pulsed laser annealing of silicon». *Applied Physics Letters.* 41:8 (1982). 700-702.

YOO, J. H., JEONG, S. H., MAO, X. L., GREIF, R., RUSSO, R. E. «Evidence for phase-explosion and generation of large particles during high power nanosecond laser ablation of silicon». *Applied Physics Letters.* 76:6 (2000). 783-785.

YOUNG, R. T., WHITE, C. W., CLARK, G. J., NARAYAN, J., CHRISTIE, W. H., MURAKAMI, M., KING, P. W., KRAMER, S. D. «Laser annealing of boron-implanted silicon». *Applied Physics Letters.* 32:3 (1978). 139-141.

WANG, J. C., WOOD, R. F., PRONKO, P. P. «Theoretical analysis of thermal and mass transport in ion-implanted laser-annealed silicon». *Applied Physics Letters.* 33:5 (1978). 455-458.

WHITE, C. W., CHRISTIE, W. H., APPLETON, B. R., WILSON, S. R., PRONKO, P. P., MAGEE, C. W. «Redistribution of dopants in ion-implanted silicon by pulsed-laser annealing». *Applied Physics Letters.* 33:7 (1978). 662-664.

WIGGINS, S. M., SOLIS, J., AFONSO, C. N. «Influence of pulse duration on the amorphization of GeSb thin films under ultrashort laser pulses». *Applied Physics Letters.* 84:22 (2004). 4445-4447.

WILLIS, D. A., XU, X. «Heat transfer and phase change during picosecond laser ablation of nickel». *International Journal of Heat and Mass Transfer.* 45:19 (2002a). 3911-3918.

WILLIS, D. A., XU, X. «In situ photography of picosecond laser ablation of nickel». *Applied Surface Science.* 197-198 (2002b). 118-123.

WILLMOTT, P. R., HUBER, J. R. «Pulsed laser vaporization and deposition». *Reviews of Modern Physics.* 72:1 (2000). 315-328.

WOOD, R. F. *Materials Research Society Symposia Proceedings.* 13 (1983). 83.

WOOD, R. F., GILES, G. E. «Macroscopic theory of pulsed-laser annealing. I. Thermal transport and melting». *Physical Review B.* 23:6 (1981). 2923-2942.

WOOD, R. F., WHITE, C. W., YOUNG, R. T. *Pulsed Laser Processing of Semiconductors.* Orlando: Academic Press, 1984. 693 p. Collection Semiconductors and Semimetals; n°23.

XU, X. «Phase explosion and its time lag in nanosecond laser ablation». *Applied Surface Science.* 197-198 (2002). 61-66.

YAVAS, O., LEIDERER, P., PARK, H. K., GRIGOROPOULOS, C. P., POON, C. C., TAM, A. C. «Enhanced acoustic cavitation following laser-induced bubble formation: Long-term memory effect». *Physical Review Letters.* 72:13 (1994). 2021-2024.

YOFFA, E. J. «Dynamics of dense laser-induced plasmas». *Physical Review B.* 21:6 (1980). 2415-2425.

YOUNG, J. F., VAN DRIEL, H. M. «Ambipolar diffusion of high-density electrons and holes in Ge, Si, and GaAs: Many-body effects». *Physical Review B.* 26:4 (1982). 2147-2158.

ZAPKA, W., ZIEMLICH, W., TAM, A. C. «Efficient pulsed laser removal of 0.2 μm sized particles from a solid surface». *Applied Physics Letters.* 58:20 (1991). 2217-2219.

ZHAKHOVSKIĬ, V. V., NISHIHARA, K., ANISIMOV, S. I., INOGAMOV, N. A. «Molecular-Dynamics Simulation of Rarefaction Waves in Media That Can Undergo Phase Transitions». *JETP Letters.* 71:4 (2000). 167-172.

ZHIGILEI, L .V. «Dynamics of the plume formation and parameters of the ejected clusters in short-pulse laser ablation». *Applied Physics A.* 76:3 (2003b). 339-350.

ZHIGILEI, L .V., GARRISON, B. J. «Microscopic mechanisms of laser ablation of organic solids in the thermal and stress confinement irradiation regimes». *Journal of Applied Physics.* 88:3 (2000). 1281-1298.

ZHIGILEI, L .V., KODALI, P. B. S., GARRISON, B. J. «On the threshold behavior in laser ablation of organic solids». *Chemical Physics Letters.* 276:3-4 (1997). 269-273.

ZHIGILEI, L .V., LEVEUGLE, E., GARRISON, B. J., YINGLING, Y. G., ZEIFMAN, M. I. «Computer Simulations of Laser Ablation of Molecular Substrates». *Chemical Reviews.* 103:2 (2003a). 321-348.

ANNEXE I

PARAMÈTRES DU MODÈLE

Le modèle combinant les techniques Monte Carlo et de dynamique moléculaire présenté au chapitre 5 comporte de nombreux paramètres dont un seul, formellement, est ajustable (*free parameter*).

Cependant, si la valeur de la vaste majorité de ces paramètres est bien connue (grâce, notamment, aux nombreux travaux expérimentaux et théoriques se retrouvant dans l'abondante littérature couvrant l'interaction de brèves impulsions laser avec la matière), un manque de données ou l'absence de consensus implique, dans certains cas, une incertitude accrue.

À cet égard, la présente annexe est consacrée à une brève revue des paramètres dont la détermination de la valeur, pour les raisons ci-haut mentionnées, a nécessité l'exercice d'une certaine forme de jugement; ceux-ci se rapportent à trois grandes catégories correspondant aux principales subdivisions du modèle.

I.1 Impulsion laser et processus d'absorption

Tel que détaillé à la section 5.2.1.1, les propriétés optiques du matériau irradié sont décrites (localement) par la permittivité complexe

$$\epsilon^* = \epsilon^*_{\mathrm{vc}}(T) + \epsilon^*_{\mathrm{fcr}}(N), \tag{I.1}$$

où $\epsilon^*_{\mathrm{vc}}(T)$ et $\epsilon^*_{\mathrm{fcr}}(N)$ représentent, respectivement, les contributions dues aux diverses transitions interbandes (à la température T) et intrabandes (à une concentration électronique N).

La principale incertitude concerne la variation du premier de ces deux termes à des températures supérieures à 1183 K pour lesquelles aucune mesure (du moins à la longueur d'onde simulée de 266 nm) n'a, à la connaissance de l'auteur, été rapportée (Sun *et al.*, 1997). Conséquemment, une extrapolation jusqu'à la température de fusion (1691 K) a été employée; ce choix n'est pas déterminant dans la mesure où la longueur de pénétration du laser varie peu et où les mécanismes d'ablation sont principalement tributaires des propriétés optiques de la phase métallique *liquide* qui sont, quant à elles, connues (Li and Fauchet, 1987).

I.2 Dynamique électronique et technique Monte Carlo

L'absorption de photons dans la cible donne lieu à la création d'électrons (et aussi de trous dans la phase solide cristalline) énergétiques dont la relaxation subséquente fait intervenir de multiples collisions par l'entremise de divers processus de diffusion.

L'émission de phonons (optiques) par les électrons et trous excités a lieu à un taux qui dépend fortement de l'énergie de ces derniers. En phase solide semi-conductrice, une relativement récente description du phénomène reposant sur un taux de collision principalement déterminé par la densité d'états est privilégiée (Fischetti and Laux, 1988; Fischetti *et al.*, 1995); en phase liquide métallique, en revanche, un temps *fixe* de collision de 10 fs (tel qu'anticipé pour un électron possédant une énergie cinétique de 1 eV) est employé. Il est à noter que l'énergie d'un "phonon" n'étant pas connue pour le silicium liquide, une valeur typique de 50 meV est utilisée.

En phase cristalline, deux processus (outre la simple diffusion en volume) influencent directement la concentration de porteurs dans la région irradiée: la recombinaison Auger ainsi que l'ionisation par impact (*impact ionization*).

Dans le premier cas, seule une évaluation théorique du temps de recombinaison ($\geq$ 6 ps) est disponible (Yoffa, 1980); cette valeur est couramment employée et, par conséquent, sa validité généralement reconnue (Lietoila and Gibbons, 1982; Agassi, 1984).

Dans le second cas, aucun consensus ne semble exister, et ce, malgré l'attention qui a été portée à ce problème complexe au cours des dernières décennies. Ainsi, un taux de collision (en fonction de l'énergie du porteur incident) basé sur de récents calculs et facile à implanter dans le modèle a été privilégié (Kamakura *et al.*, 1994; Kunikiyo *et al.*, 1996).

I.3 Dynamique atomique et technique de dynamique moléculaire

Le détail de la dynamique à l'échelle atomique dépend strictement du potentiel de Stillinger-Weber (Stillinger and Weber, 1985) utilisé dans la présente étude afin de décrire les propriétés du silicium en phases solide et liquide. Bien que certains aient modifié quelques-uns des paramètres du potentiel afin de, par exemple, mieux décrire les propriétés de la phase *amorphe* (Vink *et al.*, 2001), aucune tentative en ce sens n'a été faite.